A Total Concentration Fixed-Grid Method for Wet Chemical Etching Process

Prasenjit Rath

School of Mechanical and Aerospace Engineering

A thesis submitted to the Nanyang Technological University
in fulfilment of the requirement for the degree of
Doctor of Philosophy

2007

ABSTRACT

Chemical Etching (CE) is an important production process for the fabrication of electronic devices. CE process is widely applicable in the manufacturing of integrated circuit (IC) devices, micro-electro-mechanical-system (MEMS) devices, production of shadow mask for color TV etc. Wet chemical etching (WCE) is widely used CE process due to its low cost, high etch rate and good selectivity compared to other existing CE processes. WCE process involves dissolution of substrate by chemical reaction with liquid chemicals called as etchant. The substrate to be etched is partly protected by photoresist mask to protect it from direct contact with the etchant. The mask forms the desired pattern over the substrate surface. During the process of etching, the etched interface moves because of the dissolution of substrate by the etchant. Hence, this process is regarded as a moving boundary problem. Because of the presence of mask, the etched interface takes a very complicated shape in multidimensional etching. Predicting and understanding the etching profile growth is therefore very useful in designing the pattern structure used in fabricating IC and MEMS devices. The presence of moving boundary makes the problem highly non-linear.

The moving-grid (MG) approach is a widely used method to model the WCE process. In the MG approach, the computational domain is the etchant domain which continuously expands with time. Hence, the computation mesh has to be regenerated at every time step. However, as time progresses, because of the complicated shape of the etchfront, the computational domain is very irregular. Hence, unstructured mesh and body fitted coordinates are necessary to accurately capture the irregular moving interface. The primary focus is given on efficient mesh

generation in the MG approach which is computationally very expensive and its implementation sometimes difficult in complex geometries. This motivates to find an efficient numerical method for modeling the WCE process.

A *new* mathematical model based on the *total concentration* is developed to study the physical and chemical mechanism involved in the WCE process. The proposed model is based on the *fixed-grid* approach and is analogous to the enthalpy method used in the modeling of melting and solidification problems. The computational domain is the whole etchant and substrate domain which is discretized once at the beginning of computation. A new parameter called the total concentration is defined. The total concentration is the sum of the *unreacted* etchant concentration and the *reacted* etchant concentration. The conventional WCE model is reformulated based on the total concentration of etchant. The reacted concentration of etchant is a measure of the etchfront (the etchant-substrate interface) position during etching. With this proposed approach the etchfront position can be found implicitly. Simple Cartesian grid can be used to capture the etchfront that takes a very complicated shape in multidimensional etching.

The proposed model is applied to study the one-dimensional, two-dimensional and three-dimensional diffusion- and reaction-controlled WCE process. The etching is assumed isotropic in nature. The finite volume method is used to solve the resulting set of governing equations with prescribed initial and boundary conditions. The results obtained from the proposed model are compared with the existing moving grid (MG) methods, the analytical asymptotic solution and available experimental results. The results obtained using the proposed approach are found to be in good agreement with the existing approaches and also in good agreement with experiment. The effect of mask thickness, the rate of reaction and the initial etchant

concentration on the shape evolution of etchfront is studied. It is found that increasing the mask thickness can minimize the undercutting. The bulging effect near the mask corner is less pronounced with finite mask thickness.

ACKNOWLEDGEMENTS

After the completion of this thesis, I experience feelings of achievement and satisfaction. I wish to express my deep gratitude to all those who extended their helping hand towards me in various ways during my tenure at NTU Singapore.

It gives me immense pleasure to express my deep sense of gratitude and hearty thanks to my supervisors A/P Chai Chee Kiong, John (School of MAE) and Dr. Zheng Hong Yu (SIMTech), for their invaluable guidance and constant encouragement. They have spent a lion's share of their valuable time with me and made me feel the real zest of research work. I am highly indebted to them for their untiring devotion and willingness.

I would like to express my sincere thanks to Prof. Lam Yee Cheong and A/P V. M. Murukeshan for their invaluable guidance at different stages of my thesis work. My special thanks go to Dr. Zhu Hong for his constant help in carrying out preliminary experiment in MEMS lab at initial stage of my thesis work.

My heartfelt appreciation goes to all my former and current lab mates, Yap Yit Fatt, Ling Eng, Sohel Murshed, Gao Yandong, Liu Yongping, Harikrishnan and Marting Quang whom I have had the opportunity to interact and work with during my Ph.D. study. I especially want to thank Yap, Ling Eng, Sohel and Gao for their continuous help in and beyond my research.

Last but not the least, I would like to thank to my parents for their understanding and support.

CONTENTS

LIST OF FIGURES

LIST OF TABLES

NOMENCLATURE

SYMBOLS	DESCRIPTIONS	UNITS
a	Half width of the mask opening	-
a_E	Coefficient of the discretization equation for control volume *E*.	-
a_N	Coefficient of the discretization equation for control volume *N*.	-
a_P	Coefficient of the discretization equation for control volume *P*.	-
a_W	Coefficient of the discretization equation for control volume *W*.	-
a_S	Coefficient of the discretization equation for control volume *S*.	-
c	Unreacted etchant concentration	mol/cm^3
c_b	Bulk etchant concentration	mol/cm^3
c_s	Etchant concentration at the interface	mol/cm^3
C	Dimensionless etchant concentration	-
c_R	Reacted etchant concentration	mol/cm^3
C_R	Dimensionless reacted etchant concentration	-
c_T	Total concentration	mol/cm^3
D	Diffusion coefficient of etchant	cm^2/sec
k	Rate constant of reaction	cm/sec
M_{Sub}	Molar mass of substrate	gm/mol
m	Stoichiometric reaction parameter	-
Sh	Sherwood Number	-
t	Time	Sec

t^*	Dimensionless time	-
x	Co-ordinate direction	cm
J_x	Mass flux	mol/cm^2-sec
$c_{R,max}$	Required reacted concentration of etchant	mol/cm^3

Greek Symbols

α	Underrelaxation factor	-
Δt	Time step	Sec
ΔV	Volume of control volume	cm^3
ρ_{Sub}	Density of substrate	gm/cm^3
β	Dimensionless etching parameter	-
δ	Etch depth	μm

List of Abbreviations

CE	Chemical Etching	-
DCE	Dry Chemical Etching	-
DG	Deal Groove	-
ECV	Etching Control Volume	-
EDP	Ethylene Diamine Pyrocatecol	-
HNA	Hydrfluoric-Nitric-Acetic acid etchant	-
FG	Fixed-Grid	-
LAWCE	Laser Assisted Wet Chemical Etching	-
MEMS	Micro-Electro-Mechanical-System	-
MG	Moving Grid	-
TEAHW	Tetra Ethyl Ammonium Hydroxide Water	-
TMAH	Tetra Methyl Ammonium Hydroxide	-

WCE	Wet Chemical Etching	

Subscripts

Et	Etchant	-
E	Control Volume *E*	-
l	Lower limit of integration	-
o	Initial	-
P	Control Volume *P*	-
N	Control Volume *N*	-
W	Control Volume *W*	-
S	Control Volume *S*	-
Sub	Substrate	-
u	Upper limit of integration	-

Superscripts

o	Previous Time Step	-
n	Iteration Number	-

CHAPTER 1

INTRODUCTION

1.1 Background

Etching is a process by which materials are removed selectively from the surface of a solid body called as substrate. It is an important production process that is extensively used in the fabrication of semi-conductors, the design of specific pattern of circuit on the electronic devices such as the printed circuit board (PCB), the integrated circuit (IC) devices (Madou, 2002) etc. This process has also played a key role in designing micro-electro-mechanical-systems (MEMS) devices such as sensors and actuators (Pister et al., 1992; Mastrangelo et al., 1995). The materials are removed from the surface of the substrate either by physical or chemical means. Etching by physical means is known as sputtering. It is strongly directional in nature as the incident energetic ions allow the substrate material to be removed in a highly anisotropic manner (i.e. essentially vertical etch profiles can be produced). Unfortunately, such material removal mechanisms are also quite non-selective against both the masking material and the materials underlying the layers being etched. The selectivity, which is the ratio of the etch rate of the layer being deliberately removed by etching to that of a layer exposed to the etch but not to be intentionally removed, depends largely on sputter yield differences between materials. Sputter yield is the number of particles sputtered from the surface of a target per primary ion. Since the sputter yields for most materials are within a factor of three of each other, selectivities are typically not adequate. Furthermore, since the ejected species are frequently non-volatile, redeposition of species can occur on the sidewalls of the etched feature (Wolf and Tauber, 2000). As a result of these drawbacks, etching processes based

solely on physical removal mechanisms have not found wide use (Wolf and Tauber, 2000). On the other hand, etching processes relying strictly on chemical mechanisms for etching can exhibit very high selectivities against both mask and underlying substrate layers (Vakanas et al., 2002).

The chemical etching (CE) is a process by which material is removed from the substrate surface (or from thin films on the substrate surface) by chemical reaction with a reagent material called as etchant. When a mask layer (or resist) is used to protect specific regions of the substrate surface, the main goal of the etching is to precisely transfer the pattern created by the mask onto the substrate surface by removing the material not covered by the resist. The CE process involves three steps: a) transport of reactants to the surface; b) surface reaction; and c) transport of products from the surface.

CE process can be broadly classified into two parts: (1) the dry chemical etching (DCE) and (2) the wet chemical etching (WCE). In DCE processes, the etchant is in vapor, gas or plasma form. Typical example of DCE process is plasma etching. In plasma etching radio frequency glow discharge produces chemically reactive species (atoms, radicals, and ions) from a relatively inert molecular gas. The etching gas is selected to generate species, which react chemically with the material to be etched, and whose reaction products are volatile. The chemical mechanism of DCE process can be broken down into six steps. These steps are listed as: 1) reactive species are generated from the incoming gases by the plasma; 2) these species are transported by diffusion to the surface of the material being etched; 3) these species are adsorbed on the surface; 4) a chemical reaction occurs, with the formation of a volatile by-products; 5) the products are desorbed from the surface; and 6) the desorbed species diffuse into the bulk of the gas, and are pumped

from the chamber. If any of these steps fails to occur, the overall etch cycle ceases. Plasma etch gases used for etching Si, SiO_2, Si_3N_4 are fluorine- containing gases (e.g. CF_4 gas). The WCE is mainly performed in aqueous solutions of acids (HCl, HNO_3, H_2SO_4 and H_3PO_4) or in lyes (NaOH and KOH), or in neutral salt solutions of NaCl, $NaNO_3$, K_2SO_4, etc. The WCE process is found wide application in fabrication of microchannels for μTAS (Micro Total Analysis System) for chemical analysis of samples (Tjerkstra, 1999), in design of flow sensors, fabrication of shadow mask for color televison tubes (Hoffman, 1990) etc. The wet etching process is also used for formation of porous silicon (Ulhir, 1956) which is used for fabrication of MWμC (Multiwalled microchannels). These are the channels containing free hanging layers of porous silicon. These channels can be used in devices like microsieves, microbatteries and porous electrodes (Tjerkstra, 1999). Table 1-1 shows some key points, which differs these two CE processes.

WCE process has certain advantages over DCE, which can be summarized as follows:

- Wet chemical etchants are readily available compared to dry chemical etchants.
- Equipment set up cost is less compared to dry chemical etching process where a sealed gas chamber is required for the production of reactive species.
- When fast etching is required WCE is the best choice as it gives high etch rate compared to dry chemical etching.
- Because of ion-induced damage in DCE, it is difficult to obtain smooth etched side walls compared to WCE.

However, WCE has also some limitations in its application, as it is best suited for designing relatively large pattern structure. The WCE is not suitable when the pattern dimensions are less than 3 μm size, where etching can only be performed by DCE. The

WCE is associated with undercutting effect due to the etching of substrate below the mask. Generally undercutting appears during etching with isotropic etchants. The isotropic etchants are discussed in section 1.3.

The research work in this dissertation focuses on WCE, which is studied in detail in subsequent sections. A brief description of the WCE process with an example of its application is discussed in the next section.

1.2 The Wet Chemical Etching Process

The WCE is a widely used etching technique due to its good surface finish and fast etching property. It is used for cleaning, shaping 3D structures, removing surface damage, polishing, and characterizing structural and compositional features (Ulhir, 1956). The widespread use of WCE is based on two factors. First, wet etching technology was well established from its long use in the printing industry. Second, the liquid etchant systems are available which selectively remove only the materials to be etched and most of these also do not attack photoresist (the most common etch-mask material). WCE methods are characterized by excellent selectivity and relatively high etch rate. As discussed previously in this section, WCE is mainly performed using liquid chemicals, which may be acidic, basic, or neutral salt solutions. Based on the choice of liquid etchants, the WCE can either be isotropic or anisotropic in nature. The choice of the liquid etchants is based on its application and the substrate to be etched. Isotropic wet etching has application in designing silicon microchannels in microfluidic devices (Gravesen et al. 1993, Spiering et al. 1996, Van den Berg et al. 1998). Generally acidic etchants are isotropic in nature, where the lateral etch depth is equal to the vertical etch depth. Anisotropic etching is orientation dependent, where the etch rate in one crystallographic plane of the substrate is

different from other crystallographic planes. It is generally used when controlled lateral etch rate is required. Hence, the sidewalls of etched groove are essentially vertical in anisotropic etching. A typical application of anisotropic wet etching can be found in preparing the thin membrane resistor used for a piezoresistive pressure sensor (Elwenspoek et al. 1994). The detailed discussions of the properties of some commonly used etchants are presented in next sub-section. A common example of the application of CE process is shown in Fig. 1.1, where the WCE process is used to produce the shadow mask for a colour television tube (Kuiken, 1990). A shadow mask is a thin (~ 150 μm) iron sheet whose entire surface is made transparent by means of a dense rectangular array of minute holes (100-200 μm). This shadow mask is produced by means of wet etching.

The iron sheet is covered with a photosensitive layer. Upon this, a photonegative mask is pressed against the sheet in such a way that the photosensitive layer is in between the photonegative and the sheet (Fig. 1.1a). The design on the photonegative reflects the pattern of the holes one wishes to produce in the iron sheet. Then follows an exposure stage in which light of a required wavelength is used to harden the exposed part of the photosensitive layer (Fig. 1.1b). A rinsing stage is next in which non-exposed photosensitive material is removed, leaving a temporary selective layer on the iron sheet (Fig. 1.1c). This is called the etching mask or resist. After this, the etching can begin, which means that a highly concentrated solution of ferric chloride, the etchant, comes in contact with partly protected iron sheet to initiate the etching process (Fig. 1.1d).

1.3 Etchants

Etchants are the reactive species in the chemical etching process, which reacts with the substrate to dissolve it. It plays a key role in etching process. Etchants may be in solution

form or in gaseous form depending on the type of etching process involves. In choosing an etchant, a variety of issues must be considered such as: a) Ease of handling; b) Toxicity; c) Etch rate; d) Desired topology of the etched bottom surface; e) IC-compatibility; f) Etch stop; g) Etch selectivity over other materials; h) Mask material and thickness of the mask. Key ingredients in any wet etchant are: a) Oxidizer (e.g. H_2O_2, HNO_3); b) Acid or base to dissolve oxidized surface (e.g. H_2SO_4, NH_4OH); c) Diluent media to transport reactants and products through (e.g. H_2O, CH_3COOH). Depending on the mechanism of reaction of etchants with substrates, etchants can be divided into two categories: anisotropic and isotropic. Etchants of these two categories are discussed in detail in next sub-sections.

1.3.1 Isotropic Etchants

Isotropic etchants are otherwise called as polishing etchants. Typical properties of isotropic etchants are: a) Etch rate is same in all crystallographic directions; b) Lateral etch rate is about the same as vertical etch rate; c) Etch rate does not depend upon the orientation of the mask edge. Isotropic etchants are used at room temperature or slightly above ($<50^0$ C) (Madou, 2002). Historically they were the first Si etchants introduced by Ulhir (1956), Turner (1958), Robbins and Schwartz (1959, 1976), Klein and D'Stefan (1962) and Kern (1978). Isotropic etchants typically show diffusion limitation, which is discussed in detail in Chapter 2. For isotropic etching of Si, the most commonly used etchants are mixtures of nitric acid (HNO_3) and hydrofluoric acids (HF). Water can be used as a diluent, but acetic acid (CH_3COOH) is preferred because it prevents the dissociation of the nitric acid better and so preserves the oxidizing power of HNO_3, which depends on the undissociated nitric acid species for a wide range of dilution (Robbins and Schwartz, 1959). The etchant is called the HNA system. A useful formulation for HNA is

250 ml HF, 500 ml HNO_3, and 800 ml CH_3 COOH (Petersen, 1982). When used at room temperature, one obtains an etch rate of ≈ 4-20 μm/min (Kovacs et al., 1998). A comprehensive review of isotropic etchant solutions is given by Kern (Kern et al., 1978).

1.3.2 Anisotropic Etchants

Typical properties of anisotropic etchants are: a) Etch rate depends upon orientation to crystalline planes; b) Lateral etch rate can be much larger or smaller than vertical etch rate, depending upon orientation of mask edge to crystalline axes; c) Orientation of mask edge and the details of the mask pattern determine the final etched shape. Anisotropic etchants can be used for making complex shapes.

Some of the examples of anisotropic etchants are alkaline aqueous solutions of KOH, NaOH, LiOH, CsOH, RbOH, NH_4OH, and quarternary ammonium hydroxides, with the possible addition of alcohol. Alkaline organics such as ethylene-diamine, cholin (trimethyl-2-hydroxyethyl ammonium hydroxide), hydrazine and sodium silicates with additives such as pyrocatechol and pyrazine are employed as well. The principal characteristics of four commonly used anisotropic etchants are listed in Table 1.1 (Madou, 2002).

The most commonly used anisotropic etchants are KOH (Lee, 1969) and ethylene-diamine-pyrocatechol + water [EDP] (Finne and Klein, 1967); hydrazine-water rarely used (Declercq et. al., 1975). More recently, quarternary ammonium hydroxide solutions such as tetra-methyl-ammonium-hydroxide-water (TMAHW) and tetra-ethyl-ammonium-hydroxide-water (TEAHW) have become more popular (Tabata et al. 1990).

The review of experimental and modeling works on WCE process will now be discussed in next section.

1.4 Literature Review

A brief review of experimental and modeling works on WCE process are discussed in this section. The experimental and modeling works are discussed in the following two sub-sections.

1.4.1 Review of Experimental Works on WCE Process

In this section a brief review of experimental works, which has been studied by different researchers, so far are discussed.

Nielsen and Hackleman (1983) have studied the etch stop mechanism in CE process. They have found that the dissolution of SiO_2 in HF solutions can be stopped by the application of an electric field across the SiO_2. The field strength required is small enough to be generated in shallow-junction CMOSC circuits through photon absorption.

Kuiken and Tijburg (1983) have studied the centrifugal etching process and found it a promising tool to achieve deep etching results. In conventional etching process undercutting is the major problem, which can damage the integrated circuits through short circuit. They found that although adding convection will certainly increase the etch rate, etching methods that involve the forcing of the etchant along the hole pattern have one inherent drawback. It has in fact, been shown experimentally and explained theoretically that the emergence of every new vortex leads to a drastic reduction of the etch rate. This results in strong undercutting effects. In any case it is doubtful whether, in the end, the etch depth will ever be much larger than the final hole width. They have proposed an alternative method of etching that does involve convection but circumvents the deleterious side effects mentioned above. This method makes use of the fact that in an actual etching process, the density of

the liquid certainly is not uniform throughout the system. In many instances, the fluid will become more dense if reaction products are added to it. This means that in such cases the fluid close to the wall of the cavity is denser than the remaining pure etchant. When the complete system is put in an acceleration field, e.g. inside a centrifuge or in the ordinary gravity field, and care is taken to ensure that the acceleration vector is pointing out of the hole, the more dense polluted fluid will be drawn out, thus creating a natural convection pattern inside the etched cavity. Now there will be no trapped vortex within the cavity. Hence, fresh etchant will always come in contact with the base of the etched hole. Therefore, effect of undercutting can be minimized effectively.

Meerakker and Vegchel (1989) investigated the dissolution of silicon in aqueous CrO_3 - HF solutions by etching and electrochemical measurements. It has been shown that in CrO_3 - HF solutions with an [HF] / [CrO_3] ratio higher than 20, the reduction of Cr (VI) at silicon electrode is a valence band process. This reduction is kinetically controlled and first order in CrO_3 concentration.

Siedel et al. (1990) studied the crystal orientation dependence of anisotropic etching of crystalline silicon in alkaline solutions. They have studied the anisotropic behavior of all aqueous alkaline etchants (KOH, NaOH, LiOH etc.). They also found that concentration of KOH solution can greatly affect the etch rate. For highly concentrated KOH solutions, a decrease of the etch rate with the fourth power of the water concentration was observed. They have also studied the etching behavior of highly boron doped silicon in aqueous solutions based of ethylene-diamene, KOH, NaOH, and LiOH. They found that for all etchants, there was a strong reduction of the etch rate when boron concentrations exceeds approximately 2×10^{19} cm^{-3}. The reduction of the etch rate was found to be inversely

proportional to the fourth power of the boron concentration. For a given high boron concentration, the etch stop effect was found to be most effective for ethylene-diamine-based solutions and low concentration KOH and least effective for highly concentrated KOH. It was observed that the reduction of the etch rate on silicon doped with germanium and phosphorus is much smaller and follows a different mechanism.

Kendall (1990) presented the anisotropic etching mechanism of some of the chemical etchants like KOH solution during etching of silicon. Etch rates being about 200 times larger on the <100> and 400 times larger on the <110> than on the <111> surfaces of silicon in KOH:water solutions. He proposes that hydration complexes of the K^+ and OH^- are a dominant factor and that the <111> is blocked from the etching process by an inactive complex, $H_7O_4^-$.

Kikyuama et al. (1991) studied the principles of WCE in ULSI microfabrication. An improved chemical composition for buffered hydrogen fluoride (BHF: $NH_4F + HF + H_2O$) is determined based on fundamental research into the chemical reaction mechanism of BHF and SiO_2. The principles of WCE in silicon technology were proposed on the basis of four items: the determination of the dominant reaction (etching) species, the influence of the solubility of the etching products in BHF on etching uniformity and linearity, stability of chemical composition without solid phase segregation and an improvement of the wettability of liquid chemicals on wafer surface by the addition of a surfactant.

Kao et al. (1992) investigated the etch profile development in spray etching processes. They have observed an increase in the etch angle, resulting in more vertical sidewalls, as extent of etch undercut increases. Since spray etchers can keep a fresh supply of etchant on the board surface at all times, more consistent etch rates are possible. This type of process

offers improved etch quality, shorter etching times, and thus higher throughput. They have investigated the spray etching process for etching of copper in cupric chloride solution. However they encountered some difficulties during operation. They found the accumulation of puddles of liquid on the topside of the board during etching, which creates additional mass-transport limitations for the etching process. As a result higher spray pressures are required to aid in the transport of the etchant species through the liquid layer to the board surface.

Elwenspoek (1993) proposed a new model that explains the anisotropy of the etch rate of single crystalline silicon in certain etchants. It is based on the theories of crystal growth. He found that, it is the nucleation barrier on the <111> plane that inhibits the etching and gives rise to a larger activation energy of the etch rate and hence the etch rate in this plane is less compared to rest planes.

Georgiadou and Alkire (1993) have investigated the etching of thick copper foil masked except for a single rectangular opening having an aspect ratio of 5:1 or 1:1 in the presence of controlled laminar flow across the width of the pattern opening. It was observed that in a solution of 3.5*M* $CuCl_2$ + 0.5*M* HCl + 0.5*M* KCl, copper was found to form a surface film spontaneously to dissolve at a rate that depended upon convective-mass transfer conditions. It was concluded that anisotropic CE was related to the presence of a sparingly soluble surface film of CuCl.

Jianqiang and Yu-Chong (1993) fabricated straight one-dimensional PSG microchannels of different dimensions. One end of each channel was completely sealed, while the other end is an etching window. Typical length of the channels is 3000 μm. Widths of these channels ranges from 2 μm to 200 μm. Height of the channels which is also the PSG thickness, is 1

μm. They carried out the etching experiments under an *in situ* monitoring system. This monitoring system consists of a microscope, a video camera, a tap recorder, and a temperature-controlled hot chuck. The whole process is video recorded. They found that higher temperature increases the etching speed at least at the beginning of the etching, which shows that reaction constant is sensitive to temperature. Results show that thinner PSG channels are etched much slower than the thicker ones. This happens due to the two reasons: one is surface interaction between solid and liquid, which may either increase or reduce etching rate. The other is that flow is involved in the etching. In this case one should expect that the etching rate should increase with the channel height since the channels with larger cross-section tend to allow stronger fluid motion.

Williams et al. (1996) measured the etch rate for a wide variety of combinations of etchant and substrate material and tabulated. They found that wet etch rates can vary for reasons that are usefully divided into three groups: the etch setup, the material being etched and the layout and structure on the substrate. Etch-rate variation due to the etch setup is a function of: 1) temperature; 2) loss of reactive species; 3) loss of liquids to evaporation; 4) mixing; 5) stratification of the solution; 6) etch product blocking of chemical flow; 7) elapsed time from the start of the etch; 8) applied potential; 9) illumination; and 10) contamination. Etch rate variation due to the material being etched is affected by 11) impurities in or on the material being etched; 12) microstructure; 14) the distribution and fraction of surface area of the exposed surface layer; and 15) the structure geometry.

Kovacs et al. (1998) have given variety of possible methods for bulk etching silicon. For a given application, the appropriate choice of etching method depends upon a number of

factors, including shape of the desired structures, the resulting surface roughness, etchant cost, equipment cost, safety, process compatibility and availability. They found that for etching simple structures such as membranes, grooves, and reflective surfaces, beaker-based wet chemical etching of silicon would be entirely adequate. For undercutting of delicate micrometer-scale mechanisms, dry-etching method will be more appropriate.

Tjerkstra (1999) studied the applicability of isotropic WCE of silicon in fluoride containing solutions. It was found that this type of wet etching could be used as a tool for fabricating microchannels. Isotropic wet etching is very suitable for the fabrication of semi-circular channels with very smooth walls. Channels traveling in any direction can be made independent of crystal planes. Isotropic etching can be performed electrochemically in fluoride containing solutions, or chemically in solutions containing HF and an oxidizing agent such as HNO_3. Both methods offer the possibility of forming porous silicon. The large surface area and the very small diameters of the pores make porous silicon an interesting material in MEMS devices (Van den Berg and Grisel 1990, Drott et al. 1997, Tjerkstra et al. 2000).

Monguchi et al. (2000) developed a room temperature wet etch process, which allows control of the wavelength of photoluminescence from porous silicon. It was found that the size of the silicon crystal reduced by the repeated formation and removal of the surface oxide. It has been learned that the surface after this process does not have residual oxide.

Meerakker et al. (2000) investigated the process of photoanodic etching of deep pores in lightly doped n^- - Si wafers. Kinetic experiments revealed that etching process was diffusion-controlled in a solution containing HF, H_2O and ethanol. Electrochemical

experiments showed that H_2 evolution took place at the backside of the Si wafer and that H_2 and O_2 evolved at the Pt cathode and anode, respectively.

Sakaino et al. (2000) studied the chemically treated Si <100> surfaces in an aqueous NaOH solution at 20^0 C using spectroscopy ellipsometry (SE) and *ex situ* atomic force microscopy (AFM). They found that when the native silicon oxide is partly etch-removed, the resulting surface is very rough. This occurs because the solution does not etch surface native oxide rapidly, but attacks bulk silicon vigorously. The AFM image confirms a roughened surface of ~5.5 nm rms.

Stocker et al. (2000) demonstrate the crystallographic wet etching of p-type GaN with etch rates as high as 1.2 μm/min. Etchants used include KOH dissolved in ethylene glycol, aqueous tetra-ethyl-ammonium-hydroxide, and phosphoric acid at temperatures ranging from 90 to 260^0 C.

Striemer and Fauchet (2002) have developed an electrochemical etching technique that provides continuous control over the porosity of a porous silicon layer as a function of etching depth. Thin films with engineered porosity gradients, and thus a controllable gradient in the index of refraction, were used to demonstrate broadband antireflection properties on silicon wafer and solar cell substrate.

Cho et al. (2002) have successfully integrated InP microlenses on the backside of 1.55μm InGaAs photodiodes, using a single step diffusion-limited etching technique. They simulated the microlens surface profiles numerically based on a simple diffusion theory. Fiber coupling tolerance are also measured and compared with theoretical estimations using ray optics.

Resnik et al. (2003) have studied different approaches to obtain sharp silicon tips with a variety of aspect ratios, for potential use in advanced microelectronic applications. Tips suited for atomic force microscopy and field emission arrays were formed by WCE of <100> and <111> single crystal silicon in KOH, TMAH and HNA etchant.

1.4.2 Review of Modeling Works on WCE Process

A brief review of research works on modeling of WCE processes is discussed in this section. The modeling works include the analytical and the numerical approaches to understand the physical and chemical mechanisms involved in the WCE process. These research works are discussed below.

A mathematical approach to two-dimensional etching in a semi-infinite active surface was presented by Kuiken (Kuiken, 1984a). The mathematical model assumes that the transport of the active species occurs solely by diffusion. It is shown that, when the diffusion field propagates much faster than the etched surface, the problem can be solved by perturbation technique. In this technique the concentration distribution is first obtained without moving the interface in a given time. Then by applying the interface condition, interface displacement was evaluated. When the etched interface moves very slowly, there will be negligible effect on the concentration profile between expanded etchant domain due to small perturbation of the interface and unexpanded etchant domain in a given time. Based on the perturbation principle, the model has given a semi-analytical asymptotic solution. This asymptotic solution is valid when the etching process is diffusion-controlled (infinitely fast reaction at the etchant-substrate interface) and the interface moves slowly. Later in the same year, 1984b, the analytical model is extended for etching with mask, which will now leave open a slit-shaped area only, through which etching fluid may come into contact with

the surface of the solid body to attack its substance. As long as the diffusion field extends over a distance that is small in comparison with the width of the slit, the problem is exactly the same as discussed above. However, when the process proceeds further into the time domain, the diffusion field will eventually extend beyond the bounds set by the slit due to the etching below the mask and the solution will become quite different.

Vuik and Cuvelier (1985) presented a numerical solution to etching problem based on the moving grid (MG) approach and the variational inequality approach. In the MG approach, the computational domain is the etchant domain, which continuously expands with time. The effect of grid velocity due to expanding computational domain was taken into account in the MG approach. The same etching problem is also solved using the variational formulation, where a Baiocchi transformation (Baiocchi et al 1973) is used. In this formulation a variable is defined whose derivative with respect to time gives the etchant concentration distribution. Later Bruch et al (1993) parallelize the etching problem using the variational formulation. It has been found that the method parallelizes well and the computational time was minimized. The undercutting effect (described in section 1.4) in wet chemical etching was also discussed, which causes serious problems in integrated circuit devices fabrication especially when the feature dimension is too small ($<3\mu m$). Undercutting in etched integrated circuit devices could results in short-circuit.

Kuiken et al. (1986) presented a mathematical model that describes the diffusion-controlled etching near resist edges. To understand the role of the various physical parameters, a simple maskless one-dimensional model was studied first. An exact solution is presented for one-dimensional etching problem under diffusion-controlled limit. It is found that mathematical model under diffusion-controlled case can be solved by means of perturbation

technique that assume relatively small displacements of the etching surface. Based on the perturbation principle an analytical asymptotic solution is presented for two-dimensional etching in a semi-infinite geometry under pure diffusion and convection effect (flowing etchant). It was observed that etching profiles reveals a bulging shape near the mask edge in both diffusion-controlled and convection driven etching problems.

Shin and Economou (1989) studied the effect of fluid flow, transport, and reaction on the shape evolution of two-dimensional cavities during WCE. The finite element method (FEM) was employed to solve for the fluid velocity profiles and for the etchant concentration distribution in cavities of arbitrary shape. The MG method was used to track the shape evolution of etching cavities at different times. It was found that during etching in a quiescent solution under conditions of diffusion-control, bulging was specially pronounced for an infinitely thin mask, but the bulging was much weaker for a realistic mask having thickness ¼ of the cavity mouth width. In addition, the thicker mask resulted in significantly better etch anisotropy with only slightly different etch rate. The effect of etchant flow on etch rate and etch anisotropy was also studied. It was found that, with fluid flow across the cavity, the time average etch rate increased four times and time averaged etch anisotropy increased by 40% as compared to pure diffusion under condition studied. Later in 1990-91, the same group, have extended their earlier model to study the effect of forced and natural convection on the shape evolution of deep cavities. Effect of forced convection on the shape evolution of cavities was studied for higher values of the peclet number (up to 10^4). In addition, the effect of natural convection was investigated for values of Rayleigh number up to 10^4. Forced convection was found very ineffective for rinsing deep cavities. The etching rate decreased sharply with time as the cavity became deeper during etching. At the same time, the etching rate distribution along the active surface

became nearly uniform, degrading etch anisotropy. In contrast, natural convection was effective for rinsing the dissolution products out of the cavity. It was found that both the etch rate and etch anisotropy remained at relatively high values throughout etching, even at later times when the cavity became deeper.

Koide et al. (1991) developed a simulation program to predict the two-dimensional anisotropic etch profile. In the simulation program, the experimental database of complete etch rate distribution was used to predict the cross-section of the etchfront. With this simulation program it has become possible to predict a change in the cross-sectional shape of a silicon wafer having arbitrary crystallographic orientation and initial cross-sectional shape including concave and convex edges.

Monk et al. (1991 and 1994) presented the simple mathematical model for sacrificial phosphosilicate glass (PSG) etching in concentrated, dilute, or buffered hydrofluoric acid (HF). The mathematical analysis was based on the Deal-Grove (DG) model. It has been assumed that the reaction of PSG with HF to be first order in nature. The model further assumes that the etching to be one-dimensional and the etchant concentration is linear in the etched region. The fluosilicic acid (H_2SiF_6) formed by the reaction between PSG (SiO_2) and HF are instantaneously transported to the bulk where they do not establish any concentration profiles.

Liu and Yu-Chong (1993) studied the *in situ* monitoring and universal modeling of sacrificial PSG etching using hydrofluoric acid. They have extended the Monk et. al.'s work for wide range of HF concentrations and came to the conclusion that at higher concentration of HF, the etch depth obtained from the model had not fit well with the experimental results. Therefore, the model was modified by assuming mixed order

reactions (combination of first and second order) between PSG and HF. It was found that the results obtained with the mixed order kinetics fits well with the experimental results for a wide range of HF concentrations.

Georgiadou and Alkire (1994) developed the mathematical model for anisotropic CE of copper foil in acid chloride solutions. In this model the principal hypothesis of the etching mechanism was that, the copper surface can undergo mixed mass-transport/kinetic-control dissolution, due to non-uniformities in the etch rate created by the flow field. The flow was assumed two-dimensional, incompressible and steady for a Newtonian fluid with no body forces. They found that the effect of flow on average dissolution rate was complex. Computations indicated that for peclet number greater than 5400, etch rate deteriorated and, for low oxidant concentrations, directionality is worsen.

Adalsteinsson and Sethian (1995a) presented a level set formulation to the etching problem in a two-dimensional geometry. In the level set method, the computational problems related to evolution of the moving profile are solved formulating the front motion in terms of a master equation for a well-defined function having the moving surface as zero level. The evolution equation is Hamilton-Jacobi type equation. The level set function is a signed distance function which needs to be re-initialized at every time step. The method further extended to simulate three-dimensional etching (Adasteinsson and Sethian, 1995b). However, in the enthalpy type fixed-grid approach (Shamsundar and Sparrow 1975, Voller and his co-workers 1981, 1987-88, 1990-92), the interface condition is included in the governing equation and front motion is not directly evaluated. The fraction of the latent heat content will give the interface position. Hence, no separate front motion equation needs to be solved in this approach. Such type of fixed-grid method is developed in this

thesis to model the WCE process which will be discussed in detail in the next Chapter (Chapter-2).

Eaton et al. (1996) presented the model for sacrificial oxide (SiO_2) etching in aqueous HF solutions. They extended the work done by Monk et al. and Liu et al. They have (Eaton et al.) presented the one-dimensional model. For etching structures using either side or top etch ports, understanding the etch behavior for a given geometry can be essential to the successful fabrication of a micromachined device. They have presented the model for different geometry like bubble etch geometry of circular shape, concentric circles, rectangular etch, port to bubble, port to port etc. and presented the suitability of the models for various types of geometries.

Asaumi et al. (1997) have developed an anisotropic CE process simulation system, MICROCAD, which is equipped with a database of orientation dependent etching rates of single crystal silicon.

Li et al. (1998) presented the moving-boundary numerical scheme to predict the motion of the hydrofluoric acid (HF) and phosphosilicate-glass (PSG) etching interface. They have tested their numerical scheme in a radial geometry. From the simulated results of etch rate they found that the initial etching mechanism is dominated by reaction and is independent of device geometry. As time progresses the etching phenomenon becomes diffusion limited.

Kuiken (1998) presented a mathematical model for centrifugal etching system, which is a promising tool to control the undercutting effect in conventional etching process. The etching was studied in a axisymmetric cavity under the influence of an artificial

acceleration field generated inside a centrifuge. It is shown that the etching process is governed by a thin convective-diffusive boundary layer along the curved cavity wall. Local coordinates are used to describe this boundary layer and a similarity solution was presented.

Driesen (1999) has studied the convection driven wet chemical etching in a two-dimensional etch hole geometry using the boundary element method. A steady state concentration field was assumed inside an etch hole geometry.

Veenendaal et al. (2000) have developed a method to construct analytical functions that accurately describes anisotropic etch rate functions. A functional relationship between etch rate and crystal orientation was presented.

Vuik et al. (2000) developed a finite element based moving grid method to study the dissolution of Al_2Cu particle in an Al-Cu alloy. It is very similar to the wet etching problem where dissolution of substrate taking place by liquid etchant. Both these processes are governed by the mass diffusion equation with an interface condition describing the displacement of the interface. It has been mentioned that the enthalpy method which is a most popular fixed-grid method used for modeling melting/solidification problems needs a freezing interval. However, until now they have not able to find a related formulation based on enthalpy like approach for mass diffusion problems with moving boundaries.

La Magna et al. (2003) have implemented a code based on the level-set approach for a moving front to the simulation of the profile evolution during the selective electrochemical etching process. The code simulates the evolution of the etched profile using a phenomenological functional relation between dopant density and etch rate.

Kuiken (2003) presented a mathematical model for diffusion-controlled mask etching through a circular hole. Three dimensional diffusion field was assumed to be axisymmetric and fully developed. He considered two time regimes. First he applies when the etch depth is small in comparison with the width of the mask opening. In the second, the depth of etching is much greater than the width of the mask opening. The asymptotic method (as discussed in Kuiken 1984b) was applied to derive the approximate solutions for various time regimes. Explicit solutions are found for the shape of the etched surface as a function of the physical parameters. It is found that as long as etch pits are shallow, the etching through small apertures is faster than through large ones. The opposite is found to be true for deep pits.

Kaneko et al. (2003) developed a numerical method based on MG approach for simulating two-dimensional reaction controlled WCE. In their model they have taken into account the mesh velocity due to variation of computational region owing to the proceed of the etching.

Javierre (2003) presented an overview of different numerical methods used for modeling the dissolution problems like the WCE problem. It has been mentioned that although the enthalpy method is a most promising method for heat diffusion problems with moving boundaries like the melting/solidification problems, but it is difficult to generalize it to the concentration problems.

Salo et al. (2004) presented the modeling of sacrificial aluminium etching in complex network geometries. The modeling is based on the two-dimensional diffusion equation. A one-dimensional model for correlating etch rate and diffusion coefficient in silicon dioxide etching is extended to cover two-dimensional geometries. The two-dimensional diffusion

equation is solved numerically in the etch network geometry using the finite element simulation software FEMLAB.

Sudirham et al. (2004) applied the space-time discontinuous Galerkin finite element method to simulate the WCE of microstructures under pure diffusion and convection-diffusion conditions. The MG approach was used to track the etchant-substrate interface. The space-time DG method has a key feature that time is treated as an extra dimension which makes the method particularly useful for problems with time-dependent flow domains. The method offers great flexibility in mesh adaptation and special attention was given to the generation of an initial solution and mesh when there was no etching cavity yet.

1.5 Remarks on the Existing Works on WCE Process

From the review of modeling works it is found that the analytical solution to the multidimensional etching problem can be possible only for most simplified cases. The simplified cases are like the semi-infinite geometry and relatively slow movement of the interface as discussed by Kuiken (1984a-b) and Kuiken et al. (1986). This is because of the high non-linearity characteristics of the process due to the presence of moving boundary. The moving-grid numerical approach was widely used to model the WCE process. This approach is a very direct approach for the moving boundary problems. In this approach, the computational domain is the etchant domain, which continuously expands with time. Hence, regeneration of the computational mesh is necessary at each time step. This makes the grid size to change as etching progresses with time. The central difficulty in this approach is to efficiently capture the etchfront (the etchant-substrate interface) that takes a complicated shape in multidimensional etching. Hence, unstructured grid and body-fitted coordinates are used. The main focus in this approach is given to the mesh generation so as

to capture the etchfront accurately. This makes the approach sometime to be computationally very expensive and its implementation is not so straightforward.

The enthalpy method is a most popular method to handle the moving boundary problems in heat transfer like the melting and the solidification processes (Voller et al. 1981). Earlier attempts to formulate such fixed-grid method for moving boundary mass diffusion problems by other researchers have not been successful. Difficulties in formulating such method have been documented as early as 2000. Vuik et al. (2000) mentioned that

> "The EM (enthalpy method) allows a freezing interval, however until now we were not able to find a related formulation for our diffusion problem. Therefore, we used a front-tracking method which allows a first order reaction at the interface."

As recent as 2003, researchers (see Javierre, 2003) were still trying to formulate such a procedure. This was highlighted in the attached slide as shown in Fig 1.2.

Hence, efficient numerical modeling tool is still an open issue to study the physical and chemical mechanism associated with the WCE process.

1.6 Objective and Scope

From the current status of existing works on WCE process, it is found that the development of an efficient numerical model for this process is still an open issue. It is found that although the enthalpy method has got vast popularity in heat transfer area while modeling melting/solidification problems, it is not been successful for modeling moving boundary concentration problems as discussed in section 1.5. Looking at the

current status of modeling works for WCE process, the objectives and scopes of this thesis can be summarized as follows.

The objective of this thesis is to investigate the physical and chemical mechanism involved in the isotropic WCE process through a simple and novel mathematical model. A new numerical model is developed to simulate the WCE process. The new model is tested for simple one-dimensional etching to more realistic three-dimensional etching. The proposed model is based on a fixed-grid approach where the grid size is fixed and the computational domain is the whole etchant and substrate domain. It is analogous to the enthalpy method used to model melting and solidification problems (Shamsundar and Sparrow, 1975, Voller et al. 1981). In this new model the concept of *total concentration* is introduced which makes it feasible to formulate the problem using a fixed-grid approach analogous to the enthalpy method.

The scopes of this dissertation are:

1. To develop a novel numerical model for isotropic WCE process without laser.
2. To extend the numerical model to study the effect of rate of reaction on the etching process.
3. To evaluate the performance of the proposed model compared to the existing models.
4. To investigate the performance of the proposed approach in modeling multidimensional etching where the etchfront takes a very complicated shape because of the presence of inert mask.
5. To validate the proposed mathematical model with available experimental results.

1.7 Contribution

A novel numerical model is developed to simulate the WCE process. The proposed model is based on the fixed-grid approach analogous to the enthalpy method used for modeling melting/solidification problems. In the proposed approach the concept of total concentration is introduced, which makes it feasible to formulate the problem using a fixed-grid approach. The proposed approach is applied to model diffusion- and reaction-controlled etching. The prediction of etchfront from proposed approach compared with existing approaches. The proposed model is validated with available experimental results. The new model is applied to simulate the one-dimensional, the two-dimensional and the three-dimensional wet etching system.

1.8 Outline of the Dissertation

There are five chapters in this dissertation. The chemical etching and the wet chemical etching processes are introduced in Chapter 1. Some commonly used wet etchants are also discussed in Chapter 1. In Chapter 2, the theoretical model governing the etching process is presented. The proposed total concentration model is also presented in Chapter 2. The numerical method used to solve the governing equations with initial and boundary conditions is discussed in Chapter 3. The simulated results obtained using the proposed method are presented and discussed in Chapter 4. Finally, in Chapter 5, the conclusion and future recommendations are given.

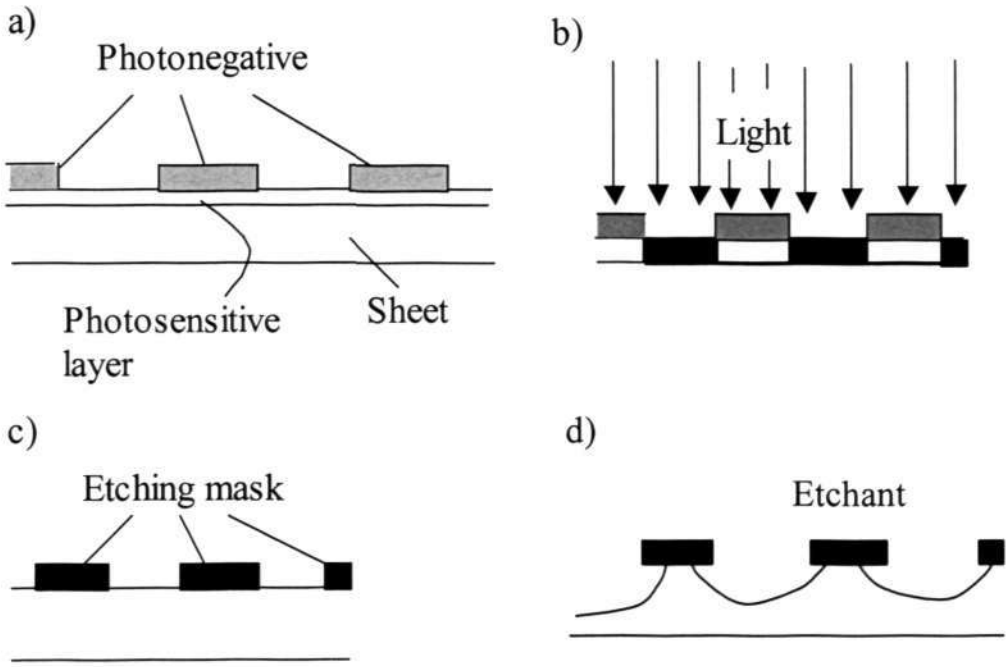

Figure 1.1 Steps in the production of shadow mask by etching.

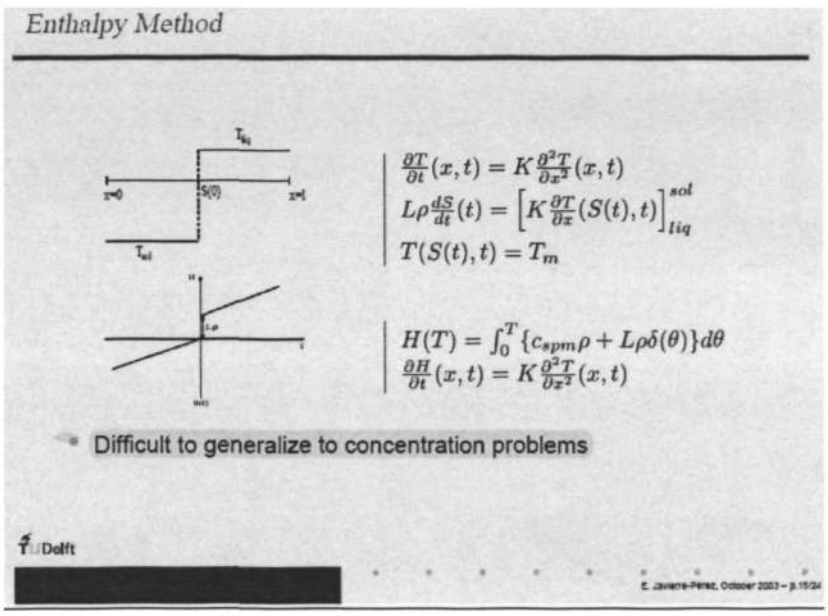

Figure 1.2 The enthalpy method for dissolution problems (Javierre, 2003).

Table 1.1 Key differences between WCE and DCE.

S. No.	WCE	DCE
1.	Liquid etchant is used for etching	Gaseous etchant is used for etching
2.	No sealed chamber is required in etch setup.	A sealed gas chamber is required in etch setup.
3.	It provides higher degree of selectivity.	Degree of selectivity is less compared to WCE.
4.	It is generally used when high etch rate is required (of the order of 1 μm/min).	It is generally used when slow etching is required (of the order of 0.1 μm/min).
5.	Smooth etched surface can be obtained.	Due to ion-induced damage, the etched surface is not very smooth.

Table 1.2 Principal characteristics of four different anisotropic etchants.

Etchant/diluent/temperature	Etch rate (μm/min)	Remarks
KOH (water) 85^0 C	1.4	IC incompatible, avoid in eyes, etches oxide fast, lots of H_2 bubbles.
Ethylenediamine pyrocatechol (water), 115^0 C	1.25	Toxic, ages fast, O_2 must be excluded, few H_2 bubbles, silicates may precipitate.
Tetramethyl ammonium hydroxide (TMAH) (water), 90^0 C	1.0	IC compatible, easy to handle, smooth surface finish.
N_2H_4 (water, isopropyl alcohol), 100^0 C	2.0	Toxic and explosive, ok at 50% water.

CHAPTER 2

THEORETICAL MODEL

The theoretical formulation of the WCE problem is presented in this Chapter. Three main formulations are given: the one-dimensional model and the two multidimensional models of WCE process respectively. The physical behavior of the WCE problem is briefly described in section 2.1. The undergoing mechanism of the etching process is discussed in section 2.2. The mathematical formulation of the problem is described in section 2.3. An exact solution for a simplified case is briefly described in section 2.4. The widely used existing MG method and some remarks are briefly described in section 2.5. The overview of the proposed approach is described in section 2.6. The proposed approach is applied to formulate the one-dimensional, the two-dimensional and the three dimensional WCE problems which are described in detail in next three subsequent sections (sections-2.7, 2.8, and 2.9) respectively. Finally, the overall solution procedure for proposed approach is summarized in section 2.10.

2.1 Problem Description

During the progress of wet etching, due to the dissolution of substrate by the liquid chemicals, the etchant-substrate interface moves. Hence, theoretically this process can be treated as a moving boundary problem, where the moving interface position is priory an unknown. It is in close resemblance with the Stefan problem governing the melting/solidification (Ozisik 1980, Crank 1984, Tarzia 2000) processes. This is shown in Table 2.1. The only difference is the boundary condition at the interface. In the wet chemical etching (WCE) problem, the concentration at the interface is obtained by the

balance between the rate of diffusion and the rate of reaction at the interface, whereas in the melting/solidification problems it is the melting temperature.

However, a diffusion-controlled WCE problem has one-to-one correspondence with the melting/solidification problems with zero melting temperature (e.g. melting of ice). It is because of the zero etchant concentration at the interface when etching is diffusion-controlled. The details about diffusion-controlled etching will be discussed later in this Chapter.

The etching process is governed by the transient mass diffusion equation according to Fick's second law with the prescribed boundary conditions and an initial condition. One of the boundary (the etchant-substrate interface) is unknown, whose position continuously changes with time because of the dissolution of substrate by the etchant. This needs an additional condition to describe the movement of the interface, known as the interface condition. The interface condition is obtained by the balance between the rate of diffusion of etchant and the rate of dissolution of substrate at the etchant-substrate interface.

2.2 Physical Mechanism of Chemical Etching Process

The physical mechanism of CE process can be of two types: 1) Diffusion-controlled etching and 2) Reaction-controlled etching depending on the mechanism of reaction at the etchant-substrate interface. These are discussed in next sub-sections.

2.2.1 Diffusion-Controlled Etching

In diffusion-controlled etching process, reaction proceeds infinitely fast compared to diffusion process. In CE process the boundary condition at the moving boundary (the

etchant-substrate interface) is obtained by balancing the rate of diffusion and the rate of reaction at the interface, which can be represented mathematically for a first order reaction kinetics as

$$-D(\hat{n}\cdot\nabla c)=Kc \tag{2.1}$$

where $\hat{n}$ is the unit vector normal to the interface that points towards the substrate, D is the diffusion coefficient of etchant, c is the etchant concentration and K is the surface rate constant of reaction. The etchant concentration at the interface depends on the relative ratio of rate of diffusion to the rate of reaction. When the reaction is infinitely fast at the interface, the etchant concentration at the interface approaches to zero. For infinitely fast reaction, the ratio D/K is infinitely small which leads to zero etchant concentration at the interface. This can be represented as

$$c=\lim_{\frac{D}{K}\to 0}\frac{D}{K}(\hat{n}\cdot\nabla c)$$

$$\Rightarrow c=0 \tag{2.2}$$

Equation (2.2) is the boundary condition at the interface for diffusion-controlled etching. The moment a molecule of etchant presents itself at the surface, it will be consumed instantaneously. Its residence time at the surface is infinitely short. Hence, the etching process is governed by the diffusion of etchant to the interface. The faster the diffusion of etchant, the faster will be the etching and hence the high etch rate.

2.2.2 Reaction-Controlled Etching

In reaction-controlled etching process, diffusion becomes infinitely efficient, so that the smallest glimpse of a depletion profile will be immediately flattened out. This means the

consumption of etchant by chemical reaction will not affect the bulk concentration of etchant in the etchant domain. Here the bulk concentration means the concentration of etchant in the etchant domain except the interface where reaction between etchant and substrate is taking place. So, the bulk concentration is nothing but the initial concentration of etchant in the etchant domain. Due to very slow reaction at the interface, concentration profile quickly relaxes to initial etchant concentration in the etchant domain. In this situation, the dissolution of substrate proceeds slowly compared to the transport of material in the etchant. When a molecule of a substrate is dissolved by the etchant it is immediately transported away from the etch surface. As a result, the concentration of etchant near the boundary will not be zero in this case unlike diffusion-controlled etching. The boundary condition at the interface for this case will be same as given in Eq. (2.1). In this type of etching the etched surface is controlled by the reaction kinetics.

2.3 Mathematical Representation of the Etching Problem

For demonstration purposes a one-dimensional WCE problem is considered. The schematic and co-ordinate system chosen is shown in Fig. 2.1. At the beginning of the etching process, the etchant at an initial concentration c_o is brought into contact with the substrate to be etched. Reaction between etchant and substrate at the etchant-substrate interface results in the decrease of the concentration of etchant and the depletion of the substrate. This leads to a moving etchfront (the etchant-substrate interface). For the problem described here, the origin of the co-ordinate is fixed at the etchant-substrate interface at time $t = 0$. With this definition, the coordinates of the region occupied by the substrate are always negative.

The WCE is a complicated process in reality, because of the complex reaction mechanism involved in the reaction between etchant and substrate. In order to simplify the mathematical model, some assumptions are made as below:

1. Product is soluble in the etchant solution.
2. Products formed by the reaction between etchant and substrate are assumed non-reactive.
3. Convection effect of etchant solution is neglected.
4. The reaction is assumed first order. In this case the rate of reaction is directly proportional to the concentration of etchant.

The mathematical form of the problem for a one-dimensional geometry (as shown in Fig 2.1) with the above assumptions can be represented as below.

Governing Equation

$$\frac{\partial c}{\partial t} = \frac{\partial}{\partial x}\left(D\frac{\partial c}{\partial x}\right) \qquad \text{in } -\delta(t) < x < \infty \text{ and } t > 0 \qquad (2.3.1a)$$

Initial Condition ($t = 0$)

$$c = c_o \qquad \text{at } t = 0 \text{ and } 0 \le x < \infty \qquad (2.3.1b)$$

Boundary Conditions ($t > 0$)

$$c = c_o \qquad \text{at } x \to \infty \qquad (2.3.1c)$$

$$D\frac{\partial c}{\partial x} = Kc \qquad \text{at } x = -\delta(t) \qquad (2.3.1d)$$

Interface Condition

$$-D\frac{\partial c}{\partial x}=\frac{m\rho_{Sub}}{M_{Sub}}\frac{dx}{dt} \qquad \text{at } x=-\delta(t) \text{ and } t>0 \qquad (2.3.1e)$$

$$\text{or } D\frac{\partial c}{\partial x}=\frac{m\rho_{Sub}}{M_{Sub}}\frac{d\delta(t)}{dt} \qquad \text{at } x=-\delta(t) \text{ and } t>0 \qquad (2.3.1f)$$

where, M_{Sub} is the molecular weight of substrate, ρ_{Sub} is the density of substrate, $\delta(t)$ is the position of etchfront at any time t and m is the stoichiometric reaction parameter of the reaction between the etchant and the substrate given as

$$S+mE\rightarrow qP \qquad (2.3.1g)$$

where, S stands for substrate, E stands for etchant and P is the product.

2.4 Exact Solution

The exact solution for one-dimensional semi-infinite geometry (shown in Fig. 2.1) under diffusion-controlled case is given as

$$\frac{c}{c_o}=\frac{\operatorname{erf}\left(\frac{x}{2\sqrt{Dt}}\right)+\operatorname{erf}(\gamma)}{1+\operatorname{erf}(\gamma)} \qquad (2.4.1)$$

where the error function is given as

$$\operatorname{erf}(x)=\frac{2}{\sqrt{\pi}}\int_0^{\infty}e^{-x^2}dx \qquad (2.4.2)$$

and the constant γ is given as

$$\gamma = \frac{\delta(t)}{2\sqrt{Dt}} \tag{2.4.3}$$

Equation (2.4.3) indicates that the etch depth varies as the square root of time. Constant γ can be found by solving the interface condition (Eq. 2.3.1f) using the concentration distribution as given in Eq. (2.4.1). Hence solving Eq. (2.4.1) and Eq. (2.3.1f) results in

$$\gamma e^{\gamma^2}\left[1+\operatorname{erf}(\gamma)\right] = \frac{1}{\beta\sqrt{\pi}} \tag{2.4.4}$$

In Eq. (2.4.4), β is the non-dimensional parameter called the etching parameter given as

$$\beta = \frac{m\rho_{Sub}}{c_o M_{Sub}} \tag{2.4.5}$$

Using the Newton-Raphson method, the constant γ can be evaluated for a given β value by solving the non-linear equation, Eq. (2.4.4).

2.5 The Moving Grid Method

The moving grid (MG) method is a widely used method for modeling WCE. The solution procedure in the moving grid (MG) method is summarized as follows.

(i) Concentration distribution is solved in the etchant domain at time $t + \Delta t$, keeping the etchant domain fixed at its original position (etchant domain at time t as shown in Fig. 2.2).

(ii) After solving the concentration distribution, interface displacement, Δx is found by using the interface condition as given in Eq. (2.3.1e). Hence the new position of the interface is given as

$$\Delta x^{t+\Delta t} = -\sigma\left(\frac{\partial c}{\partial x}\right)_{t+\Delta t} \Delta t \tag{2.5.1a}$$

where, σ is a constant given by

$$\sigma = \frac{DM_{Sub}}{m\rho_{Sub}} \tag{2.5.1b}$$

(iii) Expanded etchant domain is discretized again at time $t + \Delta t$.

(iv) Steps (i) and (ii) are repeated in the expanded etchant domain to get the new position of interface and new expanded etchant domain at the next time step.

(v) Steps (i), (ii), (iii), and (iv) are repeated until the desired etch depth is reached or the desired time is reached.

The MG method is associated with the movement of grids due to changing grid sizes as a result of expanding computational domain (the etchant domain). This makes a pure diffusion problem into a convection-diffusion problem because of the extra convective term due to the grid velocity.

While modeling multi-dimensional etching using MG method, mesh is irregular with time due to expanding grid. Hence, it is difficult to capture the complex etchfront in the MG method using cartesian grid and one must have to use the unstructured mesh and body fitted co-ordinates to capture the whole complex etchfront which is sometimes computationally very expensive.

2.6 The Total Concentration Fixed-Grid Method

A new method called as the total concentration fixed-grid (FG) method (Rath et al. 2005) is developed to simulate the wet chemical etching process. It is a fixed-grid method based on the total concentration of etchant. This proposed method is analogous to the enthalpy method used in the modeling of melting/solidification problems (Shamsundar and Sparrow 1975, Voller and his co-workers 1981, 1987-88, 1990-92, Chun and Park 2000, Hu and Agyropoulos 1996, White 1982, Prakash et al. 1987, Nedjar 2002). In this new method, the computational domain is the whole etchant and substrate domain. The computation mesh is generated once at the beginning of computation and the grid size remains fixed. Hence, there is no grid velocity unlike the MG method. Simple Cartesian grids are used to capture the complicated etchfront. The reacted concentration of etchant is a measure of the position of etchfront. The governing equation based on the total concentration includes the interface condition. The etchfront position is found implicitly.

Some new terminologies used in the proposed method are defined and presented next.

The Total Concentration (c_T)

In the proposed method, the *total concentration* (c_T) of etchant is the sum of: (i) the *unreacted* etchant concentration (c) which is the etchant concentration left after reaction and, (ii) the *reacted* etchant concentration (c_R) which is the etchant concentration consumed in the reaction process. The total concentration is defined as

$$c_T \equiv c + c_R \tag{2.6.1}$$

The reacted etchant concentration refers to the concentration of etchant reacted away during dissolution of substrate by the chemical reaction between substrate and etchant.

The Required Reacted Concentration ($c_{R,max}$)

$C_{R,max}$ is a measure of the moles of etchant required to dissolve a unit volume of substrate material by the chemical reaction. Consider an elementary volume of substrate having width Δx and cross-sectional area A_c as shown in Fig. 2.3. Now, if c_{Sub} is the concentration of substrate in the elementary volume Δx, then

Total number of moles of substrate in the elementary volume = $c_{Sub} \times A_c \Delta x$

$$= \frac{\rho_{Sub}}{M_{Sub}} \times A_c \Delta x$$

where ρ_{Sub} and M_{Sub} are the density and the molecular weight of substrate respectively. As discussed in Section 2.3 (Eq. 2.3.1g), during reaction of substrate with etchant, m moles of etchant reacted to dissolve 1 mole of substrate. Hence,

Total number of moles of etchant required to dissolve the elementary volume of substrate

$$= m \times \frac{\rho_{Sub}}{M_{Sub}} \times A_c \Delta x$$

$\therefore$ Total number of moles of etchant required per unit volume of substrate to dissolve the substrate by reaction = $m \times \frac{\rho_{Sub}}{M_{Sub}}$

This much moles of etchant is required to dissolve a unit volume of substrate, which we call it as *required reacted* concentration of etchant. Hence, if $c_{R,max}$ represents the required reacted concentration of etchant, then

$$c_{R,max} = \frac{m\rho_{Sub}}{M_{Sub}} \qquad (2.6.2)$$

The Etching-Control-Volume (ECV)

The etching-control-volume (ECV) is the elementary reaction control volume in the substrate domain adjacent to the etchant domain as shown in Fig. 2.4, where the reaction between the etchant and the substrate is taking place. The reacted concentration of etchant (c_R) varies from 0 to $c_{R,max}$ in an ECV. An ECV is said to be etched completely when c_R reaches $c_{R,max}$.

The one-dimensional, the two-dimensional and the three-dimensional etching problem formulations using the proposed total concentration approach are discussed in next subsequent sections.

2.7 One-Dimensional Etching

The one-dimensional etching problem as discussed in section 2.3 is studied in this section based on the proposed total concentration approach. The schematic of the one-dimensional etching problem is same as shown in Fig. 2.1 (section 2.3). The conventional governing equation (Eq. 2.3.1a of section 2.3) is modified due to the inclusion of reacted concentration in the proposed approach. The derivation of governing equation and interface condition based on the total concentration are presented below.

2.7.1 Derivation of Governing Equation

Consider an one-dimensional control volume of thickness Δx and cross sectional area A_c as shown in Fig. 2.5. Applying the conservation of mass in the control volume Δx, neglecting the effect of convection of etchant, we have

[Rate of moles of species enter into the control volume Δx] – [Rate of moles of species leaving the control volume Δx] = [Rate of change of total moles of species inside the control volume Δx]

$$\therefore J_x - J_{x+\Delta x} = \frac{d}{dt}(c_T A_c \Delta x) \tag{2.7.1}$$

It should be noted that, the rate of change of total concentration of (c_T) would be equal to the rate of change of unreacted concentration (c), if the elementary control volume is completely in the etchant domain (as in MG method where solution domain is only the etchant domain). It is because the reaction is taking place only at the interface. Therefore, the reacted concentration (c_R) is constant in the etchant domain. For demonstration purposes, its value is kept $c_{R,max}$ in the whole etchant domain. The reacted concentration will only vary at the etchant-substrate interface.

From Eq. (2.7.1), we have

$$J_x - \left[J_x + \frac{\partial}{\partial x}(J_x)\Delta x \right] = \frac{d}{dt}(c_T A_c \Delta x)$$

$$\Rightarrow -\frac{\partial}{\partial x}(J_x) = \frac{d}{dt}(c_T A_c \Delta x) \tag{2.7.2}$$

From Fick's law

$$J_x = -DA_c \frac{\partial c}{\partial x} \tag{2.7.3}$$

Substituting Eq. (2.7.3) in Eq. (2.7.2) and canceling A_c on both sides results in

$$\frac{\partial}{\partial x}\left(D\frac{\partial c}{\partial x}\right)=\frac{dc_{\mathrm{T}}}{dt} \tag{2.7.4}$$

Equation (2.7.4) is the governing mass diffusion equation based on the total concentration. This modified governing equation based on the total concentration includes the interface condition too. That means the proposed governing equation is equally applicable to the etchant-substrate interface in addition to pure etchant and substrate domains. The total concentration concept is used in the proposed method to include the interface condition in the governing equation itself, unlike in MG method where governing equation and the interface condition are separate as given in Eq. 2.3.1a and Eq. 2.3.1f. Equation (2.7.4) can also be applicable in the substrate domain. When Eq. (2.7.4) is applied to the etchant domain (except the interface), it will reduce to

$$\frac{\partial}{\partial x}\left(D\frac{\partial c}{\partial x}\right)=\frac{dc}{dt} \tag{2.7.5}$$

Equation (2.7.5) is same as the governing equation presented in Section 2.2 (Eq. 2.2.1a) where governing equation is used only in the etchant domain. Equation (2.7.5) is used as the governing equation in the MG method as solution domain in the MG method is etchant domain only.

When Eq. (2.7.5) is applied to the substrate domain (except the interface), it will reduce to

$$\frac{\partial}{\partial x}\left(D_{Sub}\frac{\partial c_{Sub}}{\partial x}\right)=\frac{dc_{Sub}}{dt} \tag{2.7.6}$$

where, D_{Sub} is the diffusion coefficient in the substrate and c_{Sub} is the etchant concentration in the substrate. Since the diffusion coefficient of substrate is very low (of

the order of 10^{-15} to 10^{-37} m^2/sec), diffusion is negligible in the substrate region. Hence, the etchant concentration remains constant and it is zero in the substrate domain.

Combining Eq. (2.6.1) and Eq. (2.7.4) results in

$$\frac{\partial c}{\partial t} = \frac{\partial}{\partial x}\left(D\frac{\partial c}{\partial x}\right) - \frac{\partial c_R}{\partial t} \tag{2.7.7}$$

Equation (2.7.7) is used in the computation of unreacted concentration c in the proposed FG method.

The inclusion of interface condition in the proposed governing equation based on the total concentration concept (Eq. 2.7.4) is described next.

2.7.2 Interface Condition From Proposed Governing Equation

Using Eq. (2.7.4), the integral form of the governing equation based on the total concentration for a one-dimensional control volume spanning $x_l \leq x \leq x_u$ can be written as

$$\frac{d}{dt}\int_{x_l}^{x_u} c_T\, dx = \int_{x_l}^{x_u} \frac{\partial}{\partial x}\left(D\frac{\partial c}{\partial x}\right) dx = \left(D\frac{\partial c}{\partial x}\right)_{x_u} - \left(D\frac{\partial c}{\partial x}\right)_{x_l} \tag{2.7.8}$$

Consider an elementary control volume of length L ($L = L_e + L_s$, which contains the interface) as shown in Fig. 2.6 at two time intervals. Between t and $t + \Delta t$, an Δx-thick layer of substrate has been etched away. Locations of the interface at time t and at time $t + \Delta t$ are shown in Fig. 2.6. The total concentrations at t and $t + \Delta t$ are

$$\int_{-L_s}^{L_e} c_T^t\, dx = \int_{-L_s}^{-\Delta x} (c_T^t)_{Sub}\, dx + \int_{-\Delta x}^{0} (c_T^t)_{Sub}\, dx + \int_{0}^{L_e} (c_T^t)_{Et}\, dx \tag{2.7.9}$$

and

$$\int_{-L_s}^{L_e} c_{\mathrm{T}}^{t+\Delta t}\,dx = \int_{-L_s}^{-\Delta x} (c_{\mathrm{T}}^{t+\Delta t})_{Sub}\,dx + \int_{-\Delta x}^{0} (c_{\mathrm{T}}^{t+\Delta t})_{Et}\,dx + \int_{0}^{L_e} (c_{\mathrm{T}}^{t+\Delta t})_{Et}\,dx \tag{2.7.10}$$

where the subscripts *Et* and *Sub* represent the total concentration of etchant in the etchant and the substrate regions respectively. Subtracting Eq. (2.7.9) from Eq. (2.7.10), gives

$$\begin{aligned}\int_{-L_s}^{L_e} \left(c_{\mathrm{T}}^{t+\Delta t} - c_{\mathrm{T}}^{t}\right) dx = {} & \int_{-L_s}^{-\Delta x} (c_{\mathrm{T}}^{t+\Delta t} - c_{\mathrm{T}}^{t})_{Sub}\,dx + \int_{-\Delta x}^{0} \left[(c_{\mathrm{T}}^{t+\Delta t})_{Et} - (c_{\mathrm{T}}^{t})_{Sub}\right] dx \\ & + \int_{0}^{L_e} (c_{\mathrm{T}}^{t+\Delta t} - c_{\mathrm{T}}^{t})_{Et}\,dx\end{aligned} \tag{2.7.11}$$

Dividing both sides by Δt, and taking limits as $\Delta t \to 0$ in Eq. (2.7.11) gives

$$\frac{d}{dt}\int_{-L_s}^{L_e} c_{\mathrm{T}}\,dx = \frac{d}{dt}\int_{-L_s}^{-\Delta x} (c_{\mathrm{T}})_{Sub}\,dx + \lim_{\Delta t\to 0}\int_{-\Delta x}^{0} \frac{\left[(c_{\mathrm{T}}^{t+\Delta t})_{Et} - (c_{\mathrm{T}}^{t})_{Sub}\right]}{\Delta t} dx + \frac{d}{dt}\int_{0}^{L_e} (c_{\mathrm{T}})_{Et}\,dx \tag{2.7.12}$$

Using Eq. (2.7.8), Eq. (2.7.12) can be written as

$$\begin{aligned}\frac{d}{dt}\int_{-L_s}^{L_e} c_{\mathrm{T}}\,dx = {} & \left(D\frac{\partial c}{\partial x}\right)_{Sub,-\Delta x} - \left(D\frac{\partial c}{\partial x}\right)_{-L_s} + \lim_{\Delta t\to 0}\int_{-\Delta x}^{0} \frac{\left[(c_{\mathrm{T}}^{t+\Delta t})_{Et} - (c_{\mathrm{T}}^{t})_{Sub}\right]}{\Delta t} dx \\ & + \left(D\frac{\partial c}{\partial x}\right)_{L_e} - \left(D\frac{\partial c}{\partial x}\right)_{Et,0}\end{aligned} \tag{2.7.13}$$

Equation (2.7.13) can be rearranged as

$$\frac{d}{dt}\int_{-L_s}^{L_e} c_T\,dx - \left[\left(D\frac{\partial c}{\partial x}\right)_{L_e} - \left(D\frac{\partial c}{\partial x}\right)_{-L_s}\right] = \lim_{\Delta t\to 0}\int_{-\Delta x}^{0}\frac{\left[(c_T^{t+\Delta t})_{Et} - (c_T^{t})_{Sub}\right]}{\Delta t}dx + \left(D\frac{\partial c}{\partial x}\right)_{Sub,-\Delta x} - \left(D\frac{\partial c}{\partial x}\right)_{Et,0} \tag{2.7.14}$$

Using Eq. (2.7.8), Eq. (2.7.14) reduces to

$$\left(D\frac{\partial c}{\partial x}\right)_{Et,0} - \left(D\frac{\partial c}{\partial x}\right)_{Sub,-\Delta x} = \lim_{\Delta t\to 0}\int_{-\Delta x}^{0}\frac{\left[(c_T^{t+\Delta t})_{Et} - (c_T^{t})_{Sub}\right]}{\Delta t}dx \tag{2.7.15}$$

In the substrate, the unreacted etchant concentration is zero. As a result, the second term of Eq. (2.7.15) vanishes and Eq. (2.7.15) becomes

$$\left(D\frac{\partial c}{\partial x}\right)_{Et,0} = \lim_{\Delta t\to 0}\int_{-\Delta x}^{0}\frac{\left[(c_T^{t+\Delta t})_{Et} - (c_T^{t})_{Sub}\right]}{\Delta t}dx \tag{2.7.16}$$

As $\Delta t \to 0$, the ratio $dx/\Delta t$ approaches v, where v is the local normal velocity of the interfacial surface element towards the substrate region. Attention is now focused on the remaining terms. At time t, the interface is occupied by the substrate. As the interface is occupied by the substrate, the reacted concentration is zero. The unreacted etchant concentration at the interface is finite. As a result, the total concentration is

$$(c_T^{t})_{Sub} = c^{t} + c_R^{t} = c^{t} \tag{2.7.17}$$

At time $t + \Delta t$, the total concentration is

$$(c_T^{t+\Delta t})_{Et} = c^{t+\Delta t} + c_R^{t+\Delta t} \tag{2.7.18}$$

As shown in Fig. (2.6b), a layer of substrate has been etched away and the vacated space is now filled with the etchant. As $\Delta t \rightarrow 0$, the unreacted concentration $c^{t+\Delta t} \rightarrow c^t$ and the reacted concentration $c_R^{t+\Delta t} \rightarrow c_{R,max}$. Hence Eq. (2.7.18) reduces to

$$(c_T^{t+\Delta t})_{Et} = c^t + c_{R,max} \tag{2.7.19}$$

Using Eq. (2.7.17) and (2.7.19), Eq. (2.7.16) becomes

$$D\frac{\partial c}{\partial x} = c_{R,max} \mathrm{v} \tag{2.7.20}$$

Combining Eq. (2.6.2) and Eq. (2.7.20), gives

$$D\frac{\partial c}{\partial x} = \frac{m\rho_{Sub}}{M_{Sub}} \mathrm{v} \tag{2.7.21}$$

Equation (2.7.21) is same as Eq. (2.3.1e) for representing the interface condition. Thus the modified governing equation reduces to the interface condition at the interface.

2.7.3 Mathematical Representation

The governing equation for a one-dimensional etching problem with corresponding initial and boundary conditions are presented in this sub-section using the proposed approach. The schematic of the etching problem is shown in Fig. 2.7. The modified governing equation with prescribed initial and boundary conditions are given as follows:

Modified Governing Equation

$$\frac{\partial c}{\partial t} = \frac{\partial}{\partial x}\left(D\frac{\partial c}{\partial x}\right) - \frac{\partial c_R}{\partial t} \qquad \text{in } -L < x < \infty \text{ and } t > 0 \tag{2.7.22a}$$

Initial Condition ($t = 0$)

$$c = c_o,\ c_R = c_{R,max} \qquad \text{in } 0 \le x < \infty \qquad (2.7.22b)$$

$$c = 0,\ c_R = 0 \qquad \text{in } -L \le x < 0 \qquad (2.7.22c)$$

Boundary Conditions ($t > 0$)

$$c = c_o,\ c_R = c_{R,max} \qquad \text{at } x \to \infty \text{ and } t > 0 \qquad (2.7.22d)$$

$$c_R = 0 \qquad \text{in } -L \le x < -s \text{ and } t > 0 \qquad (2.7.22e)$$

$$D\frac{\partial c}{\partial x} = Kc \qquad \text{at } x = -s \qquad (2.7.22f)$$

where, c is the unreacted etchant concentration, c_R is the reacted concentration of etchant. It is to be noted that the c_R value remains constant in the etchant and substrate domains except the ECV. As discussed earlier in section 2.6, the c_R value changes from 0 to $c_{R,max}$ in an ECV. Hence an update procedure of c_R in an ECV is needed to complete the proposed formulation which is derived in next sub-section.

2.7.4 Procedure to Update c_R

A procedure to calculate the reacted etchant concentration c_R is presented in this Sub-section. As the reacted concentration is constant away from the etchant-substrate interface, Eq. (2.7.22a) reduces to the original governing equation (Eq. 2.3.1a) except at the etchant-substrate interface. At the etchant-substrate interface, the reacted etchant concentration is a measure of the amount of substrate being etched. In the proposed FG method, a control volume where etching is taking place is identified which is called the ECV as shown in Fig. 2.8. In the ECV, c_R changes from 0 to its maximum possible value $c_{R,max}$. A procedure to update c_R in the ECV is described in this sub-section. The finite

volume discretized equation (using implicit scheme) of Eq. (2.7.22a) for a control volume P (control volume undergoing etching i.e. ECV) as shown in Fig. 2.8 is given as

$$a_P c_P^m = \sum a_{nb} c_{nb}^m + a_P^o c_P^o - (c_{\mathrm{R},P}^m - c_{\mathrm{R},P}^o)\frac{\Delta x_P}{\Delta t} \tag{2.7.23}$$

where m, o, P, nb, a, Δx and Δt are the m^{th} iteration of the current time step, the previous time step, the control volume P, the neighboring control volumes, the coefficients of the discretization equation, the volume of a control volume, and the time step respectively. Equation (2.7.23) is valid for all control volumes. However, as c_{R} is constant in the etchant and substrate, the last term on the right side of Eq. (2.7.23) is zero except in the ECV. At the $(m+1)^{\text{th}}$ iteration, Eq. (2.7.23) can be written as

$$a_P c_P^{m+1} = \sum a_{nb} c_{nb}^{m+1} + a_P^o c_P^o - (c_{\mathrm{R},P}^{m+1} - c_{\mathrm{R},P}^o)\frac{\Delta x_P}{\Delta t} \tag{2.7.24}$$

Subtracting Eq. (2.7.24) from Eq. (2.7.23) and rearranging, gives

$$c_{\mathrm{R},P}^{m+1} = c_{\mathrm{R},P}^m + \frac{\Delta t}{\Delta x_P}\left[a_P(c_P^m - c_P^{m+1}) + \sum a_{nb}(c_{nb}^{m+1} - c_{nb}^m)\right] \tag{2.7.25}$$

When the solution converges, the last term of Eq. (2.7.25) will be zero. However, during the initial iteration process, it is most likely a non-zero term. Realizing that it is zero upon convergence, this term can be ignored from the calculation and Eq. (2.7.25) becomes

$$c_{\mathrm{R},P}^{m+1} = c_{\mathrm{R},P}^m + \alpha\, a_P \frac{\Delta t}{\Delta x_P}(c_P^m - c_P^{m+1}) \tag{2.7.26}$$

where α is the under-relaxation parameter whose value lies between 0 and 1. Equation (2.7.26) is used in updating the reacted concentration in the ECV. In Eq. (2.7.26), c_P^{m+1} is

calculated using the boundary condition at the interface as given in Eq. (2.7.22f). Hence, the c_P^{m+1} is approximated as

$$c_P^{m+1} = \frac{c_E^m}{1 + \frac{K_e \Delta x_{PE}}{D_e}} \tag{2.7.27}$$

where c_E^m is the etchant concentration in an etchant control volume at the east of ECV as shown in Fig. 2.8b. It is to be noted that, when the reaction rate is much faster, the ratio K_e/D_e will be very large, which leads to nearly zero etchant concentration in the ECV during etching. This happens in diffusion-controlled etching as discussed in section 2.2. Hence, in diffusion-controlled etching, the c_P^{m+1} is approximated as

$$c_P^{m+1} = \lim_{\frac{K}{D} \to \infty} \frac{c_E^m}{1 + \frac{K_e \Delta x_{PE}}{D_e}} = 0 \tag{2.7.28}$$

When etching starts, the initial unreacted etchant concentration needs to be evaluated in the ECV. This is presented next.

2.7.5 Initial Unreacted Etchant Concentration in the ECV

When etching starts, the initial unreacted etchant concentration (c_o) may be finite at the etchant-substrate interface depending on the rate of reaction compared to diffusion. Generally, in diffusion-controlled etching because of infinite rate of reaction, the unreacted etchant concentration at the interface is zero. However, when the reaction rate is slow compared to diffusion, there is always a finite etchant concentration at the interface as evident from the boundary condition at the interface (Eq. 2.7.22f). In the

proposed approach the interface is contained in the ECV itself. Hence, using the boundary condition at the interface, the initial unreacted etchant concentration in a fresh ECV (as shown in Fig. 2.8a) is approximated as

$$c_P^o = \frac{c_E^m}{1 + \frac{K_e \Delta x_{PE}}{D_e}} \tag{2.7.29}$$

2.8 Two-Dimensional Etching

In this section a two-dimensional wet etching model and formulation of the problem using the proposed approach is presented. In two-dimensional etching, the etchfront takes a very complicated shape because of the inclusion of inert mask, which prevents some parts of the substrate from being etched. Due to the lateral etching of substrate by the etchant below the mask, the etchfront takes a very irregular shape. The two-dimensional etching problem considered here is described below. Two limiting conditions are studied namely- the diffusion-controlled and the reaction-controlled WCE.

2.8.1 Problem Description

The schematic and computational domain for the two-dimensional problem considered here is shown in Fig. 2.9. A gap of width $2a$ is to be etched in a substrate (Fig. 2.9a). For demonstration purposes, the width of the mask on both sides of the gap is assumed to be large enough so that the concentration of etchant far away from the gap will remain unaltered at the initial concentration. The initial concentration of etchant at $t = 0$ is c_o. At $t > 0$, the reaction between the etchant and the substrate at the etchant-substrate interface results in the reduction of the concentration of etchant adjacent to the etchant-substrate interface and the depletion of the substrate. The concentration of etchant on the boundaries

far away from the gap is kept at the initial concentration, i.e. $c = c_o$. The etching is assumed diffusion-controlled where reaction rate is infinitely fast. The origin of the coordinate system is set to the etchant-substrate interface at the center of the gap. Since the problem is symmetrical about the origin, only half of the domain is considered as shown in Fig. 2.9b. The governing equation, the interface condition and the boundary conditions are presented next.

Governing Equation

For a stationary etchant solution, the etchant concentration within the etchant domain is governed by the mass diffusion equation given by

$$\frac{\partial c}{\partial t} = \frac{\partial}{\partial x}\left(D\frac{\partial c}{\partial x}\right) + \frac{\partial}{\partial y}\left(D\frac{\partial c}{\partial y}\right) \quad \text{in } \Omega(t) \tag{2.8.1a}$$

The initial and boundary conditions are

Initial Condition ($t = 0$)

$$c = c_o \qquad \text{in } \Omega(t) \tag{2.8.1b}$$

Boundary Conditions ($t > 0$)

$$\frac{\partial c}{\partial x} = 0 \qquad x = 0 \tag{2.8.1c}$$

$$c = c_o \qquad y = h + l_3 \tag{2.8.1d}$$

$$c = c_o \qquad x = a + l_1,\ h \le y \le h + l_3 \tag{2.8.1e}$$

$$J_y = -D\frac{\partial c}{\partial y} = 0 \qquad y = h,\ a \le x \le a + l_1 \text{ and } y = 0,\ a \le x \le a + x_o(t) \tag{2.8.1f}$$

$$J_x = -D\frac{\partial c}{\partial x} = 0 \qquad x = a,\ 0 \le y \le h \tag{2.8.1g}$$

$$-D(\hat{n}\cdot\nabla c) = Kc \qquad \text{on } f(t) \tag{2.8.1h}$$

where $\hat{n}$ is the unit normal vector at the interface $f(t)$ pointing towards the substrate domain.

Interface Condition for $t > 0$ on $f(t)$

$$\vec{v} = -\frac{DM_{Sub}}{m\rho_{Sub}}\nabla c \tag{2.8.1k}$$

Parameters in the above equations are same as described in section 2.3. The normal speed of the etchant-substrate interface $v_{\hat{n}}$ is obtained by dotting both sides of Eq. (2.8.1k) with the unit vector $\hat{n}$ normal to the interface which points towards the substrate region. This can be written as

$$\vec{v}\cdot\hat{n} = -\frac{DM_{Sub}}{m\rho_{Sub}}\nabla c\cdot\hat{n}$$

$$\Rightarrow v_{\hat{n}} = -\frac{DM_{Sub}}{m\rho_{Sub}}\frac{\partial c}{\partial \hat{n}} \tag{2.8.1m}$$

2.8.2 Formulation using Total Concentration Approach

The two-dimensional etching problem is reformulated using the proposed total concentration approach using the similar procedure as discussed in previous sub-section. In the proposed procedure, the computational domain is the whole etchant and substrate domain. The schematic of the computational domain is shown in Fig. 2.10. The etchant and substrate domains are shown as $\Omega(t)$ and $\Omega_s(t)$ respectively, which changes with time

due to the dissolution of substrate by the etchant. The mask region is shown as Ω_m which is fixed at all times as the mask is inert to etchant. Γ_3 is the extreme boundary at right hand side above the mask. The modified governing equation with associated boundary and initial conditions are given below.

Modified Governing Equation

$$\frac{\partial c}{\partial t} = \frac{\partial}{\partial x}\left(D\frac{\partial c}{\partial x}\right) + \frac{\partial}{\partial y}\left(D\frac{\partial c}{\partial y}\right) - \frac{\partial c_R}{\partial t} \qquad \text{in } \Omega(t), \Omega_s(t), \text{ and } \Omega_m \qquad (2.8.2a)$$

Initial Conditions

$$c = c_o,\ c_R = c_{R,max} \qquad \text{in } \Omega(0) \qquad (2.8.2b)$$

$$c = 0,\ c_R = 0 \qquad \text{in } \Omega_s(0) \text{ and } \Omega_m \qquad (2.8.2c)$$

Boundary Conditions

$$\frac{\partial c}{\partial x} = 0,\ \frac{\partial c_R}{\partial x} = 0 \qquad \text{at } \Gamma_1 \qquad (2.8.2d)$$

$$c = c_o,\ \frac{\partial c_R}{\partial y} = 0 \qquad \text{at } \Gamma_2 \qquad (2.8.2e)$$

$$c = c_o,\ \frac{\partial c_R}{\partial x} = 0 \qquad \text{at } \Gamma_3 \qquad (2.8.2f)$$

$$c_R = 0 \qquad \text{in } \Omega_s(t) \text{ and } \Omega_m \qquad (2.8.2g)$$

$$-D(\hat{n}\cdot\nabla c) = Kc \qquad \text{on } f(t) \qquad (2.8.2h)$$

The interface condition which describes the movement of the interface is contained in the modified governing equation (Eq. 2.8.2a). How the modified governing equation will

represent the interface condition at the interface in two-dimensional etching is described in next sub-section.

2.8.3 Interface Condition from Modified Governing Equation

The interface condition derived from the modified governing equation through a simple analysis for one-dimensional etching problem (discussed in section 2.7.2). However, in multidimensional problems the treatment is slightly different. Hence, a more general approach for the derivation of interface condition from the modified governing equation is presented below applicable for multidimensional etching problems.

Using the definition of total concentration as given in Eq. 2.6.1 in section 2.6, Eq. 2.8.2a can be written as,

$$\frac{dc_T}{dt} = \frac{\partial}{\partial x}\left(D\frac{\partial c}{\partial x}\right) + \frac{\partial}{\partial y}\left(D\frac{\partial c}{\partial y}\right) \tag{2.8.3}$$

The integral form of Eq. 2.8.3 is given as

$$\int_A \nabla c \cdot \hat{n} dA = \frac{d}{dt}\int_V c_T \, dV \tag{2.8.4}$$

where A is the surface area and $\hat{n}$ is outward normal on the surface A. Consider an elementary control volume V (which contains the interface) as shown in Fig. 2.11 at two time intervals. At $t + \Delta t$, ΔV volume of the substrate is etched away from the elementary control volume V. At time t, the interfacial surface Σ divides the control volume V into a etchant portion V_{Et} and a substrate portion V_{Sub} and divides the surface area A of V into two parts namely, A_{Et} and A_{Sub}. After a small increment in time Δt, the interface occupies a new

position Σ' and during this time ΔV volume of substrate has been etched away. Now the integral on the right hand side of Eq. (2.8.4) is examined at time t and $t + \Delta t$. At time t,

$$\int_V c_T^t \, dV = \int_{V_{Et}} \left(c_T^t\right)_{Et} dV + \int_{V_{Sub}-\Delta V} \left(c_T^t\right)_{Sub} dV + \int_{\Delta V} \left(c_T^t\right)_{Sub} dV \tag{2.8.5}$$

where the subscripts *Et* and *Sub* represent the etchant and the substrate respectively.

At time $t + \Delta t$,

$$\int_V c_T^{t+\Delta t} \, dV = \int_{V_{Et}} \left(c_T^{t+\Delta t}\right)_{Et} dV + \int_{V_{Sub}-\Delta V} \left(c_T^{t+\Delta t}\right)_{Sub} dV + \int_{\Delta V} \left(c_T^{t+\Delta t}\right)_{Et} dV \tag{2.8.6}$$

Subtracting Eq. (2.8.5) from Eq. (2.8.6), gives

$$\begin{aligned} \int_V \left(c_T^{t+\Delta t} - c_T^t\right) dV = & \int_{V_{Et}} \left(c_T^{t+\Delta t} - c_T^t\right)_{Et} dV + \int_{V_{Sub}-\Delta V} \left(c_T^{t+\Delta t} - c_T^t\right)_{Sub} dV \\ & + \int_{\Delta V} \left[\left(c_T^{t+\Delta t}\right)_{Et} - \left(c_T^t\right)_{Sub}\right] dV \end{aligned} \tag{2.8.7}$$

Dividing both sides of Eq. (2.8.7) by Δt, and taking limits as Δt approaches zero. It should be noted that as $\Delta t \to 0$, $(V_{Sub} - \Delta V) \to V_{Sub}$. Hence Eq. (2.8.7) reduces to

$$\frac{d}{dt}\int_V c_T \, dV = \frac{d}{dt}\int_{V_{Et}} \left(c_T\right)_{Et} dV + \frac{d}{dt}\int_{V_{Sub}} \left(c_T\right)_{Sub} dV + \lim_{\Delta t \to 0} \int_{\Delta V} \frac{\left[\left(c_T^{t+\Delta t}\right)_{Et} - \left(c_T^t\right)_{Sub}\right]}{\Delta t} dV \tag{2.8.8}$$

Using Eq. (2.8.4), the integrals over V_{Et} and V_{Sub} can be replaced as

$$\frac{d}{dt}\int_V c_T \, dV = \int_{A_{Et}+\Sigma} \left(\nabla c\right)_{Et} \cdot \hat{n} dA + \int_{A_{Sub}+\Sigma} \left(\nabla c\right)_{Sub} \cdot \hat{n} \, dA + \lim_{\Delta t \to 0} \int_{\Delta V} \frac{\left[\left(c_T^{t+\Delta t}\right)_{Et} - \left(c_T^t\right)_{Sub}\right]}{\Delta t} dV \tag{2.8.9}$$

Now considering the last term of Eq. (2.8.9), at time t the interface is occupied by the substrate. As the interface is occupied by the substrate, the reacted concentration is zero. Therefore,

$$\left(c_T^t\right)_{Sub} = c^t + c_{\mathrm{R}}^t = c^t \tag{2.8.10}$$

At time $t + \Delta t$, the total concentration is

$$\left(c_{\mathrm{T}}^{t+\Delta t}\right)_{Et} = c^{t+\Delta t} + c_{\mathrm{R}}^{t+\Delta t} \tag{2.8.11}$$

As $\Delta t \to 0$, the unreacted etchant concentration $c^{t+\Delta t} \to c^t$ and the reacted concentration $c_{\mathrm{R}}^{t+\Delta t} \to c_{\mathrm{R,max}}$. Again as $\Delta t \to 0$, the ratio $dV/\Delta t$ approaches $\mathrm{v}_{\hat{n}}\, d\Sigma$, where $\mathrm{v}_{\hat{n}}$ is the local normal speed of the interfacial surface element $d\Sigma$ towards the substrate region. Also, the space that is enclosed by ΔV shrinks to the surface Σ, so that the region of integration becomes Σ. If $\hat{n}$ represents the local outward normal to Σ towards the substrate region, then for a portion of the integrals over Σ, $\hat{n} = \hat{n}$ and $\hat{n} = -\hat{n}$ for the etchant and the substrate side respectively. As a result, Eq. (2.8.9) reduces to

$$\frac{d}{dt}\int_V c_{\mathrm{T}}\, dV = \int_A \nabla c \cdot \hat{n}\, dA + \int_\Sigma \left[\left(\frac{\partial c}{\partial \hat{n}}\right)_{Et} - \left(\frac{\partial c}{\partial \hat{n}}\right)_{Sub}\right] d\Sigma + \int_\Sigma c_{\mathrm{R,max}}\, \mathrm{v}_{\hat{n}}\, d\Sigma \tag{2.8.12}$$

Using Eq. (2.8.4), Eq. (2.8.12) reduces to

$$\int_\Sigma \left[\left(\frac{\partial c}{\partial \hat{n}}\right)_{Et} - \left(\frac{\partial c}{\partial \hat{n}}\right)_{Sub} + c_{\mathrm{R,max}}\, \mathrm{v}_{\hat{n}}\right] d\Sigma = 0$$

$$\Rightarrow \left(\frac{\partial c}{\partial \hat{n}}\right)_{Et} - \left(\frac{\partial c}{\partial \hat{n}}\right)_{Sub} + c_{\mathrm{R,max}}\, \mathrm{v}_{\hat{n}} = 0 \tag{2.8.13}$$

In the substrate, the etchant concentration is zero. As a result, the second term of Eq. (2.8.13) will be zero. Hence Eq. (2.8.13) reduces to

$$\frac{\partial c}{\partial \hat{n}} = -c_{\mathrm{R,max}}\, \mathrm{v}_{\hat{n}} \tag{2.8.14}$$

Substituting $c_{\mathrm{R,max}}$ from Eq. (2.6.2) in the above equation and rearranging results in

$$\mathrm{v}_{\hat{n}} = -\frac{DM_{Sub}}{m\rho_{Sub}} \frac{\partial c}{\partial \hat{n}}$$

Above relation is the interface condition given in Eq. (2.8.1m).

2.8.4 Procedure to Update c_{R}

In two-dimensional etching the update procedure of reacted concentration c_{R} is similar to the update procedure as described in section 2.7 for one-dimensional etching. However, the previous update procedure is applicable only for diffusion-controlled etching for a two-dimensional case. This is because the previous update procedure is applicable as long as the concentration along the interface is constant. But in two-dimensional reaction-controlled etching, the etchant concentration along the interface generally not constant and it varies along the interface. The etchant concentration variation is highly non-linear especially in the mask corner region. Due to the abrupt rise and fall of the etchant concentration near the mask corner, the previous iterative update procedure of c_{R} fails to capture the front accurately. Hence, a different update procedure is developed for reaction-controlled etching which will be described next. For two-dimensional diffusion-controlled etching, by setting $c_P^{m+1} = 0$ in Eq. (2.7.26) as described for one-dimensional etching in sub-section 2.7.4, gives the update expression for c_{R} as

$$c_{\mathrm{R},P}^{m+1} = c_{\mathrm{R},P}^{m} + \alpha\, a_P \frac{\Delta t}{\Delta V_P} c_P^m \tag{2.8.15}$$

where ΔV is the volume and subscript P denotes the nodal point of an ECV. Other symbols are same as described in sub-section 2.7.4.

Procedure to Update c_{R} in Reaction-Controlled Etching

A new procedure to update c_{R} in the etching-control-volumes (ECVs) is presented in this section. The new update procedure is applicable to diffusion- as well as reaction-controlled etching. Later in Chapter 4 in the discussion of results, the etchfronts are compared using two c_{R} update procedures for diffusion-controlled case and it is found that both update procedures produce the same etchfront. Hence, it can be said that the current c_{R} update procedure converges to conventional c_{R} update procedure in diffusion-controlled etching, where concentration along the etchant-substrate interface is zero.

In the proposed update procedure, the interface condition (Eq. 2.8.1m) is used to update c_{R}. As discussed earlier, the reacted concentration c_{R} is a measure of the interface displacement. Note that the normal displacement of the interface can be decomposed into horizontal and vertical components. Both the horizontal and vertical displacements lead to changes in the c_{R} value of a control volume. In the proposed procedure the change in the c_{R} value of a control volume is the maximum of the changes in c_{R} due to the horizontal and vertical displacements. For a two-dimensional problem, this can be written as

$$\Delta c_{\mathrm{R}} = \max\left(\Delta c_{\mathrm{R},E}, \Delta c_{\mathrm{R},W}, \Delta c_{\mathrm{R},N}, \Delta c_{\mathrm{R},S}\right) \tag{2.8.16}$$

In Eq. (2.8.16), $\Delta c_{\mathrm{R},E}$ and $\Delta c_{\mathrm{R},W}$ are the changes in the reacted concentrations due to the horizontal displacements δx_E and δx_W respectively. The remaining two terms in Eq.

(2.8.16) are the reacted concentrations due to the vertical displacements. The relation between $\Delta c_{R,N}$ and the vertical displacement δy_N can be written as

$$\delta y_N(x,t) = \frac{\Delta c_{R,N}}{c_{R,\max}} \Delta y_P \tag{2.8.17}$$

where δy_N, $\Delta c_{R,N}$ and Δy_P are the vertical displacement due to etching by the etchant adjacent to the north interface, the resulting change in the reacted etchant concentration and the height of the control volume P respectively. A procedure to calculate the displacement and the resulting reacted concentrations is described next.

Figure 2.12 shows the locations of the etchfront at two consecutive times namely, t and $t + \Delta t$. At a given x location, the vertical displacement δy is related to the speed normal to the etchfront by

$$v_{\hat{n}} = \frac{\Delta n}{\Delta t} = \frac{\delta y \, \mathrm{Cos}\theta}{\Delta t} \tag{2.8.18}$$

In Eq. (2.8.18), Δn is the displacement *normal* to the etchfront and θ is the angle subtends by the normal with the vertical. The term δy can be approximated as

$$\delta y = y(x,t+\Delta t) - y(x,t) \approx \frac{\partial y}{\partial t} \Delta t \tag{2.8.19}$$

Combining Eq. (2.8.18) and (2.8.19), gives

$$v_{\hat{n}} \approx \frac{\partial y}{\partial t} \mathrm{Cos}\theta \tag{2.8.20}$$

From the interface condition (Eq. 2.8.1m), the same speed can be obtained from the normal concentration gradient via

$$v_{\hat{n}} = -\frac{DM_{Sub}}{m\rho_{Sub}}\left[Sin\theta\frac{\partial c}{\partial x} - Cos\theta\frac{\partial c}{\partial y}\right] \tag{2.8.21}$$

Combining Eq. (2.8.20) and (2.8.21), results in

$$\frac{\partial y}{\partial t} = \frac{DM_{Sub}}{m\rho_{Sub}}\left[\frac{\partial c}{\partial y} - \frac{\partial c}{\partial x}\tan\theta\right] = \frac{DM_{Sub}}{m\rho_{Sub}}\left[\frac{\partial c}{\partial y} + \frac{\partial c}{\partial x}\frac{\partial y}{\partial x}\right] \tag{2.8.22}$$

The proposed c_R update procedure is obtained by combining Eq. (2.8.17) and (2.8.22). This can be written as

$$c_{R,N} = \frac{c^{o}_{R,P} + \frac{\Delta tD}{\Delta y_P}\frac{\partial c}{\partial y} - \frac{\Delta t}{\Delta x_w}\frac{D}{c_{R,\max}}\frac{\partial c}{\partial x}c_{R,W}}{1 - \frac{\Delta t}{\Delta x_w}\frac{D}{c_{R,\max}}\frac{\partial c}{\partial x}} \tag{2.8.23}$$

Equation (2.8.23) is the recursive equation for the c_R value due to the vertical displacement of the interface in contact with an etchant at the north interface of the ECV. The concentration gradient terms in Eq. (2.8.23) can be evaluated in each ECVs (as shown in Fig. 2.13a) as

$$\frac{\partial c}{\partial y} = \frac{c_N - c_{P,I}}{\Delta y_n} \tag{2.8.24a}$$

$$\frac{\partial c}{\partial x} = \frac{c_{P,I} - c_W}{\Delta x_w} \tag{2.8.24b}$$

where $c_{P,I}$ is the interface unreacted etchant concentration in the ECV evaluated by using the boundary condition at the interface (Eq. 2.8.1h), c_W and c_N are the unreacted etchant

concentrations in the neighboring control volumes at west and north of ECV respectively, $\Delta x_w = x_P - x_W$ and $\Delta y_n = y_N - y_P$. Following the same procedure as discussed above, a recursive equation for $c_{R,S}$ can be obtained, when the vertical displacement of the interface is due to the etchant at the south interface of ECV.

With a similar approach, it can be shown that the horizontal motion of the interface is given by

$$\frac{\partial x}{\partial t} = -\frac{DM_{Sub}}{m\rho_{Sub}}\left[\frac{\partial c}{\partial x} - \frac{\partial c}{\partial y}\frac{\partial x}{\partial y}\right] \tag{2.8.25}$$

The horizontal displacement δx_W is related to change in the reacted concentration $\Delta c_{R,W}$ as

$$\delta x_W(y,t) = \frac{\Delta c_{R,W}}{c_{R,\max}}\Delta x_P \tag{2.8.26}$$

where δx_W, $\Delta c_{R,W}$ and Δx_P are the horizontal displacement of the interface due to etching by the etchant adjacent to the west interface, the resulting change in the reacted etchant concentration and the width of the control volume P respectively. Combining Eqs. (2.8.25) and (2.8.26), gives c_R due to the horizontal displacement of the interface as

$$c_{R,W} = \frac{c^{o}_{R,P} - \dfrac{\Delta t D}{\Delta x_P}\dfrac{\partial c}{\partial x} - \dfrac{\Delta t}{\Delta y_s}\dfrac{D}{c_{R,\max}}\dfrac{\partial c}{\partial y}c_{R,S}}{1 - \dfrac{\Delta t}{\Delta y_s}\dfrac{D}{c_{R,\max}}\dfrac{\partial c}{\partial y}} \tag{2.8.27}$$

Above equation represents the recursive equation for the c_R value due to the horizontal displacement of the interface in contact with an etchant at the west of the ECV. The

concentration gradient $\partial c/\partial x$ in Eq. (2.8.27) can be obtained by using Eq. (2.8.24b) and $\partial c/\partial y$ can be evaluated in each ECVs (as shown in Fig. 2.13b) as

$$\frac{\partial c}{\partial y} = \frac{c_{P,I} - c_S}{\Delta y_s} \tag{2.8.28}$$

where c_S is the unreacted etchant concentration in the neighboring control volume at south of ECV and $\Delta y_s = y_P - y_S$. Following the similar procedure a recursive equation for $c_{R,E}$ can be obtained, when the horizontal displacement of the interface is due to the etchant at the east interface of ECV. The final c_R value for an ECV is taken as the maximum of the c_R values due to the horizontal and the vertical displacement of the interface as given in Eq. (2.8.16). The other two c_R updates in Eq. (2.8.16) can be similarly derived without any new concept.

2.8.5 Initial Unreacted Etchant Concentration in the ECV

As discussed earlier in section 2.7 while formulating the one-dimensional etching problem, the initial unreacted etchant concentration in a fresh ECV needs to be evaluated. A similar approach is applied as discussed in sub-section 2.7.5 for approximating the initial unreacted etchant concentration in a fresh ECV in two-dimensional etching. When etching starts in an ECV in the current time step, the initial unreacted etchant concentration (concentration from previous time step) of the ECV is approximated using the boundary condition of the interface as given in Eq. (2.8.1h). The initial unreacted etchant concentration is the maximum of the interface concentrations due to the chemical reaction from all possible directions. This can be written as

$$c_P^o = \max\left(c_{P,E}^o, c_{P,W}^o, c_{P,N}^o, c_{P,S}^o\right) \tag{2.8.29a}$$

$$c_{P,E}^{o} = \frac{c_E^m}{1 + \frac{k_P \Delta x_e}{D_P}} \tag{2.8.29b}$$

$$c_{P,W}^{o} = \frac{c_W^m}{1 + \frac{k_P \Delta x_w}{D_P}} \tag{2.8.29c}$$

$$c_{P,N}^{o} = \frac{c_N^m}{1 + \frac{k_P \Delta y_n}{D_P}} \tag{2.8.29d}$$

$$c_{P,S}^{o} = \frac{c_S^m}{1 + \frac{k_P \Delta y_s}{D_P}} \tag{2.8.29e}$$

where $c_{P,E}^{o}$, $c_{P,W}^{o}$, $c_{P,N}^{o}$, and $c_{P,S}^{o}$ are the initial unreacted etchant concentration due to the chemical reaction from east, west, north, and south interfaces of the ECV respectively.

2.9 Three-Dimensional Etching

The proposed total concentration approach is further extended to model three-dimensional wet etching in order to get in-depth knowledge of the more realistic wet etching processes. In two-dimensional etching, one of the dimensions is assumed to be long enough as for example the etching in a long channel. However, in some cases when a small hole needs to be etched, etching in all the three directions need to be considered. In those cases, a three-dimensional etching model is more appropriate to study the etching process and the etch surface evolution. For demonstration purposes, a diffusion-controlled case is studied as most of the isotropic etching processes are diffusion limited (Tjerkstra 1999, Madou 2002). A test problem is described to study the three-dimensional etching behavior and it is reformulated using the proposed approach.

2.9.1 Problem Description

The schematic and computational domain for the three-dimensional etching problem considered is shown in Fig. 2.14. An opening of square cross-section ($2a \times 2a$) is to be etched in a substrate (Fig. 2.14a). The remainder of the substrate surface is covered by a photoresist mask at the top. For demonstration purposes, the width of the masks on all the four sides of the opening is located sufficiently far from the opening so that the concentration of etchant far away from the opening will remain unaltered at the initial etchant concentration. The initial concentration of etchant at $t = 0$ is c_o. At $t > 0$, the reaction between the etchant and the substrate at the etchant-substrate interface results in the reduction of the concentration of etchant adjacent to the etchant-substrate interface and the depletion of the substrate. The concentration of etchant on the boundaries far away from the opening is kept at the initial concentration, i.e. $c = c_o$. The etching is assumed diffusion-controlled which is associated with infinitely fast reaction rate at the interface. The origin of the coordinate system is set to the etchant-substrate interface at the center of the opening. Since the problem is symmetrical about the origin, only one-quarter of the domain is considered as shown in Fig. 2.14b. $\Gamma_4(t)$ denotes the outer-surface of mask which is changing with time because of the underetching below the mask. $\Gamma_5(t)$ denotes two symmetry surfaces in XZ- and YZ-planes which are changing with time because of the dissolution of substrate by the etchant. The governing equation, the interface condition and the boundary conditions are presented next.

Governing Equation

For a stationary etchant solution, the etchant concentration within the etchant domain is governed by the mass diffusion equation given by

$$\frac{\partial c}{\partial t} = \frac{\partial}{\partial x}\left(D\frac{\partial c}{\partial x}\right) + \frac{\partial}{\partial y}\left(D\frac{\partial c}{\partial y}\right) + \frac{\partial}{\partial z}\left(D\frac{\partial c}{\partial z}\right) \qquad \text{in } \Omega(t) \qquad (2.9.1a)$$

The initial and boundary conditions are

Initial Condition at $t = 0$

$$c = c_o \qquad \text{in } \Omega(0) \qquad (2.9.1b)$$

Boundary Conditions for $t > 0$

$$c = c_o \qquad \text{on } \Gamma_1, \Gamma_2 \text{ and } \Gamma_3 \qquad (2.9.1c)$$

$$\frac{\partial c}{\partial \hat{n}} = 0 \qquad \text{on } \Gamma_4(t) \text{ and } \Gamma_5(t) \qquad (2.9.1d)$$

$$c = 0 \qquad \text{on } f(t) \qquad (2.9.1e)$$

Interface Condition for $t > 0$ on $f(t)$

The interface condition is obtained by the balance between rate of diffusion and rate of reaction at the etchant-substrate interface. This gives the interface velocity as

$$\vec{v} = -\frac{DM_{Sub}}{m\rho_{Sub}}\nabla c \qquad (2.9.1f)$$

where $\vec{v}$ is the velocity of the etchant-substrate interface. The normal speed of the etchant-substrate interface $v_{\hat{n}}$ is obtained by dotting both sides of Eq. (2.9.1f) with the unit vector $\hat{n}$ normal to the interface which points towards the substrate region. This can be written as

$$\vec{v} \cdot \hat{n} = -\frac{DM_{Sub}}{m\rho_{Sub}}\nabla c \cdot \hat{n}$$

$$\Rightarrow v_{\hat{n}} = -\frac{DM_{Sub}}{m\rho_{Sub}}\frac{\partial c}{\partial \hat{n}} \qquad (2.9.1h)$$

2.9.2 Formulation Using Total Concentration

The above three-dimensional etching problem is reformulated using the total concentration approach. The schematic of the modified computational domain is shown in Fig. 2.15. $\Omega(t)$ and $\Omega_s(t)$ are the region occupied by the etchant and the substrate respectively, which are changing with time because of the dissolution of substrate. Ω_m is the mask region which is fixed and do not vary with time. Γ_1 and Γ_2 are the boundary surfaces above the mask. Γ_3 denote the top boundary surface in the etchant region. The two perpendicular symmetry surfaces are denoted as Γ_4. The modified governing equation, the initial condition and the boundary conditions are presented next.

Modified Governing Equation

$$\frac{\partial c}{\partial t} = \frac{\partial}{\partial x}\left(D\frac{\partial c}{\partial x}\right) + \frac{\partial}{\partial y}\left(D\frac{\partial c}{\partial y}\right) + \frac{\partial}{\partial z}\left(D\frac{\partial c}{\partial z}\right) - \frac{\partial c_R}{\partial t} \qquad \text{in } \Omega(t), \Omega_s(t), \text{ and } \Omega_m \qquad (2.9.2a)$$

Initial Conditions

$$c = c_o,\ c_R = c_{R,max} \qquad \text{in } \Omega(0) \qquad (2.9.2b)$$

$$c = 0,\ c_R = 0 \qquad \text{in } \Omega_s(0) \text{ and } \Omega_m \qquad (2.9.2c)$$

Boundary Conditions

$$c = c_o,\ \frac{\partial c_R}{\partial \hat{n}} = 0 \qquad \text{at } \Gamma_1, \Gamma_2, \text{ and } \Gamma_3 \qquad (2.9.2d)$$

$$\frac{\partial c}{\partial n} = 0, \frac{\partial c_R}{\partial \hat{n}} = 0 \qquad \text{at } \Gamma_4 \qquad (2.9.2e)$$

$$c = 0 \qquad \text{on } f(t) \qquad (2.9.2f)$$

where $\hat{n}$ is the unit normal vector to a surface. The modified governing equation includes the interface condition. The interface condition can be extracted from the modified governing equation using the same procedure as discussed in sub-section 2.8.3 of section 2.8. The iterative update procedure of c_R is also same as discussed before for diffusion-controlled two-dimensional wet etching (Eq. 2.8.15).

2.10 The Overall Solution Procedure

The overall solution procedure for the proposed FG method based on the total concentration used to model the one-dimensional, the two-dimensional and the three-dimensional WCE is summarized in this section. Both diffusion- and reaction-controlled WCE is considered in the solution procedure. The overall solution procedure can be summarized as follows:

1. Specify the etchant, the substrate, and the mask (if any) domains. Ensure that the etchant-substrate interface lies on the interface between two control volumes and the same applies to the mask-substrate and the mask-etchant interfaces.
2. Set the initial etchant concentration as c_o in the etchant domain, 0 in the substrate domain and the mask region (if any).
3. Initially set c_R to 0 in the substrate domain including the mask (if any) and $c_{R,max}$ in the etchant domain respectively.
4. Advance the time step to $t + \Delta t$.

5. Identify the etching-control-volumes (ECVs). These are the substrate control volumes with adjacent etchant control volumes.
6. Set the initial etchant concentration (c_o) in the fresh ECVs using Eq. (2.7.29) for one-dimensional etching and Eq. (2.8.29a) for two-dimensional etching when the reaction is about to start.
7. Set the unreacted etchant concentration to zero in the mask and substrate regions (except the ECVs). A simple procedure of doing this is described in next Chapter (Chapter 3).
8. Calculate c_P^o in the ECVs to ensure that the interface condition is satisfied with a finite time step size.
9. Set c_P to c_P^o as the initial guess.
10. Solve the modified governing equation (Eqs. 2.7.22a, 2.8.2a, 2.9.2a) for the concentration.
11. Update the reacted concentration in the ECVs using the respective iterative update equation based on diffusion/reaction-controlled etching (Eqs. 2.7.26 or 2.8.15 or 2.8.16).
12. Check for convergence.
    a. If solution has not converged, check the calculated reacted concentration.
       - If $c_R < c_{R,max}$, repeat (7) to (11).
       - If $c_R \geq c_{R,max}$, then set $c_R = c_{R,max}$ and repeat (5) to (11).
    b. If solution has converged, then check if the number of time steps has been reached. If yes, stop. If not, repeat (4) to (11).

In the above solution procedure, the steps 6, 8 and 9 are generally not required if the etching is diffusion-controlled. This is because, in diffusion-controlled limit, the initial etchant concentration c_P^o in the fresh ECVs is actually zero as the ratio K/D is very large due to infinitely fast reaction at the interface. Therefore, its effect is negligible in the overall calculation procedure.

In the next Chapter the numerical method used to solve the resulting set of governing equations with associated initial and boundary conditions is described.

Table 2.1 Similarity between an etching problem and the Stefan problem.

Parameters	**Wet Chemical Etching Problem**	**The Stefan Problem** (Melting)
Governing Equation	$\frac{\partial c}{\partial t} = \frac{\partial}{\partial x_j}\left(D\frac{\partial c}{\partial x_j}\right);\ j = 1, 2, 3$ (The mass diffusion equation)	$\frac{\partial(\rho c_P T_l)}{\partial t} = \frac{\partial}{\partial x_j}\left(k\frac{\partial T_l}{\partial x_j}\right)$ (The heat diffusion equation)
Boundary Condition at the Interface	$-D\frac{\partial c}{\partial \hat{n}} = Kc$	$T_l = T_m$
Interface Condition	$-D\frac{\partial c}{\partial \hat{n}} = \frac{m\rho_{Sub}}{M_{Sub}} v_{\hat{n}}$	$-k\frac{\partial T_l}{\partial \hat{n}} = \rho L v_{\hat{n}}$

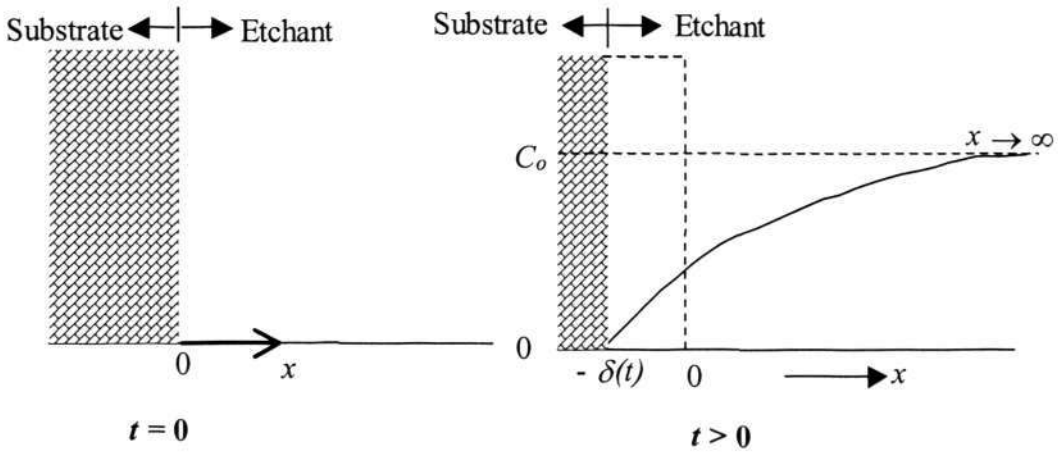

Figure 2.1 Schematic of the etching problem and co-ordinate system.

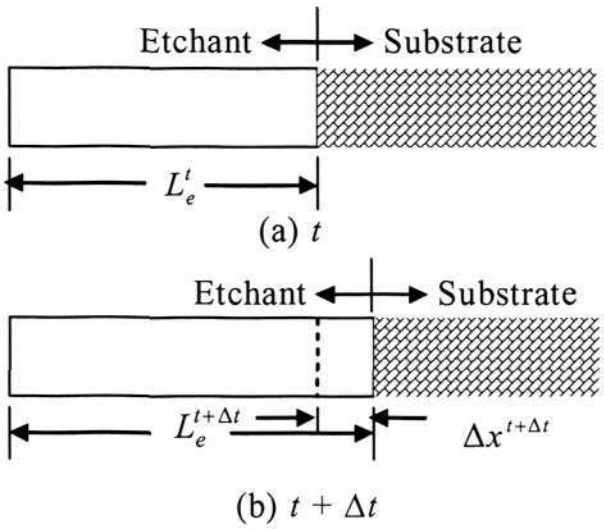

Figure 2.2 Etchant domain at two time steps.

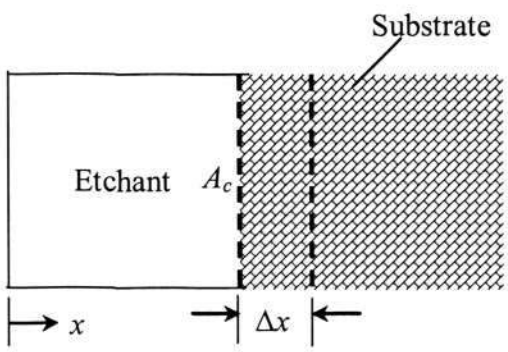

Figure 2.3 An elementary volume of substrate to be etched.

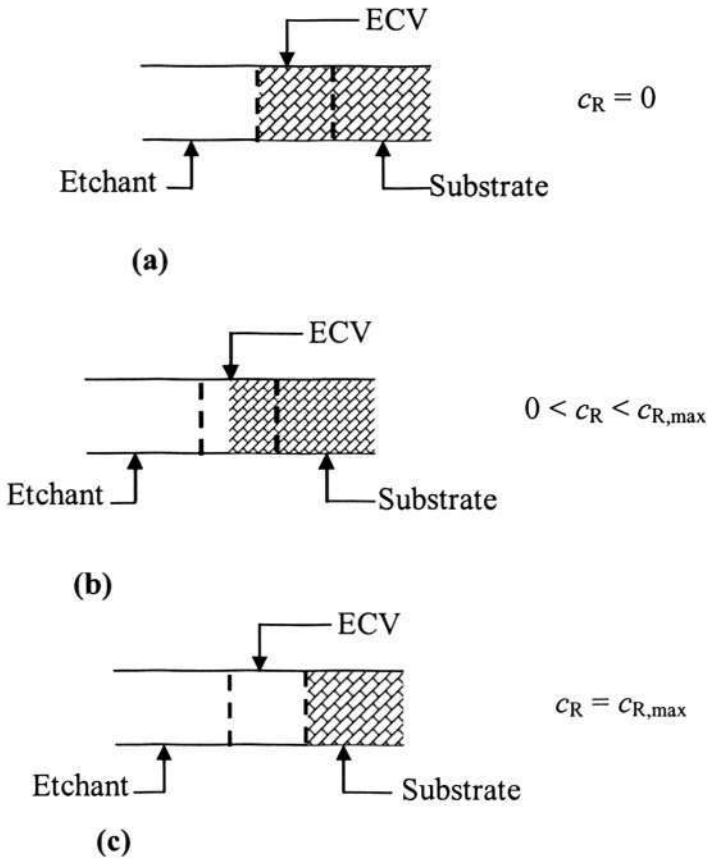

Figure 2.4 Schematic of an etching-control-volume (ECV) undergoing etching: (a) the etching about to start in the ECV; (b) during progress of etching in the ECV; (c) a completely etched ECV.

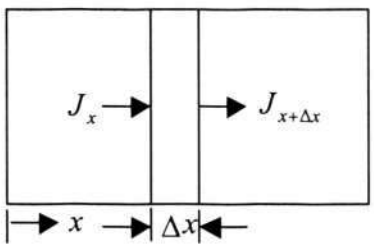

Figure 2.5 Schematic of one dimensional control volume.

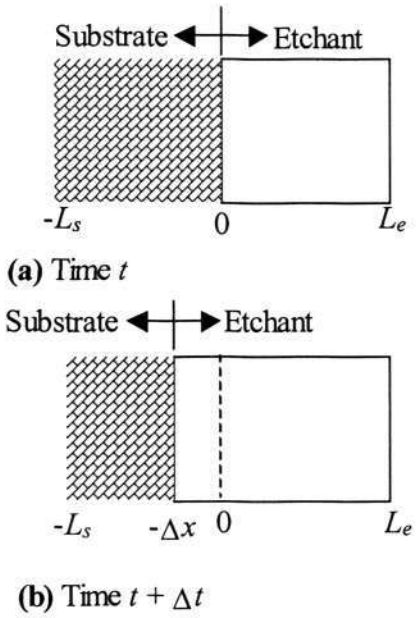

Figure 2.6 Etchant-substrate interface locations at two time steps.

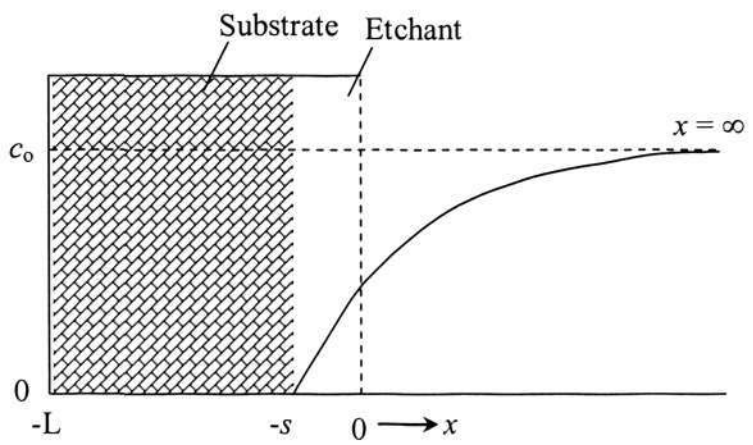

Figure 2.7 Schematic of one-dimensional etching problem.

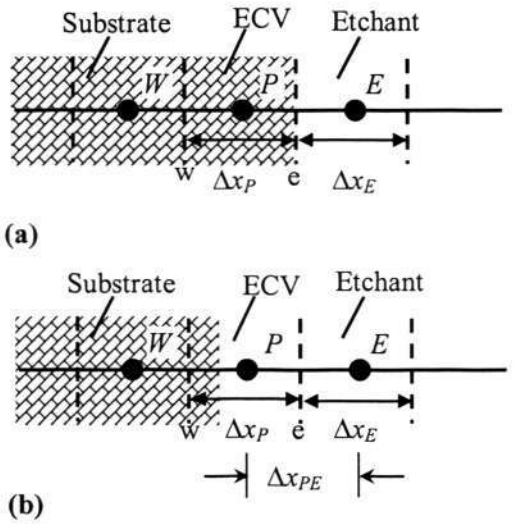

Figure 2.8 A control volume (P) undergoing etching: (a) the ECV when etching starts and (b) the ECV during etching.

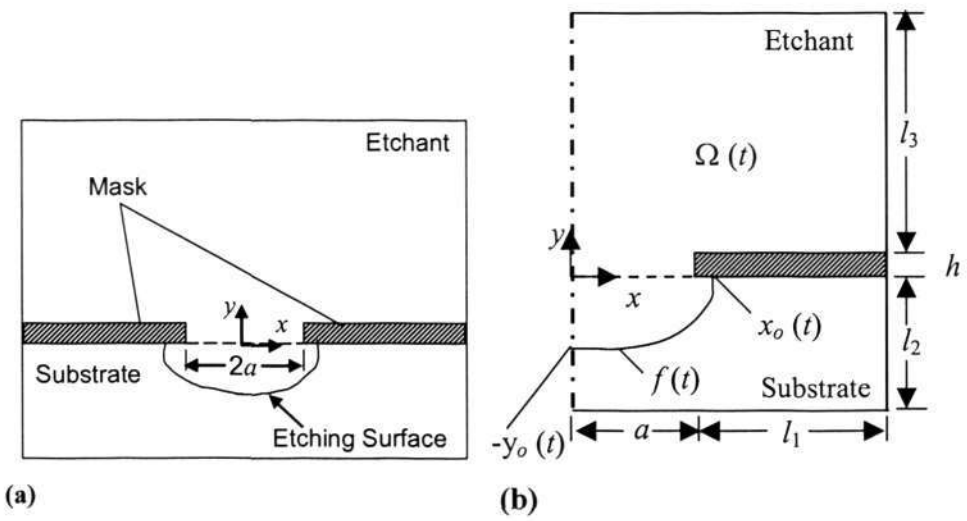

Figure 2.9 Schematic of the two-dimensional etching problem:(a) a full schematic; (b) the computational domain.

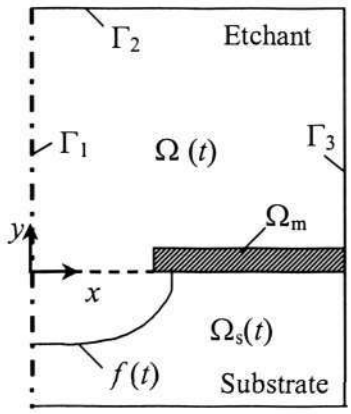

Figure 2.10 Schematic of computational domain used for two-dimensional etching using proposed procedure.

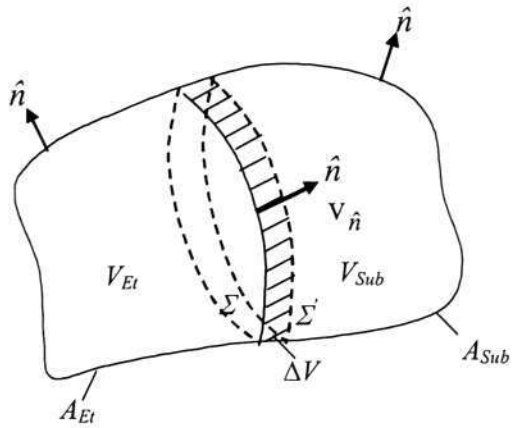

Figure 2.11 A control volume containing the etchant-substrate interface.

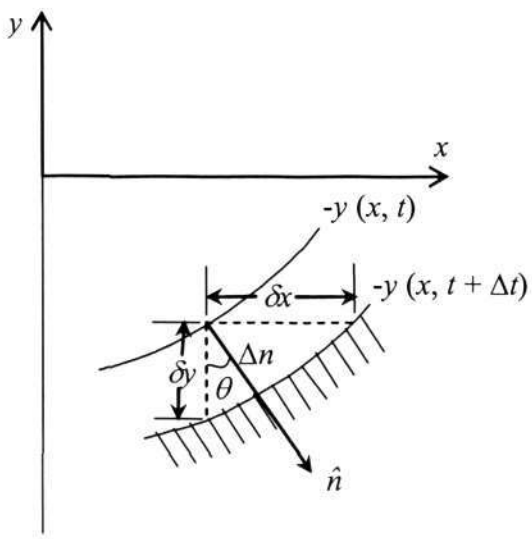

Figure 2.12 Sketch for evaluation of normal concentration gradient at the interface.

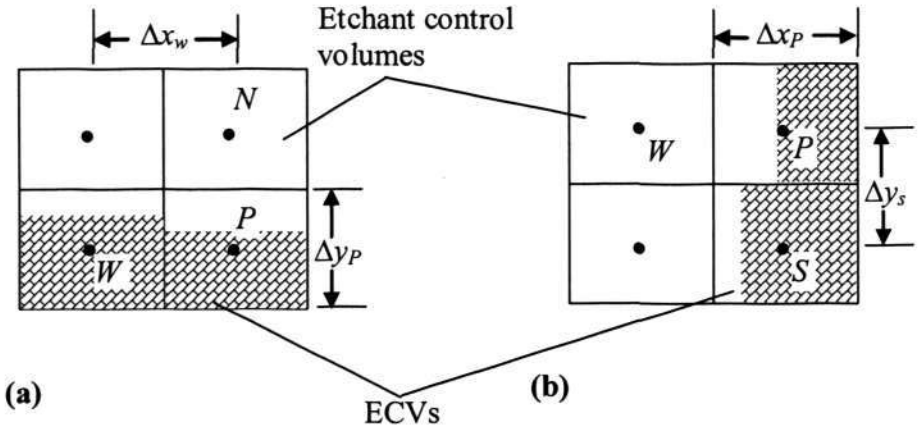

Figure 2.13 Etching control volumes undergoing etching: (a) vertical displacement of interface; (b) horizontal displacement of interface.

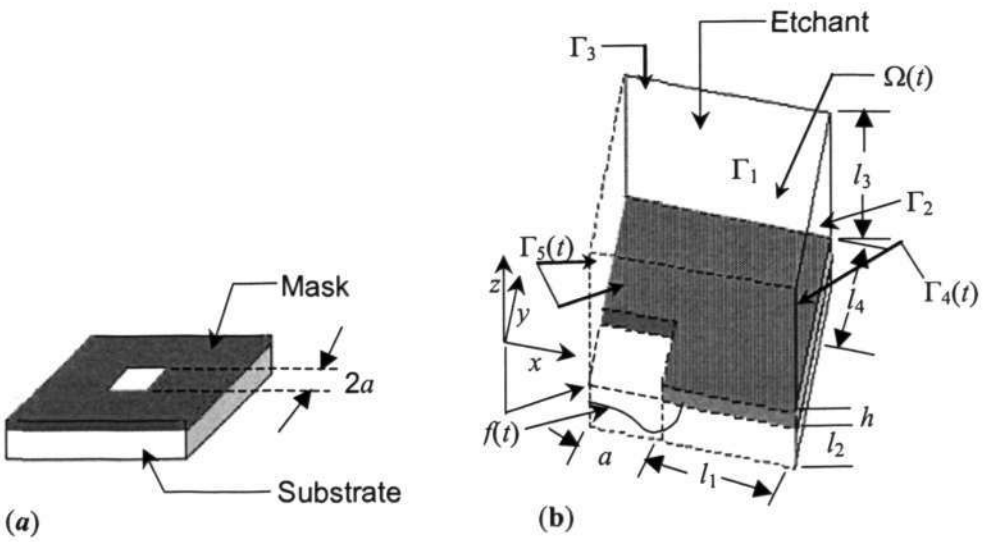

Figure 2.14 Schematic and computational domain of the three-dimensional (3D) etching.

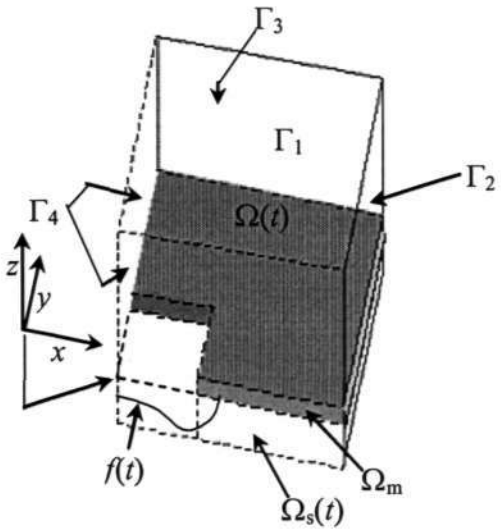

Figure 2.15 Schematic of the computational domain based on proposed approach.

CHAPTER 3

NUMERICAL METHOD

In this Chapter, the numerical method used in the modeling of wet chemical etching process is described. This process is basically referred to as a transient mass diffusion problem with heterogeneous chemical reaction. That means the reaction is taking place only at the interface and the governing equation does not include any source term due to species generation/degradation as found in the problems on diffusion with homogeneous chemical reaction. In section 3.1, the general form of the governing equation is presented. Then the Finite Volume Method is described in section 3.2. The discretization of the Partial Differential Equation is discussed in section 3.3. In section 3.4, the under-relaxation procedure to avoid divergence during computation is discussed. The solution methodology for solving the system of linear algebraic equations is described in section 3.5. The implementation of the different kinds of boundary conditions is discussed in section 3.6 and a brief discussion on convergence criteria is presented in section 3.7.

3.1 Governing Equations

The governing mass diffusion equation in its standard form is given as

$$\underbrace{\frac{\partial c}{\partial t}}_{Transient\ \ term} = \underbrace{\frac{\partial}{\partial x_i}\left(D\frac{\partial c}{\partial x_i}\right)}_{Diffusion\ \ term} + \underbrace{S}_{Source\ \ term} \tag{3.1.1}$$

where c, D and S are the concentration, the diffusion coefficient of etchant and the source term due to generation of chemical species by chemical reaction, respectively. The governing

equation was discussed in more detail in Chapter 2. They are solved by the Finite Volume Method, which is discussed in next section. In the etching problem the source term (S) is absent as reaction is heterogeneous in nature. Hence, Eq. (3.1.1) will reduce to

$$\frac{\partial c}{\partial t} = \frac{\partial}{\partial x_i}\left(D\frac{\partial c}{\partial x_i}\right) \tag{3.1.2}$$

As discussed before (in Chapter 2) with the proposed approach, the above governing equation is modified as

$$\frac{\partial c}{\partial t} = \frac{\partial}{\partial x_i}\left(D\frac{\partial c}{\partial x_i}\right) - \frac{\partial c_R}{\partial t} \tag{3.1.3}$$

where c is the unreacted etchant concentration and c_R is the reacted concentration of etchant.

3.2 The Finite Volume Method

In Finite Volume method, the domain is divided into a number of control volumes. The grid points are located at the center of control volume. This method is also called as control volume method since the conservation principles are applied to a fixed region in the control volume. The integral form of the conservation equation is integrated over each control volume to derive an algebraic equation with values of unknown variable (as for example c in the present problem). The discretization equation expresses the conservation principle for a finite control volume.

Typical two-dimensional Cartesian control volumes are shown in Fig. 3.1. The control volume interface is subdivided into four place faces for two-dimensional problem, which are denoted

by lower case letters- e, w, n, and s corresponding to their direction along east, west, north and south respectively with respect to the central node P. Similarly, the adjacent control volume nodes are denoted by capital letters E, W, N, and S corresponding to their direction with respect to the central node P.

3.3 Discretization of the Governing Equation

In this section the finite volume discretized governing equation is derived using the integral procedure and finite difference schemes. In the finite volume approach, the governing equation is integrated over the control volume and the derivative terms in the integral equation is approximated using conventional finite difference schemes. Finally, the original governing equation reduces to a linear algebraic equation. The detail procedure of getting a linear discretized form of governing equation is described next.

The Discretization Equation

The finite volume formulation procedure is described here taking the example of a two-dimensional etching problem. Using the similar procedure the finite volume formulation can be obtained for one-dimensional and three dimensional etching problems.

The total flux through a control volume interface is given as

$$J_i = D\frac{\partial c}{\partial x_i} \tag{3.3.1}$$

Treating last term in Eq. (3.1.3) as the source term in the proposed approach, Eq. (3.1.3) can be written as

$$\frac{\partial c}{\partial t} = \frac{\partial}{\partial x_i}\left(D\frac{\partial c}{\partial x_i}\right) + S \tag{3.3.2}$$

where S is the source term. It can be linearized as

$$S = S_C + S_P c \tag{3.3.3}$$

where S_C and S_P are constants. S_P is always set to a negative big number (of the order of -10^{20}) in the substrate domain (except the ECVs) to make the concentration of etchant to zero in the substrate domain (discussed later in this section) and S_C is given as

$$S_C = -\frac{\partial c_R}{\partial t} \tag{3.3.4}$$

The integration of Eq. (3.3.2) over a two-dimensional control volume ΔV ($\Delta V = \Delta x \times \Delta y$) as shown in Fig. 3.1 and over a time interval from t to $t + \Delta t$, gives

$$\int_t^{t+\Delta t}\int_{\Delta V}\frac{\partial c}{\partial t}\,dV dt = \int_t^{t+\Delta t}\int_{\Delta V}\frac{\partial}{\partial x_i}\left(D\frac{\partial c}{\partial x_i}\right)dV dt + \int_t^{t+\Delta t}\int_{\Delta V} S\,dV dt$$

Using fully implicit scheme and applying the divergence theorem to the second term, above equation can be simplified as

$$\left[c_P^{t+\Delta t} - c_P^t\right]\Delta V = \left[A_e\left(D\frac{\partial c}{\partial x}\right)_e^{t+\Delta t} + A_n\left(D\frac{\partial c}{\partial y}\right)_n^{t+\Delta t} - A_w\left(D\frac{\partial C}{\partial x}\right)_w^{t+\Delta t} - A_s\left(D\frac{\partial c}{\partial y}\right)_s^{t+\Delta t}\right]\Delta t + \bar{S}\,\Delta t\Delta V \tag{3.3.5}$$

where A_w, A_e, A_n, and A_s are the surface areas of control volume P at west, east, north and south interfaces respectively (as shown in Fig 3.1). The term $\bar{S}$ is the average source term over the control volume P given as

$$\bar{S} = \bar{S}_C + \bar{S}_P c \tag{3.3.6a}$$

where the value of $\bar{S}_P$ is as described before and $\bar{S}_C$ is given as

$$\bar{S}_C = -\frac{c_{\mathrm{R},P}^{t+\Delta t} - c_{\mathrm{R},P}^{t}}{\Delta t} \tag{3.3.6b}$$

For a two-dimensional control volume shown in Fig. 3.1, the surface areas are given as

$$A_e = A_w = \Delta y \tag{3.3.7a}$$

$$A_n = A_s = \Delta x \tag{3.3.7b}$$

Using the finite difference scheme in discretizing the spatial derivative terms in Eq. (3.3.5), results in

$$\begin{aligned}\left[c_P^{t+\Delta t} - c_P^{t}\right]\Delta V = &\left[A_e\left\{D_e \frac{c_E - c_P}{\Delta x_e}\right\}^{t+\Delta t} + A_n\left\{D_n \frac{c_N - c_P}{\Delta y_n}\right\}^{t+\Delta t}\right]\Delta t \\ &-\left[A_w\left\{D_w \frac{c_P - c_W}{\Delta x_w}\right\}^{t+\Delta t} + A_s\left\{D_s \frac{c_P - c_S}{\Delta y_s}\right\}^{t+\Delta t}\right]\Delta t + \bar{S}\,\Delta t \Delta V\end{aligned} \tag{3.3.8}$$

Dividing both sides by Δt in the above equation, gives

$$\left[c_P^{t+\Delta t} - c_P^t\right]\frac{\Delta V}{\Delta t} = \left[A_e\left\{D_e\frac{c_E - c_P}{\Delta x_e}\right\}^{t+\Delta t} + A_n\left\{D_n\frac{c_N - c_P}{\Delta y_n}\right\}^{t+\Delta t}\right] - \left[A_w\left\{D_w\frac{c_P - c_W}{\Delta x_w}\right\}^{t+\Delta t} + A_s\left\{D_s\frac{c_P - c_S}{\Delta y_s}\right\}^{t+\Delta t}\right] + \bar{S}\,\Delta V \tag{3.3.9}$$

If superscript o denotes time t, then Eq. (3.3.9) can be written as

$$\left[c_P - c_P^o\right]\frac{\Delta V}{\Delta t} = \left[A_e\left\{D_e\frac{c_E - c_P}{\Delta x_e}\right\} + A_n\left\{D_n\frac{c_N - c_P}{\Delta y_n}\right\}\right] - \left[A_w\left\{D_w\frac{c_P - c_W}{\Delta x_w}\right\} + A_s\left\{D_s\frac{c_P - c_S}{\Delta y_s}\right\}\right] + \bar{S}\,\Delta V$$

Above equation can be rearranged to a standard linear form as

$$a_P c_P = a_P^o c_P^o + a_W c_W + a_E c_E + a_N c_N + a_S c_S + b \tag{3.3.10a}$$

where the coefficients in the above linear equation are given as

$$a_P = a_P^o + a_W + a_E + a_N + a_S - \bar{S}_P \Delta V \tag{3.3.10b}$$

$$a_W = \frac{D_w}{\Delta x_w} \tag{3.3.10c}$$

$$a_E = \frac{D_e}{\Delta x_e} \tag{3.3.10d}$$

$$a_N = \frac{D_n}{\Delta y_n} \tag{3.3.10e}$$

$$a_S = \frac{D_s}{\Delta y_s} \tag{3.3.10f}$$

$$a_P^o = \frac{\Delta V}{\Delta t} \tag{3.3.10g}$$

$$b = \bar{S}_C \Delta V \tag{3.3.10h}$$

where c_P and c_P^o are the variables which are solved at present time step and previous time step. A negative big number is assigned to $\bar{S}_P$ (as discussed before in this sub-section) in the substrate region except the ECVs to make the unreacted concentration of etchant to zero which is evident from Eq. (3.3.10a). In the whole etchant domain and in the ECVs, S_P is set to zero. This operation is performed to capture the whole etchant and substrate region as the solution domain in the proposed approach.

In this simulation, linear interpolation scheme is assumed to find fluxes and diffusion coefficient at the interface of the control volume. The linear interpolation of concentration (c) at the interface e (as shown in Fig. 3.2) can be expressed as

$$c_e = f_e c_P + (1 - f_e) c_E \tag{3.3.11}$$

where $f_e = \frac{(\delta x)_{e+}}{(\delta x)_e}$

The assumption of linear profile between the node points P and E can also offer a simple approximation of the gradient, which is needed for the evaluation of diffusive fluxes,

$$\left(\frac{\partial c}{\partial x}\right)_e \approx \frac{c_E - c_P}{\delta x_e} \tag{3.3.12}$$

To obtain the interface diffusion coefficient, D_e, equating the flux at the interface, gives

$$J_e = \frac{D_e(c_E - c_P)}{\delta x_e} = \frac{D_P(c_e - c_P)}{(\delta x)_{e-}} = \frac{D_E(c_E - c_e)}{(\delta x)_{e+}} \tag{3.3.13}$$

From above Eq. (3.3.13), the effective diffusion coefficient at the east interface can be obtained as,

$$D_e = \frac{(\delta x)_e}{\frac{(\delta x)_{e-}}{D_P} + \frac{(\delta x)_{e+}}{D_E}} = \frac{1}{\frac{1-f_e}{D_P} + \frac{f_e}{D_e}} \tag{3.3.14}$$

Similarly effective diffusion coefficient at the west, north, and south interfaces can also be found following the above procedure.

3.4 Under-relaxation for Nonlinear Problems

The coefficients of the discretized equations may depend on the variables. For example, the diffusion coefficient may depend on the concentration in diffusion equation. In that case, the discretized equations are nonlinear equations. The nonlinear equations can be solved using iterative method. First, the coefficients in the discretized equations are calculated by substituting the guessing or estimating variable values. Then, new variable values are calculated by solving the linearized algebraic equations. The coefficients are recalculated using the new values to solve the discretized equations again. This process is repeated until the convergent results are obtained.

However, the divergence might happen during iteration process, in which the iterated result is away from the real solution. In order to avoid divergence during iterative process, implementing under-relaxation method can slow down the variable changes from iteration to iteration. The under-relaxation method is presented below.

On the N'th iteration, the algebraic equation for general variable ϕ_P can be written as

$$a_P \phi_P^{N'} = \sum a_{nb} \phi_{nb}^{N'} + b \tag{3.4.1}$$

$$\phi_P^{N'} = \frac{\sum a_{nb} \phi_{nb}^{N'} + b}{a_P} \tag{3.4.2}$$

An under-relaxation method can be written as

$$\phi_P^{N'} = \phi_P^{N'-1} + \theta(\phi_P^{N'} - \phi_P^{N'-1}) \tag{3.4.3}$$

where $0 < \theta \leq 1$. Substituting Eq (3.4.2) into Eq. (3.4.3) gives

$$\frac{a_P}{\theta} \phi_P^{N'} = \sum a_{nb} \phi_{nb}^{N'} + b + (1-\theta)\frac{a_P}{\theta} \phi_P^{N'-1} \tag{3.4.4}$$

Optimum under-relaxation factor θ is problem dependent. For the etching problem considered here, the under-relaxation factor is taken as 0.8.

3.5 Solution of Linear Equations

In previous sections, the diffusion equations are discretized using finite volume method. The discretization process leads to a system of algebraic equations, which can be linear or non-linear according to the nature of the partial differential equations. In the non-linear case, the discretized equations must be solved by an iterative technique that involves guessing a solution, linearizing the equations about the solution, and improving the solution. The iteration process is repeated until a converged result is achieved. Efficient methods are required for solving linear systems of the algebraic equations. The most widely used solution method to solve the system of linear algebraic equations is discussed next.

3.5.1 TDMA (TriDiagonal Matrix Algorithm) Method

The TriDiagonal Matrix Algorithm (TDMA) also known as Thomas algorithm is used to solve the system of linear algebraic equations. The solution procedure using TDMA to solve one-dimensional, two-dimensional and three-dimensional problems are briefly described below.

Application of TDMA to One-Dimensional Problems

For one-dimensional problems, the discretized algebraic equations have a simple structure. A typical one-dimensional node point distribution is shown in Fig. 3.3. The linear algebraic equation is applied to each node points and a system of algebraic equations will result comprises of all nodal points. The coefficient matrix is a tridiagonal matrix, in which the non-zero terms exist only on its main diagonal and the diagonals immediately above and below it. The algebraic equation for a one-dimensional problem can be written as

$$a_i\phi_i = b_i\phi_{i+1} + c_i\phi_{i-1} + d_i \qquad i = 2,3,\ldots N-1 \tag{3.5.1}$$

ϕ_1 and ϕ_N are the boundary conditions (as shown in Fig. 3.3). The forward elimination and backward substitution can be used to solve this algebraic equation.

In the forward elimination ϕ_{i-1} is substituted by ϕ_i

$$\phi_{i-1} = P_{i-1}\phi_i + Q_{i-1} \tag{3.5.2}$$

Substituting Eq. (3.5.2) into Eq. (3.5.1) gives

$$\phi_i = \frac{b_i}{a_i - c_i P_{i-1}}\phi_{i+1} + \frac{c_i Q_{i-1} + d_i}{a_i - c_i P_{i-1}} \tag{3.5.3}$$

The backward substitution equation is

$$\phi_i = P_i\phi_{i+1} + Q_i \tag{3.5.4}$$

where,

$$P_i = \frac{b_i}{a_i - c_i P_{i-1}}, \quad Q_i = \frac{c_i Q_{i-1} + d_i}{a_i - c_i P_{i-1}} \tag{3.5.5}$$

$$P_1 = \frac{b_1}{a_1} = 0, \quad Q_1 = \frac{d_1}{a_1} = \phi_1 \tag{3.5.6}$$

There are two kinds of iterations, which are called inner iteration and outer iteration respectively. The inner iteration refers to the solution of the linear algebraic equations. In every inner iterative step, the coefficients are constant. The outer iteration refers to the solution

of the nonlinear problem. The coefficients and source terms must be updated after every outer iterative step.

Application of TDMA to Two-Dimensional Problems

The TDMA is applied iteratively to solve a system of linear algebraic equations for two-dimensional problems. Consider the two-dimensional grid system shown in Fig. 3.4. The standard two-dimensional discretized transport equation is given as

$$a_P\phi_P = a_W\phi_W + a_E\phi_E + a_N\phi_N + a_S\phi_S + b \tag{3.5.7}$$

To solve the system, TDMA is applied along chosen, for example north-south (*N*-*S*) lines as shown in Fig. 3.4. Equation (3.5.7) is re-arranged in the form

$$-a_S\phi_S + a_P\phi_P - a_N\phi_N = a_W\phi_W + a_E\phi_E + b \tag{3.5.8}$$

The right hand side of Eq. (3.5.8) is assumed to be temporarily known. Equation (3.5.8) is in the form of Eq. (3.5.1) where $a_P \equiv a_i$, $a_N \equiv b_i$, $a_S \equiv c_i$, $a_W\phi_W + a_E\phi_E + b \equiv d_i$. The system of equations can be solved along the *N*-*S* direction of the chosen line for values j = 2, 3, 4, …, *N*-1 as shown in Fig. 3.4. Subsequently the calculation is moved to the next *N*-*S* line. The sequence in which lines are chosen is known as the sweep direction. If sweep from west (*W*) to east (*E*) the values of ϕ_W to the west of point *P* are known from the calculations on the previous line. Values of ϕ_E to its east, however, are unknown so the solution process must be iterative. At each iteration cycle ϕ_E is taken to have its value at the end of the previous iteration or a given initial value at the first iteration. The line-by-line calculation procedure is repeated several times until a converged solution is obtained.

Application of TDMA to Three-Dimensional Problems

For three-dimensional problems the TDMA method is applied line-by-line on a selected plane and then the calculation is moved to the next plane, scanning the domain plane by plane. For example, to solve along an *N-S* line in the *x-y* plane as shown in Fig. 3.5, a discretized transport equation is written as

$$-a_S\phi_S + a_P\phi_P - a_N\phi_N = a_W\phi_W + a_E\phi_E + a_B\phi_B + a_T\phi_T + b \tag{3.5.9}$$

The values at W and E as well as those at B and T on the right hand side of Eq. (3.5.9) are considered to be temporarily known. Using the TDMA procedure values of ϕ along a selected *N-S* line (as shown in Fig. 3.5) are computed. The calculation is moved to the next line and subsequently swept through the whole plane until all unknown values on each line have been calculated. After completion of one plane the process is moved onto the next plane.

3.6 Boundary Conditions

The algebraic equation relates the variable value at the center of that control volume to the values at several neighbor control volumes. If the boundary variable values are given, the number of equations and unknowns are equal to the number of control volumes. So, the algebraic equations can be solved.

The boundary values can be given as follows:

1. Boundary values are given;
2. Boundary fluxes are given;

3. Boundary fluxes were expressed as a combination of interior values and boundary data.

If the boundary values are given, the equations can be solved directly. For the given boundary fluxes, the boundary conditions can be inserted into the discretized equations by suppression of the link to boundary side and modification of the source terms. The appropriate coefficient of the discretized equation is set to zero and the boundary side flux is introduced through source term S_C and S_P. This method is discussed next.

For example, if the flux is given, see Fig. 3.6a, the source term is

$$S_{extra} = \frac{J_B(\text{area})}{(\text{volume})}; S_{C,\text{extra}} = S_{\text{extra}} \text{ and } S_{P,\text{extra}} = 0 \tag{3.6.1}$$

If the diffusion coefficient D is given, the extra source term can be calculated (as shown in Fig. 3.6b) as

$$q_B = \frac{\phi_B - \phi_P}{\delta/D} \tag{3.6.2}$$

$$S_{\text{extra}} = \frac{q_B(\text{area})}{\text{volume}} = \frac{\phi_B - \phi_P}{\delta/D}\frac{(\text{area})}{(\text{volume})} \tag{3.6.3}$$

$$S_{C,\text{extra}} = \frac{\phi_B}{\delta/D}\frac{(\text{area})}{(\text{volume})}, \; S_{P,\text{extra}} = \frac{-1}{\delta/D}\frac{(\text{area})}{(\text{volume})} \tag{3.6.4}$$

Hence, the overall source term is given as

$$S_{\text{total}} = S_{C,\text{total}} + S_{P,\text{total}}\, c = S + S_{\text{extra}}$$

where

$$S_{C,\text{total}} = S_C + S_{C,\text{extra}} \text{ and } S_{P,\text{total}} = S_P + S_{P,\text{extra}}$$

The above modification in the source term is necessary when flux is known at one end of etchant domain away from interface.

3.7 Convergence Criteria

The solution is deemed converged with the difference in the values of a given variable between two successive iterations is less than a prescribed tolerance. For the etching problem considered here, the variables which are calculated at each iteration are the unreacted etchant concentration (c) and the reacted etchant concentration (c_R). The tolerance value is set to 10^{-11} for both c and c_R.

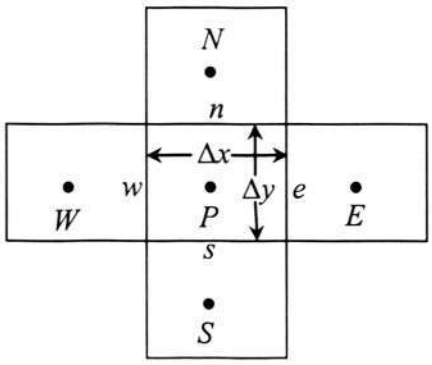

Figure 3.1 A typical two-dimensional control volume with specified notations.

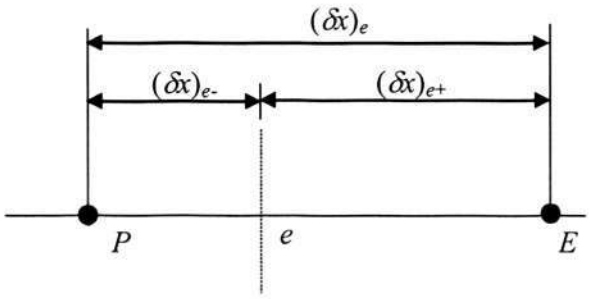

Figure 3.2 Distances related with the interface *e*.

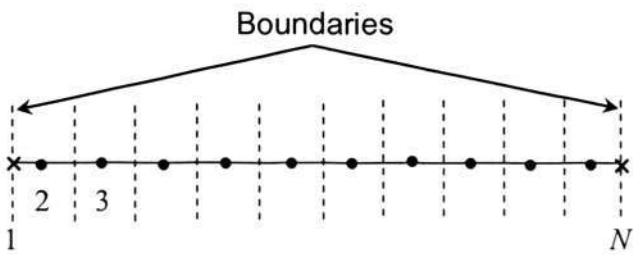

Figure 3.3 The control volume node points in one-dimensional problem. (Note: • points where the variable values are calculated; × known boundary values)

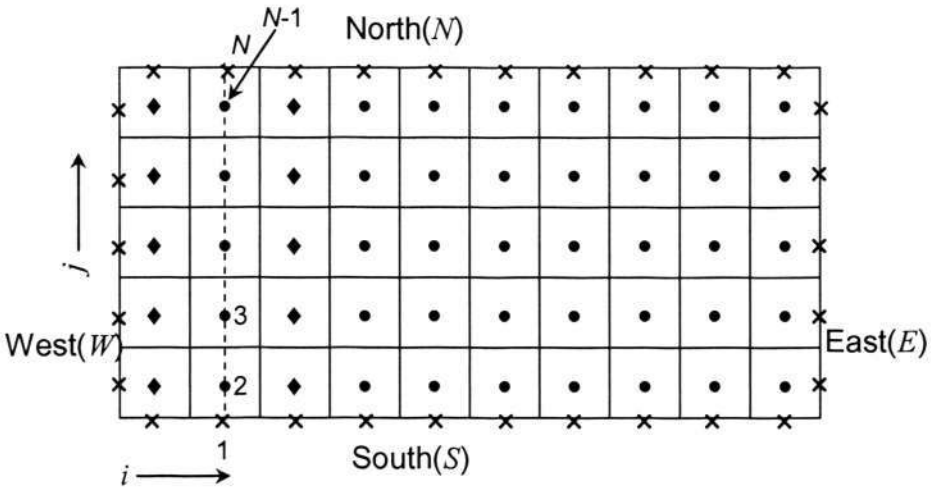

Figure 3.4 Line-by-line application of the TDMA in two-dimensional geometry. (Note: • the points at which values are calculated; ♦ the points at which the values are considered to be temporarily known; × known boundary values)

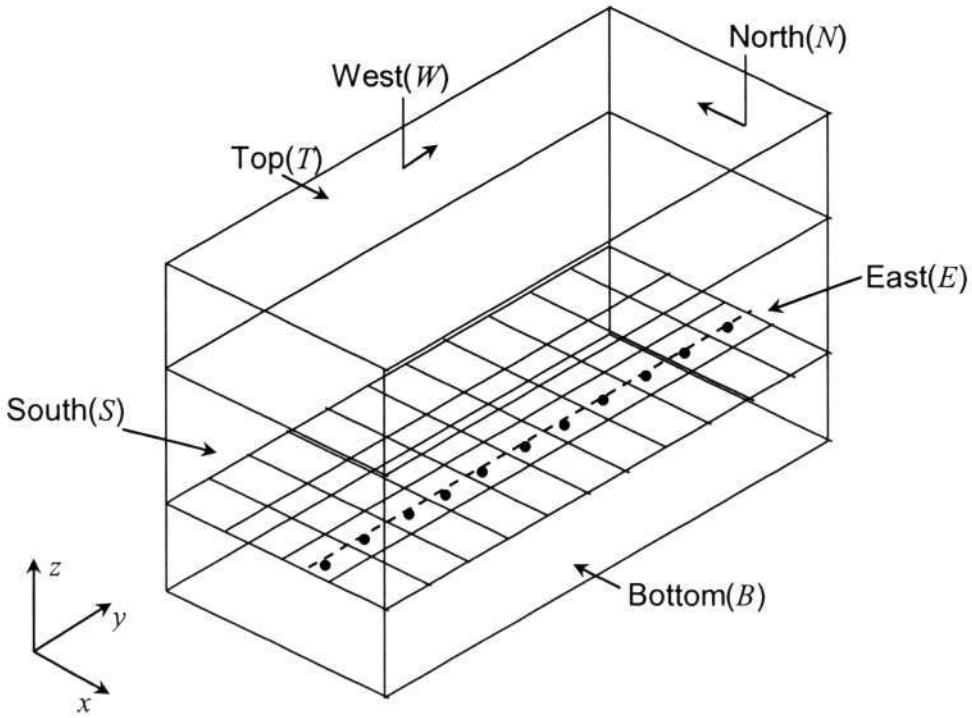

Figure 3.5 Application of TDMA in a three-dimensional geometry. (Note: • the points at which the variable values are calculated in a given *xy*-plane)

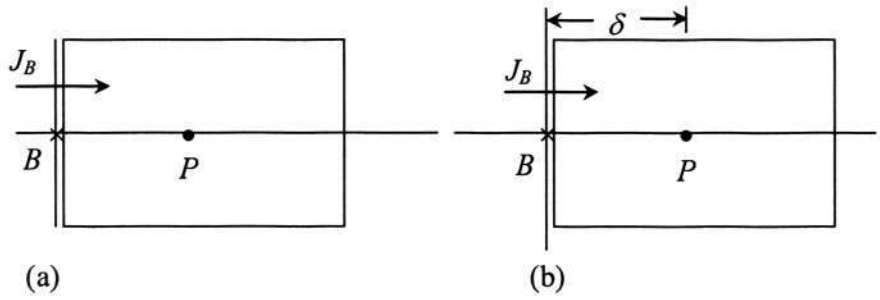

Figure 3.6 Boundary conditions.

CHAPTER 4

RESULTS AND DISCUSSIONS

The simulated results of wet chemical etching (WCE) model obtained using the proposed total concentration fixed-grid (FG) method are discussed in this chapter. The results are discussed for three etching models, namely,- the one-dimensional, the two-dimensional and the three-dimensional WCE models respectively. The physical significance of the dimensionless etching parameter β, which plays an important role in characterizing the wet chemical etching process is discussed in section 4.1. The simulated results of the three WCE models are discussed in sections 4.2, 4.3 and 4.4 respectively. The validation of the proposed model with available experimental results is presented in section 4.5. The simulated results mainly include the etchfront evolution with time as etching progresses and the etchant concentration distribution. The results are discussed for two limiting conditions: the diffusion-controlled etching and the reaction-controlled etching.

4.1 Physical Significance of β

The dimensionless etching parameter, β is an important parameter characterizing the WCE process. The etch profile shape evolution and the speed of the etchfront are directly related to β. Hence, the etch rate which is basically the speed of the etchfront also depends on the value of β. β is also a measure of the initial etchant concentration before etching starts. It is expressed as

$$\beta = \frac{m\rho_{Sub}}{c_o M_{Sub}} \tag{4.1.1}$$

where m is the stoichiometric reaction parameter, ρ_{Sub} is the density of substrate, M_{Sub} is the molecular weight of substrate, c_o is the initial etchant concentration. For a given substrate to be etched, β is inversely proportional to the initial etchant concentration. The relation between the speed of the etchfront and β is obtained by non-dimensionalizing the interface condition governing the movement of the interface. As discussed in chapter 2, the interface condition at the etchant-substrate interface is given as

$$\frac{d\hat{n}}{dt} = -\frac{DM_{Sub}}{m\rho_{Sub}}\frac{\partial c}{\partial \hat{n}} \tag{4.1.2}$$

where D is the diffusion coefficient of etchant and $\hat{n}$ is the unit normal vector at the etchant-substrate interface pointing towards the substrate region. Equation (4.1.2) is non-dimensionalized using following variables,

$$\hat{N} = \frac{\hat{n}}{L},\ C = \frac{c}{c_o},\ t^* = \frac{tD}{L^2} \tag{4.1.3}$$

where L is any reference length and c_o is the reference initial etchant concentration. Using the above dimensionless variables, Eq. (4.1.2) will reduce to

$$\frac{d\hat{N}}{dt^*} = -\frac{c_o M_{Sub}}{m\rho_{Sub}}\frac{\partial C}{\partial \hat{N}} \tag{4.1.4}$$

Combining Eqs. (4.1.1) and (4.1.4), results in

$$\frac{d\hat{N}}{dt^*} = -\frac{1}{\beta}\frac{\partial C}{\partial \hat{N}} \tag{4.1.5}$$

From Eq. (4.1.5) it is seen that the normal speed of the etchant-substrate interface is inversely proportional to the etching parameter β. As expected, high initial etchant

concentration should lead to faster etching which can be explained using Eq. (4.1.5). From Eq. (4.1.1), it can be said that, the high initial etchant concentration will result in low value of the etching parameter β for a given substrate to be etched. As a result, the speed of the etchfront increases as it is inversely proportional to β. Hence, the etching will be faster.

4.2 One-Dimensional Etching

The simulated results of the one-dimensional WCE model as discussed in section 2.7 of chapter 2 are presented in this section. The simulated results are obtained using the proposed total concentration based fixed-grid (FG) method. The details of the proposed approach are discussed in chapter 2. The variation of etch depth with time and the etchant concentration distribution as etching progresses is investigated based on the dimensionless etching parameterβ. The initial etchant and substrate thicknesses are set to 0.03 cm and 51 μm respectively. The substrate to be etched is silicon dioxide (SiO_2). The etchant solution used for etching is hydrofluoric acid (HF). The diffusion coefficient of etchant is 10^{-5} cm^2/sec. The density and molecular weight of the substrate are 2.1 g/cm^3 and 60 respectively. The reaction between the etchant HF and the substrate SiO_2 is given as

$$SiO_2 + 6HF \rightarrow H_2SiF_6 + 2H_2O \qquad (4.2.1)$$

From the above reaction system, the stoichiometric reaction parameter (m) is found to be 6, as 6 moles of HF required to dissolve 1 mole of SiO_2.

4.2.1 Grid-Independence Test

A grid refinement study was performed to ensure the solutions are grid (temporal and spatial) independent. Four grid sizes namely,- 12 μm, 6 μm, 3 μm and 1.5 μm respectively are taken to study the effect of control volumes sizes on temporal variation of etch depth. From time independent numerical experiments, the time step size is found to be Δt = 0.001 sec. Further reduction in time step size does not alter the solution. The etching is assumed diffusion-controlled where interface reaction is infinitely fast. Figure 4.1 shows the variation of etch depth and etchant concentration distribution for dimensionless etching parameter, $\beta = 2$. Figure 4.1a shows the variation of etch depth with time for 4 second of etching with four grid sizes as mentioned above. The etch depth variation from each control volume size is compared with the exact solution (discussed in chapter 2). It is seen that all the four grid sizes capture the etchfront accurately. Figure 4.1b shows the etchant concentration distribution in the etchant domain and the etched region at 4 second with four control volume sizes. It is seen that the etchant concentration distribution also in good agreement with the exact solution for all four grid sizes.

4.2.2 Comparison

Results from the proposed total concentration approach are compared with the existing approaches for diffusion-controlled and reaction-controlled etching conditions. For diffusion-controlled etching, the results from the proposed approach are compared with the exact solution described in Chapter 2. For ready reference, the exact solution for etch depth variation is given as

$$\delta(t) = 2\gamma\sqrt{Dt} \tag{4.2.2}$$

where γ is a constant depends on β. The exact solution for concentration distribution in the etchant domain and the etched region is given as

$$\frac{c}{c_o} = \frac{erf\left(\frac{x}{2\sqrt{Dt}}\right) + erf(\gamma)}{1 + erf(\gamma)} \tag{4.2.3}$$

where *erf* is the error function. Figure 4.2 shows the comparison of etch depth variation and concentration distribution obtained from total concentration fixed-grid (FG) approach with the exact solution. The comparison are shown for four β values- 1, 2, 4, and 50, which stands for four different initial etchant concentrations before etching starts. The variation of etch depth with time for 1 second of etching is shown in Fig. 4.2a and the dimensionless concentration distribution in the etchant domain including the etched region is shown in Fig. 4.2b. Both the etch depth variation and concentration distribution are found to be in good agreement with the exact solution for all four β values. A quantitative comparison of etch depth with the exact solution is presented in Table 4.1a-b for two β values- 2 and 50. It is seen that the percentage error is less than 1% in both the cases. As found from the exact solution, the etch depth varies as the square root of time (Eq. 4.2.2). As expected, the etch depth is higher when β value is low. The low value of β implies high initial etchant concentration for a given substrate to be etched and hence faster etching as more etchant particles are available for etching, which leads to higher etch depth in a given time. It is seen from Fig. 4.2b that far away from the etched interface, the etchant concentration remain unaltered at the initial etchant concentration. Hence, the etchant domain are said to be semi-infinite. If the length of the etchant domain is much higher than the diffusion length (of the order of $\sqrt{Dt}$), then it can said to be semi-infinite domain. In the present case, the length of the etchant domain is 0.03 *cm*

while the diffusion length for 1 second of etching is $3.1623 \times 10^{-3}\ cm$ which is almost 10 times less than the actual length.

The results for reaction-controlled etching conditions obtained from proposed FG approach are compared with the existing moving grid (MG) approach (discussed in chapter 2) and an approximate analytical Deal-Grove (DG) model given by Monk et al., 1991 and Liu et al., 1993. The DG model assumes a first order reaction at the interface and the etchant consumed in the reaction process does not affect the bulk concentration. The bulk concentration is the etchant concentration in the etchant domain except the interface. That is the DG model assumes a very slow rate of reaction at the interface. According to DG model, the etchant concentration is assumed to be linear in the etched region. Hence,

$$J_d = -D\frac{\partial c}{\partial x} = D\frac{(c_b - c_s)}{\delta} \tag{4.2.4}$$

where c_b is the bulk etchant concentration, c_s is the etchant concentration at the interface and δ is the etch depth i.e. the interface displacement due to the dissolution of substrate by chemical reaction with the etchant. The interface concentration is obtained by equating the rate of diffusion (J_d) with rate of reaction. Hence, for a first order reaction this balance is given as

$$D\frac{(c_b - c_s)}{\delta} = kc_s \tag{4.2.5}$$

where k is rate constant of reaction at the interface. Again, the interface condition governing the movement of the interface is given as

$$D\frac{(c_b - c_s)}{\delta} = \frac{m\rho_{Sub}}{M_{Sub}}\frac{d\delta}{dt} \tag{4.2.6}$$

Solving Eq. (4.2.5) and Eq. (4.2.6) for δ results in

$$\delta = -\frac{D}{k} + \sqrt{\left(\frac{D}{k}\right)^2 + \frac{2c_b M_{Sub} D}{m\rho_{Sub}}t} \tag{4.2.7}$$

Above equation represents the variation of etch depth with time using the DG model. From Eq. (4.2.7), it can be said that for small etching time, the etch depth varies linearly with time. Figure 4.3 shows the variation of etch depth and concentration distribution for four β values under reaction-controlled etching condition. The rate constant of reaction at the interface is taken as $k = 10^{-5}$ cm/sec. Figure 4.3a shows the variation of etch depth with time obtained using the proposed FG approach for 4 second of etching. The etch depth variations for each β values are compared with the existing MG method and an analytical DG model. It is seen that the etch depth prediction from proposed FG approach is in good agreement with the MG method. However, the DG model over predicts the etch depth especially when the β value is small. It is because the DG model assumes negligible change in the bulk etchant concentration due to the consumption of etchant by reaction at the interface. But in reality as etching progresses, after certain time the bulk concentration will decrease due to consumption of etchant at the interface. This decrease in bulk concentration is accounted for in the FG and MG method as shown in Fig. 4.3b.

4.2.3 Effect of the Rate of Reaction

The effect of the rate of reaction on the etching process is studied by varying the rate constant of reaction between the etchant and the substrate at the interface. Figure 4.4

shows the etch depth variation and concentration distribution for five different rate constant values. The non-dimensional etching parameter is taken as $\beta = 1$. Figure 4.4a shows the etch depth variation with time for 1 second of etching. It is seen that when the rate of reaction is slow i.e. when the rate constant (k) value is small, the etch depth varies linearly with time. Beyond $k \geq 10^{-2}$ cm/sec, the etch depth variation is non-linear as found in diffusion-controlled etching. When k increases, the etch depth increases at a given time. The increase in k means the reaction rate increases at the interface. Hence the dissolution of substrate is increased which leads to larger etch depth at a given time. Under a limiting case when the reaction rate is infinitely fast i.e. $k >> D$, the etching process is said to be diffusion-controlled. From Fig. 4.4 it is seen that when $k \geq 10^{-1}$ cm/sec, the etching can be considered diffusion-controlled as further increase in k does not alter the etch depth and concentration distributions. For a given diffusion coefficient of etchant, the highest etch depth in a given time is obtained when the etching is diffusion-controlled. The etch depth variation is compared with the existing MG method for all five range of k values. It is seen that the proposed FG approach predicting the etch depth accurately for all five range of k values ranging from slow to fast reaction.

From Fig. 4.4b, it is seen that the etchant concentration at the etchant-substrate interface remains almost at the initial concentration when $k = 10^{-5}$ cm/sec. At this value of k, the reaction is very slow and any etchant consumed in the etching process is replenished via diffusion. The etchant concentration at the interface decreases as the value of k increases. The etchant concentration at the interface is almost zero when $k \geq 10^{-1}$ cm/sec. The concentration distributions obtained with the proposed FG approach are compared with the MG method. The concentration distribution is found to be in good agreement with the existing MG method.

4.3 Two-Dimensional Etching

In this section results for two-dimensional wet chemical etching model are discussed. The simulated results are obtained using the proposed total concentration FG approach. Two limiting conditions namely,- the diffusion-controlled and the reaction-controlled etching are investigated. The effect of the initial etchant concentration and mask thickness on the shape evolution of etchfront and the concentration distribution in the etchant domain is investigated. The initial etchant concentration is varied by varying the dimensionless etching parameter β. The computational domain is as shown in Fig. 2.10 of chapter 2. The results are presented in dimensionless form using the dimensionless variables defined below.

$$X \equiv x/a,\ L_1 \equiv l_1/a \tag{4.3.1a}$$

$$Y \equiv y/a,\ L_2 \equiv l_2/a,\ L_3 \equiv l_3/a,\ H \equiv h/a \tag{4.3.1b}$$

$$C \equiv c/c_o \tag{4.3.1c}$$

$$C_R \equiv c_R/c_o \tag{4.3.1d}$$

$$t^* \equiv tD/a^2 \tag{4.3.1e}$$

$$\hat{N} \equiv \frac{\hat{n}}{a} \tag{4.3.1f}$$

$$Sh \equiv \frac{Ka}{D} \tag{4.3.1g}$$

Sh in Eq. (4.3.1g) represents the dimensionless rate constant of reaction called as Sherwood number. Using the above dimensionless quantities, the non-dimensional form of the governing equation with initial and boundary conditions are given as follows.

Governing Equation

$$\frac{\partial C}{\partial t^*} = \frac{\partial^2 C}{\partial X^2} + \frac{\partial^2 C}{\partial Y^2} - \frac{\partial C_R}{\partial t^*} \qquad \text{in } \Omega(t^*), \Omega_s(t^*), \text{ and } \Omega_m \qquad (4.3.2)$$

Initial Conditions

$$C = 1 \ , \ C_R = C_{R,max} \qquad \text{in } \Omega(0) \qquad (4.3.3a)$$

$$C = 0 \ , \ C_R = 0 \qquad \text{in } \Omega_s(0), \text{ and } \Omega_m \qquad (4.3.3b)$$

Boundary Conditions

$$\frac{\partial C}{\partial X} = 0 \qquad X = 0 \qquad (4.3.4a)$$

$$C = 1 \qquad Y = H + L_3 \qquad (4.3.4b)$$

$$C = 1 \qquad X = 1 + L_1, \ H \le Y \le H + L_3 \qquad (4.3.4c)$$

$$C_R = 0 \qquad \text{in } \Omega_m \text{ and } \Omega_s(t^*) \qquad (4.3.4d)$$

$$-\frac{\partial C}{\partial \hat{N}} = Sh\, C \qquad \text{on } f(t^*) \qquad (4.3.4e)$$

The dimensionless width of the mask is taken as $L_1 = 6.5$ and the dimensionless height of etchant is taken as $L_3 = 6.5$. The width and thickness of the substrate are taken as $L_{Sub} = 1 + L_1 = 7.5$ and $L_2 = 4.0$ respectively. Results for two mask thicknesses namely,- infinitely thin and finite thicknesses are discussed. For infinitely thin mask, the non-dimensional mask thickness is taken as $H = 0.005$. Further decrease in mask thickness does not alter the solution. For finite mask thickness, the thickness of the mask is taken as one-fourth of the gap width i.e. $H = 0.5$.

4.3.1 Diffusion-Controlled Etching

Results obtained using the present FG approach under diffusion-controlled etching condition, are discussed in this sub-section. As discussed before in chapter 2, the reaction at the etchant-substrate interface is infinitely fast in diffusion-controlled etching. As a result, the concentration at the interface is closes to zero. The present approach assumes zero unreacted etchant concentration at the interface. Hence, Eq. (4.3.4e) reduces to

$$C = 0 \qquad \text{on } f(t^*) \qquad (4.3.5)$$

4.3.1.1 Grid-Independence Test

A grid refinement study was performed to ensure the solution to be grid independent- both temporal as well as spatial. Figure 4.5 shows the evolution of etch profiles at four different times for $\beta = 100$ and infinitely thin mask. Three grid sizes- 32 × 29, 72 × 53 and 144 × 104 respectively are chosen to study the effect of control volume size on etchfront evolution. The evolution of etch profiles with above three grid sizes are shown in Fig. 4.5a. For each grid size the time independent etch profiles are shown. For the grid sizes of 32 × 29 and 72 × 53, the time step size is found to be $\Delta t^* = 0.01$. For the grid size 144 × 104, the time step size is found to be $\Delta t^* = 0.001$. For completeness, a time independent test is shown in Fig. 4.5b for the grid size 72 × 53. It is seen that the time step sizes $\Delta t^* = 0.01$ and 0.001 produces the same etchfront at a given time. Hence, $\Delta t^* = 0.01$ is chosen for the grid size 72 × 53. A similar experiment is performed for other two grid sizes to get the time step size at which the etchfront at a given time is independent of the time step size. It is seen from Fig. 4.5a that the grid sizes 72 × 53 and 144 × 104 produced the same etch profile for the four given times. As a result, 72 × 53 control

volumes with $\Delta t^* = 0.01$ are used for further presentation of results under diffusion-limited condition.

4.3.1.2 Comparison

The etchfronts predicted by proposed FG method is compared with the analytical asymptotic solution (Kuiken, 1984b) and the MG method (Shin and Economou, 1989). The comparison of etch profiles at four different times are shown in Fig. 4.6a for etching parameter $\beta = 100$ and infinitely thin mask. For dimensionless time, $t^* = 5$, the comparison is shown between the present FG method and the asymptotic solution. It is seen that the present approach predicting the etch profiles accurately. Some bulging effect is seen near the corner of the mask. The etching is faster near the mask corner region compared to the region away from the corner. Figure 4.6b shows the concentration contours at $t^* = 30$. It is seen that the concentration contours have gone deep into the etched region near the corner of the mask. Hence, the concentration gradient is higher near the mask region. As a result the etching is faster in this region which results in bulging of etch profiles.

Figure 4.7a shows the comparison of etch profiles at five different times for $\beta = 10$ and infinitely thin mask. The etch profiles obtained using present approach are compared with the variational inequality approach of Bruch et al., 1993. It is seen that the etch profiles from present approach comparing well with the variational inequality approach. Figure 4.7b shows the concentration contours at $t^* = 20$ for $\beta = 10$ and infinitely thin mask. It is seen that the concentration contours have gone deep at the center of the gap which results in enlarged bulging region from mask corner to the center compared to the case with $\beta =$ 100 as discussed before. This is because of the high initial etchant concentration for $\beta =$

10, which results in faster etch rate. The bulging effect is localized near the mask corner only at early time when the β value is small.

Figure 4.8a shows the comparison of the etch profiles evolution at different times for finite mask thickness. The dimensionless etching parameter is taken as $\beta = 100$. The etch profiles obtained using present approach compare well with the MG solutions (Shin and Economou, 1989). Figure 4.8b shows the concentration contours at $t^* = 126$. It is seen that the concentration contours in the etched region are nearly uniform. As a result, the concentration gradients are also uniform. Hence there is no significant bulging of etch profiles is seen unlike the case with infinitely thin mask.

4.3.1.3 Effect of Mask Thickness

Effect of mask thickness on the etchfront evolution is investigated. Figure 4.9 shows the etch profiles at two different time levels obtained with both mask thicknesses- infinitely thin and finite thickness. The dimensionless etching parameter is taken as $\beta = 100$. It is seen that the bulging effect and the underetching (etching below the mask) reduces with increase in mask thickness. It is because of the larger diffusion length of the etchant from the area above the inert mask to the etching surface. Hence fresh etchant is less readily available near the mask corner as thickness of the mask increases which results in slow etch rate near the mask corner.

4.3.1.4 Effect of Initial Etchant Concentration

The effect of initial etchant concentration on the shape evolution of etchfront is investigated based on the dimensionless etching parameter, β. As discussed before, for a given substrate to be etched, the initial etchant concentration depends inversely on the

etching parameter β (Eq. 4.3.1f). Figure 4.10 shows the evolution of etchfronts for four different β values at time $t^* = 20$. The mask is taken as infinitely thin. As expected, the etch profiles goes deep with decrease in the β value. This is because of the increase in the initial etchant concentration with decrease in β. It is seen from Fig. 4.10 that the etchfront position varies approximately, as β^1 at the center of the gap while it's position varies as $\beta^{2/3}$ near the mask corner. The etchfront speed depends on the β value. For high value of β, the front moves slowly. However, since the diffusion rate of etchant is higher near the mask corner, the dissolution rate of substrate will also be higher. Hence bulging is pronounced. At low value of β, there is no significant difference between the diffusion rates of etchant near the mask corner and away from the mask corner due to fast movement of the interface. As a result, the bulging effect is not significant.

4.3.2 Reaction-Controlled Etching

Results obtained for reaction-controlled etching using the present FG approach is discussed in this section. As discussed before, in reaction-controlled etching, the reaction proceeds very slowly at the interface i.e. the ratio $K/D \ll 1$. Therefore, the dimensionless parameter, Sh is very small. As a result, there is finite etchant concentration at the interface when etching is reaction limited.

As discussed in chapter 2, the conventional iterative update procedure of c_R can not be applicable in this case. The conventional c_R update procedure is applicable when the etchant concentration along the interface does not vary i.e. the interface is an iso-concentration interface. But in the present case because of the presence of inert mask, the etchant concentration varies along the interface due to the non-uniform diffusion rate of

etchant to the interface. Hence a new update procedure is developed which is discussed in detail in Chapter 2. The etch profiles obtained using two update procedures are compared when the etching is diffusion-limited. Figure 4.11 shows the comparison of two update procedures in predicting the etchfronts in one-dimensional and two-dimensional etching. Figure 4.11a shows the comparison of two c_R update procedures in predicting the etchfront in one-dimensional etching under diffusion and reaction-controlled etching condition. The one-dimensional etching system is taken same as discussed before in section 4.2. Two values of rate constant (k) are taken to test the applicability of new c_R update procedure in two limiting conditions i.e. the diffusion- and the reaction-controlled etching. $k = 0.1$ *cm/sec* represents the diffusion-controlled etching and $k = 10^{-3}$ *cm/sec* represents the reaction-controlled etching. These limits of k values for this one-dimensional etching system are discussed before in section 4.2. It is seen that the new c_R update procedure is predicting the same etchfront as predicted by the conventional c_R update procedure. Hence the new c_R update procedure can equally be applicable for diffusion- as well as reaction-controlled one-dimensional etching. Figure 4.11b shows the comparison of two c_R update procedures in predicting the evolution of etchfront under diffusion-limited condition. The dimensionless etching parameter is taken as $\beta = 10$. For diffusion-limited condition, since the reaction rate is very fast at the interface, the dimensionless rate constant is taken as $Sh = 1000$. From numerical experiment it is seen that further increase in Sh does not alter the solution. When $Sh = 1000$, it is seen that the etchant concentration, $c \approx 0$ at the interfacen as shown in Fig. 4.11c. It is seen that the new c_R update procedure produces the same etchfront as obtained with the conventional c_R update procedure. Hence, the new update procedure of c_R can equally be applicable to diffusion- as well as reaction-controlled etching. However, the conventional c_R update procedure is easy to implement as it does not require evaluating the normal concentration

gradient while updating c_R. Evaluating the normal concentration gradient is not so straight forward in multidimensional etching and therefore increases the complexity of the problem. Hence, the conventional c_R update procedure remains a desirable update procedure in diffusion limited etching condition due to its easiness of implementation.

4.3.2.1 Grid-Independence Test

A numerical experiment is conducted to test the effect of control volume size on the final solution for reaction limited etching condition. Figure 4.12 shows the evolution of etch profiles at four different times for dimensionless etching parameter, β = 100 and Sherwood number, Sh = 1. The mask is taken as infinitely thin (H = 0.005). Three dimensionless grid sizes namely,- 0.04, 0.02 and 0.01 are chosen for this study. From time independent test, the time step size for all the three grid sizes is found to be Δt^* = 0.01. It is found that by decreasing the control volume size beyond 0.02 does not alter the etchfront. Hence, 0.02 × 0.02 control volume size is used for further presentation of results.

4.3.2.2 Comparison and Etchfront Shape Evolution

Figure 4.13 shows the etch profiles obtained using the present FG approach under reaction-controlled etching condition and compared with the finite element based MG method proposed by Sudirham et al., 2004. The dimensionless etching parameter is β = 100 and Sherwood number is Sh = 1. It is seen that the present FG method is predicting the etch profiles accurately.

Figure 4.14 shows the etchfront evolution when the reaction rate at the interface is relatively slow. The effect of finite reaction rate on etch profile evolution is investigated

using two values of *Sh*- namely, 1 and 0.1. It is seen that the bulging effect is less pronounced near the mask region and the etch rate is slow compared to case with diffusion-controlled condition where the bulging is significantly pronounced and the etch rate is faster. This is because the etching process in reaction-controlled etching is controlled by rate of reaction at the interface. Due to the slow rate of reaction at the interface, the etch rate is slower as compared to diffusion-controlled case. As a result, the etchfront moves slowly as shown in Fig. 4.14a. It is seen from Fig. 4.14b that for Sh = 0.1, the etch profiles at equal intervals of time are nearly equidistant. This is because of the nearly constant concentration gradient at the etchant-substrate interface. When the rate of reaction at the interface is very slow, the decrease in the etchant concentration at the interface due to its consumption by reaction with the substrate has negligible effect on the bulk etchant concentration. Hence, the concentration gradient is nearly constant. The speed of the interface related to the concentration gradient as

$$v_{\hat{n}} = -\frac{DM_{Sub}}{m\rho_{Sub}}\frac{\partial c}{\partial \hat{n}} \tag{4.3.6}$$

Equation (4.3.6) is the interface condition as discussed in chapter 2. It is seen from Eq. (4.3.6) that the speed of the interface is directly proportional to the concentration gradient. Since the concentration gradient is constant for very slow rate of reaction as is the case with Sh = 0.1, the speed of the etchfront is also constant. As a result, the etch profiles are equidistant when Sh = 0.1.

4.3.2.3 Concentration Distribution

Figure 4.15 shows the etchant concentration distribution in the etchant domain and in the etched region of substrate with finite reaction rate at the interface. The dimensionless

etching parameter is taken as $\beta = 10$. Figure 4.15a shows the concentration contours for $Sh = 0.1$ and Fig. 4.15b shows it for $Sh = 1.0$ at time $t^* = 20$. As expected, with increase in Sh from 0.1 to 1.0, the concentration of etchant near the interface decreases. This is because of the increase in the reaction rate at the interface with increase in Sh. As the reaction rate increases, the consumption of etchant at the reaction interface is also increases which results in decreased etchant concentration near the interface.

4.3.2.4 Effect of the Rate of Reaction

The effect of the reaction rate on the etch profile evolution is investigated based on the value of Sherwood number (Sh) as shown in Fig. 4.16. The dimensionless etching parameter is taken as $\beta = 10$. The etch profiles shown at $t^* = 20$ for two values of Sh- 1 and 1000. It is seen that the tangent to the etch profile with $Sh = 1.0$ subtends an angle with the mask layer which is less than the corresponding angle subtend by the tangent with $Sh = 1000$. This can be explained by considering the horizontal motion of the interface below the mask for the above two values of Sh. As discussed in chapter 2 (Eq. 2.8.25 of sub-section 2.8.4), the horizontal motion of the interface is given as

$$\frac{\partial x}{\partial t} = -\frac{DM_{Sub}}{m\rho_{Sub}}\left[\frac{\partial c}{\partial x} - \frac{\partial c}{\partial y}\frac{\partial x}{\partial y}\right] \tag{4.3.7}$$

When the value of Sh is large, the concentration of etchant at the interface closes to zero. Hence, the concentration gradient along y-direction is negligibly small. As a result, the second term on the right hand side of Eq. (4.3.7) is negligible. But when the value of Sh is small, the concentration gradient at the interface is finite due to significant variation of etchant concentration along the interface. This makes the second term of Eq. (4.3.7) to have significant effect on the displacement of the interface in horizontal direction below

the mask. So, this gives an additional horizontal displacement of the interface below the mask, thus results in smaller angle.

4.4 Three-Dimensional Etching

Results obtained using the present FG method for three-dimensional WCE model is discussed in this section. The etching is diffusion limited, i.e the concentration at the interface is zero due to infinitely fast reaction at the interface. The computational domain is as discussed in chapter 2 (shown in Fig. 2.14). For presentation of results, following dimensionless variables are defined.

$$X \equiv x/a,\ L_1 \equiv l_1/a \tag{4.3.8a}$$

$$Y \equiv y/a,\ L_4 \equiv l_4/a \tag{4.3.8b}$$

$$Z \equiv z/a,\ L_2 \equiv l_2/a,\ L_3 \equiv l_3/a,\ H \equiv h/a \tag{4.3.8c}$$

$$C \equiv c/c_o \tag{4.3.8d}$$

$$C_R \equiv c_R/c_o \tag{4.3.8e}$$

$$t^* \equiv tD/a^2 \tag{4.3.8f}$$

$$\hat{N} \equiv \frac{\hat{n}}{a} \tag{4.3.8g}$$

Using the above dimensionless variables, the dimensionless form of the governing equation with initial and boundary conditions are given as

Governing Equation

$$\frac{\partial C}{\partial t^*} = \frac{\partial^2 C}{\partial X^2} + \frac{\partial^2 C}{\partial Y^2} + \frac{\partial^2 C}{\partial Z^2} - \frac{\partial C_R}{\partial t^*} \qquad \text{in } \Omega(t^*),\ \Omega_s(t^*), \text{ and } \Omega_m \tag{4.3.9}$$

Initial Conditions

$C = 1\ ,\ C_R = C_{R,max}$ in $\Omega(0)$ (4.3.10a)

$C = 0\ ,\ C_R = 0$ in $\Omega_s(0)$, and Ω_m (4.3.10b)

Boundary Conditions

$\frac{\partial C}{\partial X} = 0$ Γ_5, $X = 0$ (4.3.11a)

$\frac{\partial C}{\partial Y} = 0$ Γ_5, $Y = 0$ (4.3.11b)

$C = 1$ $Y = H + L_3$ (4.3.11c)

$C = 1$ $X = 1 + L_1$, $Y = 1 + L_4$, $H \le Z \le H + L_3$ (4.3.11d)

$C_R = 0$ in Ω_m and $\Omega_s(t^*)$ (4.3.11e)

$C = 0$ on $f(t^*)$ (4.3.11f)

The values of L_1 and L_4 are taken as 6.5 each. The dimensionless thickness of substrate is taken as L_2 = 2.0. The dimensionless height of etchant is taken as L_3 = 6.5. Two mask thicknesses namely,- infinitely thin and finite mask thicknesses are chosen for presentation of results. For infinitely thin mask, the dimensionless mask thickness is taken as H = 0.005. For finite mask thickness, the thickness of the mask is taken as one-fifth of the substrate thickness, i.e. H = 0.4.

4.4.1 Grid Independence Test

A grid refinement test is performed to ensure the solutions are grid independent: temporal as well as spatial. Figure 4.17 shows the evolution of sectional etchfronts at three different sections at distances 0.05, 0.45 and 0.95 from the origin in XZ- and YZ- plane cuts at three

time levels. The dimensionless etching parameter is taken as $\beta = 10$ and the mask is infinitely thin. Three control volume sizes namely, 0.2 × 0.2 × 0.2 (18 × 18 × 31 number of control volumes) , 0.1 × 0.1 × 0.1 (25 × 25 × 41 number of control volumes) and 0.05 × 0.05 × 0.05 (45 × 45 × 58 number of control volumes) are taken to carry out this test. These control volume sizes are taken near the opening region of the substrate. Away from the opening an expanding grid is used, as the grid sizes away from the etchant-substrate interface have no significant effect on the solution. For each control volume size the time independent etchfronts are shown. The time step size for all three control volume sizes is found to be $\Delta t^* = 0.01$. It is seen that there is no significant difference in the prediction of etchfronts from control volume sizes of 0.1 × 0.1 × 0.1 and 0.05 × 0.05 × 0.05. Hence it can be said that the control volume size 0.1 × 0.1 × 0.1 produced the grid independent solution.

4.4.2 Sectional Etch Profiles

Figure 4.18 shows the sections of the etchfronts taken from two perpendicular planes namely, XZ and YZ. Etchfronts are shown at three different sections at distances 0.05, 0.45 and 0.95 from the origin. It is seen that the sections of the etchfronts taken from the above two perpendicular planes at equal distances from the origin are same. This is in accordance with the symmetry of the problem considered here. Since the boundary conditions in two perpendicular planes are symmetrical and the opening is also square in size, hence the etchfronts are also symmetrical in two perpendicular planes (XZ and YZ) at equal distances from the origin. The bulging effect is pronounced near the mask corner at an early time ($t^* = 5$) as shown in Fig. 4.18. This is because of the faster diffusion rate of etchant near the mask corner. Diffusion length increases approximately as the square root of time. At an early time, the diffusion length is small which restricts to mask corner and thus having

higher diffusion rate near mask corner. As time progresses, the effect of diffusion of etchant also expands near the interface. As a result, the bulging region spreads towards the origin. Figure 4.19 shows the sections of etchfronts for $\beta = 50$. The etch depth in this case is relatively small compared to the former case. This is because of the decrease in the initial etchant concentration with increase in β value for a given etchant substrate combination as discussed before in section 4.1. When the value of β increases to 50, the bulging effect is more clearly seen even for longer time compared to $\beta = 10$. This is because of the narrowing of bulging region with increase in the value of β.

4.4.3 Evolution of Etch Surfaces

Figures 4.20 and 4.21 show the evolution of etch surfaces with time for infinitely thin and thick mask conditions respectively. The dimensionless etching parameter is $\beta = 50$. It is seen that the bulging of etch surfaces is not pronounced when mask thickness is finite as found in two-dimensional diffusion-limited etching. The vertical etch depth is nearly uniform whole along the surfaces. This is because of the large diffusion length of etchant particles near the mask corner due to finite mask thickness. Therefore, the effect of the diffusion of etchant to the interface from the sides of the mask is less compared to the diffusion of etchant to the interface from top. Hence fresh etchant is less readily available near the mask corner as thickness of the mask increases which results in slow etch rate near the mask corner with increase in mask thickness. As a result, the bulging is not pronounced even at early etching time.

4.4.4 Concentration Distribution

Figure 4.22 shows the concentration distribution at $t^* = 20$ for $\beta = 10$ and infinitely thin mask. The etchant-substrate interface is near the contour $C = 0.05$. The etchant concentration is less near the etchant-substrate interface compared to away from the interface and is nearly unchanged with initial etchant concentration far away from the interface. This is because of the consumption of etchant at the interface to dissolve the substrate during etchant-substrate reaction.

4.4.5 Two-Dimensional Etch Profiles from Three-Dimensional Etching

The schematic of the problem considered to study the transformation of a three-dimensional etching problem to a two-dimensional etching problem is shown in Fig. 4.23. A substrate covered with a photoresist mask at the top leaving behind a rectangular opening (Fig. 4.23a), which is exposed for direct contact of etchant with the substrate. The cross sectional dimension of the opening is taken as $2a \times 15a$. Because of the symmetry of the problem about the center of the opening, only one-quarter of the domain is considered with the origin set at the center as shown in Fig. 4.23b. The boundary conditions are same as discussed in the schematic of the previous three-dimensional etching problem. Figure 4.24 shows the evolution of the etched surface at $t^* = 20$ for $\beta = 10$. It is seen that away from the mask corner (towards the origin) in the y-direction, the vertical etch depth is almost constant. The effect of the diffusion of etchant at the mask corner (due to the consumption of etchant at the interface) is not significantly affect the etchant concentration far away from the mask corner in the y-direction. Hence the etch depth is nearly uniform far away from the mask corner towards the origin. Figure 4.25 shows the comparison of cross-sectional etchfronts at different time levels taken from the

YZ-plane near the origin with the two-dimensional etchfronts. It is seen that the sections of the etchfronts from YZ-plane near the origin are actually giving the two-dimensional etchfronts. Hence it can be said that, a three-dimensional etchfront transformed to a two-dimensional etchfront away from the mask corner.

4.5 Validation with Experiment

The proposed model is validated with available experimental results for diffusion-controlled etching. Notten et al. (1986) conducted an experiment to etch Gallium Arsenide (GaAs) in a mixture etchant solution consists of hydrochloric acid, hydrogen peroxide and water ($HCl/H_2O_2/H_2O$). A diffusion-controlled etching has been reported for this etchant-substrate combination. The stoichiometric reaction parameter of this etchant-substrate reaction is $m = 3$ (Kuiken et al., 1986). The density of GaAs substrate is found to be 5.32 g/cm^3 and the molar mass is 144.6446 g/mol. The initial etchant concentration is 0.46×10^{-3} mol/cm^3 (Notten et al. 1986). The diffusion coefficient of etchant is $D = 10^{-5}$ cm^2/sec. For the present model the maximum possible value of the reacted concentration ($c_{R,max}$) needs to be known. For the above etchant-substrate combination it is evaluated as

$$\begin{aligned} c_{R,max} &= \frac{m\rho_{Sub}}{M_{Sub}} \\ &= \frac{3\times 5.32}{144.6446} \\ &= 0.11034\, g/cm^3 \end{aligned} \tag{4.5.1}$$

For the above initial etchant concentration, the dimensionless etching parameter is

$$\begin{aligned} \beta &= \frac{m\rho_{Sub}}{c_o M_{Sub}} \\ &= \frac{3\times 5.32}{0.46\times 10^{-3}\times 144.6446} \\ &\approx 240 \end{aligned} \tag{4.5.2}$$

For this experimental test case, the present model's computational domain and boundary conditions are shown in Fig. 4.26. The mask is taken infinitely thin with thickness of 0.05 μm. The width of the mask is taken as 0.1 cm. The thickness and width of the substrate is taken as 6 μm and 0.14 cm respectively. The height of the etchant domain is taken as 0.1 cm.

Figure 4.27 shows the evolution of etch profiles at the mask corner region at three different etching times. The etch profiles are shown using scaled spatial variables. The actual spatial variables are scaled to dimensionless form as

$$\mathrm{X} = x(Dt)^{-1/2}\beta^{2/3} \tag{4.5.3a}$$

$$\mathrm{Y} = y(Dt)^{-1/2}\beta^{2/3} \tag{4.5.3b}$$

It is seen that the etch profiles in the above scaled variables remains same irrespective of different etching time. This confirms that the etchfront varies as the square root of time.

The etch profile obtained using the present FG method is compared with an analytical asymptotic solution for semi-infinite geometry (Kuiken et al., 1986) and the experiment as shown in Fig. 4.28 for the experimental condition as discussed at the beginning of this section. It is seen that the present FG method is in good agreement with the experimental etchfront and the analytical asymptotic solution. This confirms the validity of the present FG method with the experiment.

Figure 4.29 shows the complete etchfront obtained using the FG method. The etchfront is compared with the exact solution (Kuiken et al., 1986) for one-dimensional etching. It is seen that far away from the mask corner, the etchfront is actually one-dimensional. This

means the concentration gradient along x-direction is negligible far away from the mask corner, hence giving the one-dimensional profile. This confirms that the domain considered in the present model (shown in Fig. 4.26) is semi-infinite.

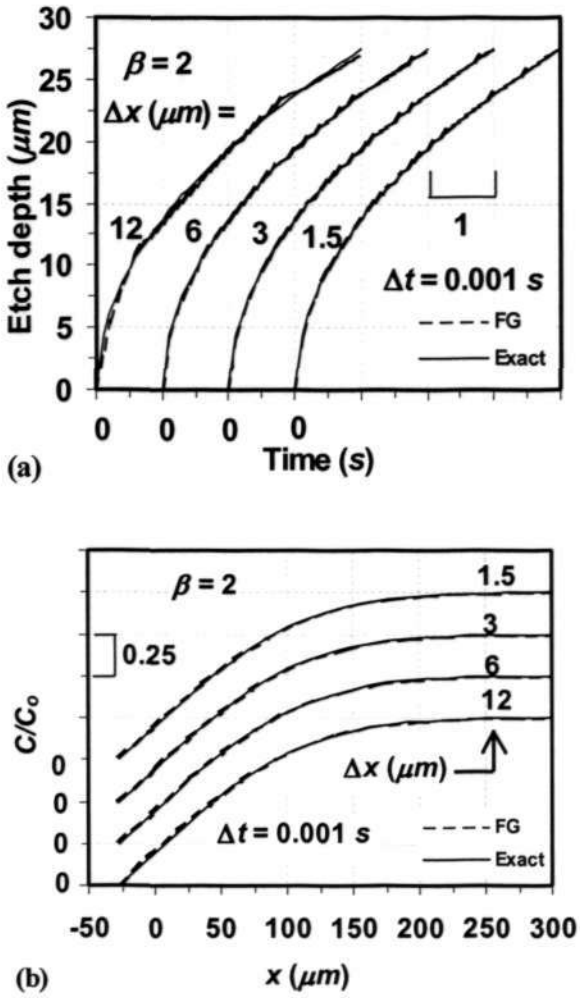

Figure 4.1 Grid independence test for $\beta = 2$ and $D = 10^{-5}\ cm^2/sec$ in diffusion-controlled etching ($k >> D$): (a) variation of etch depths for 4 seconds of etching and (b) concentration distributions at $t = 4\ s$.

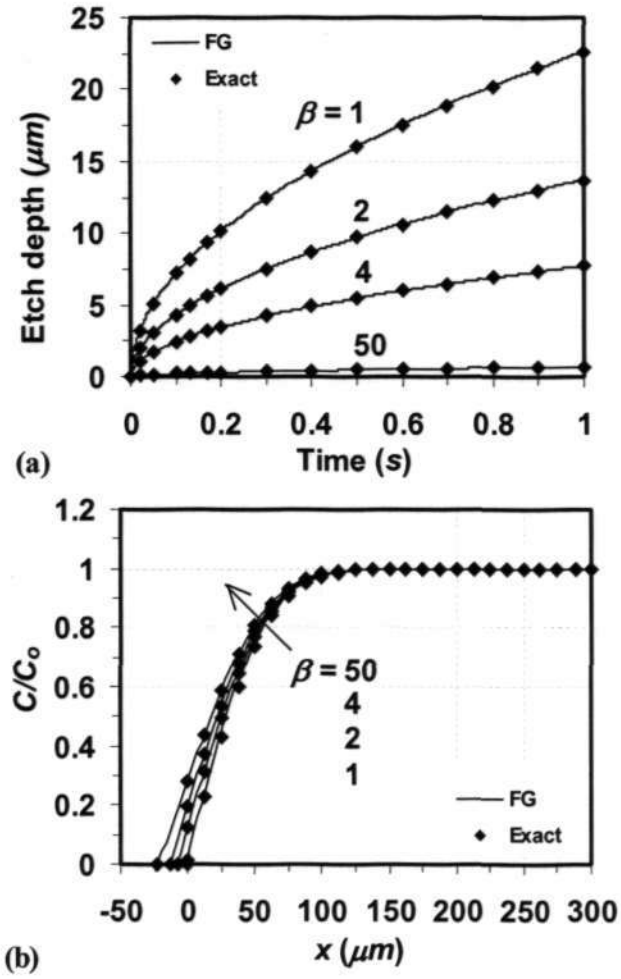

Figure 4.2 Comparisons of FG and exact solution (Kuiken et al., 1986) for $D = 10^{-5}$ cm^2/sec and four β values in diffusion-controlled etching ($k >> D$): (a) variation of etch depths for 1 second of etching and (b) concentration distributions at $t = 1$ s.

Table 4.1a. Comparison of the etch-depths (in μm) for $\beta = 50$.

Time (Sec.)	Exact	FG	% Error $\left(\left\|\frac{\text{Exact} - \text{FG}}{\text{Exact}}\right\| \times 100\right)$
0.2	0.315	0.312	0.952
0.4	0.446	0.444	0.448
0.6	0.546	0.545	0.183
0.8	0.630	0.631	0.159
1.0	0.705	0.706	0.142

Table 4.1b. Comparison of the etch-depths (in μm) for $\beta = 2$.

Time (Sec.)	Exact	FG	% Error $\left(\left\|\frac{\text{Exact} - \text{FG}}{\text{Exact}}\right\| \times 100\right)$
0.2	6.134	6.135	0.016
0.4	8.675	8.759	0.968
0.6	10.625	10.603	0.207
0.8	12.269	12.263	0.049
1.0	13.717	13.710	0.051

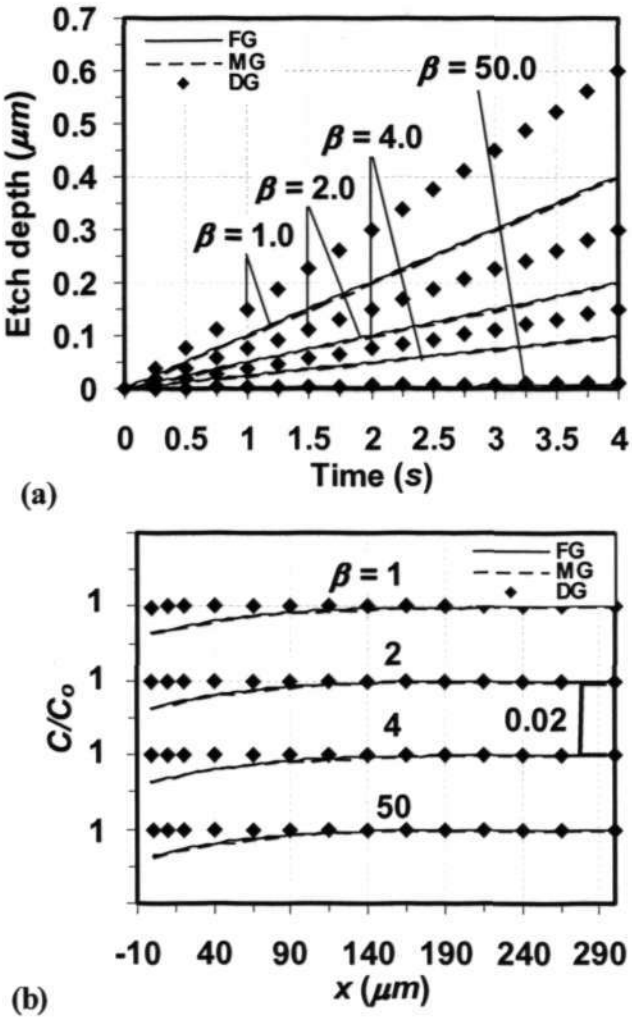

Figure 4.3 Comparisons of FG, MG and DG models for four β values in reaction-controlled etching with $k = 10^{-5}$ *cm*/sec and $D = 10^{-5}$ cm^2/sec : (a) variation of etch depths for 4 seconds of etching and (b) concentration distributions at $t = 4$ *s*.

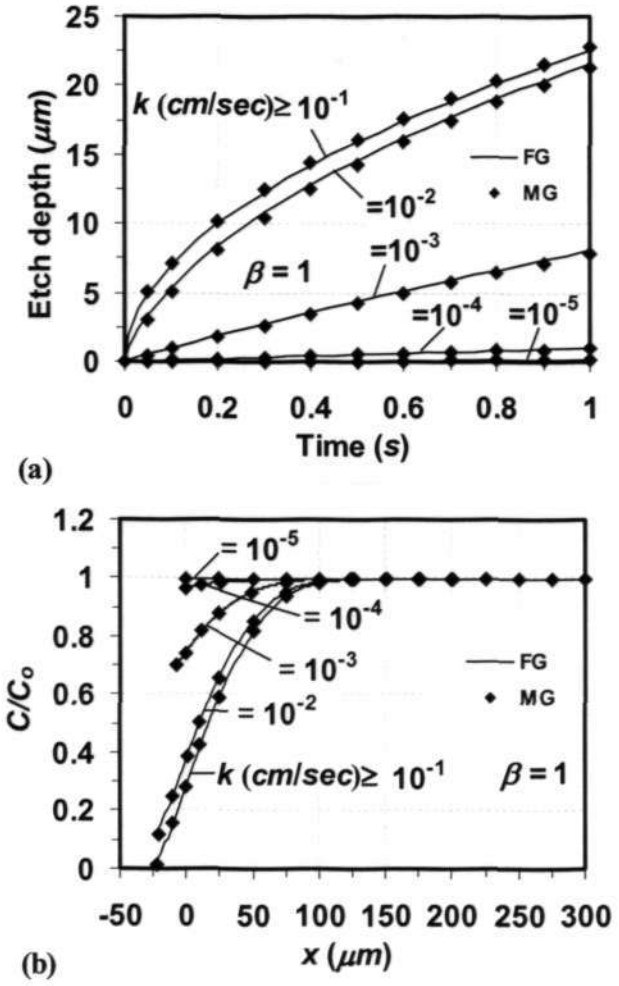

Figure 4.4 Comparisons of FG and MG methods for a range of k values with $D = 10^{-5}$ cm^2/sec and $\beta = 1$: (a) variation of etch depths for 1 second of etching and (b) concentration distributions at $t = 1$ s.

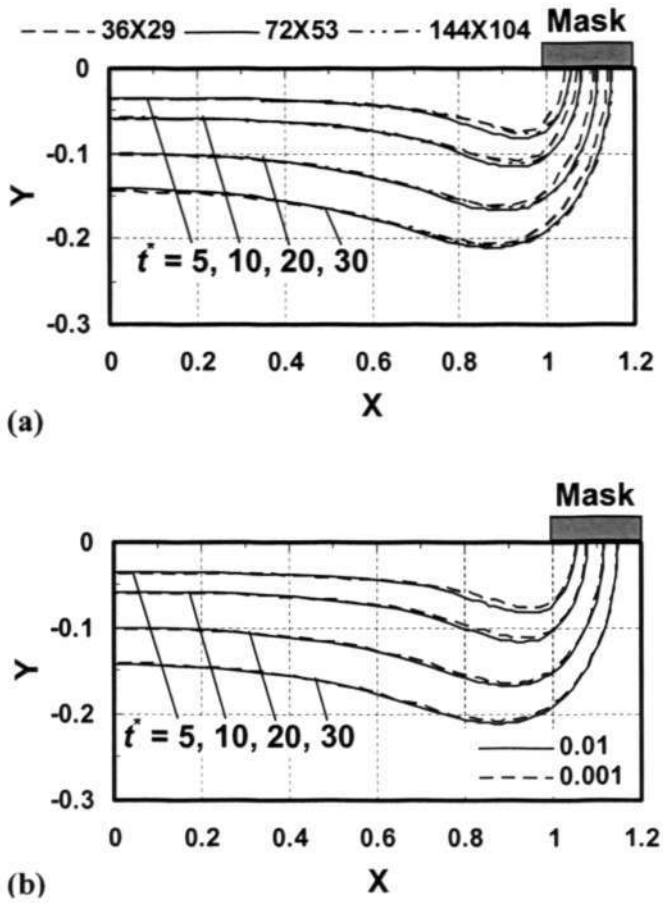

Figure 4.5 Grid independence study for $\beta = 100$ and infinitely thin mask: (a) Effect of spatial grid sizes on evolution of etch profiles; (b) Effect of time step size (Δt) on etch profile evolution for the grid size 72 × 53.

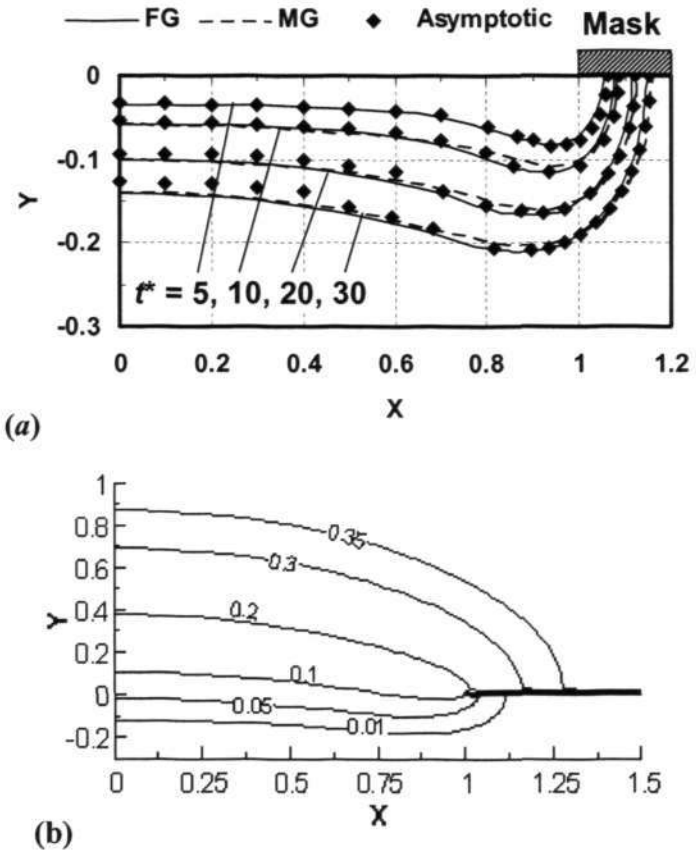

Figure 4.6 Etched profiles and concentration distribution for $\beta = 100$ and infinitely thin mask: (*a*) comparison of etched profiles with asymptotic solution (Kuiken, 1984b) and MG method (Shin and Economou, 1989); (b) concentration contours at $t^* = 30$.

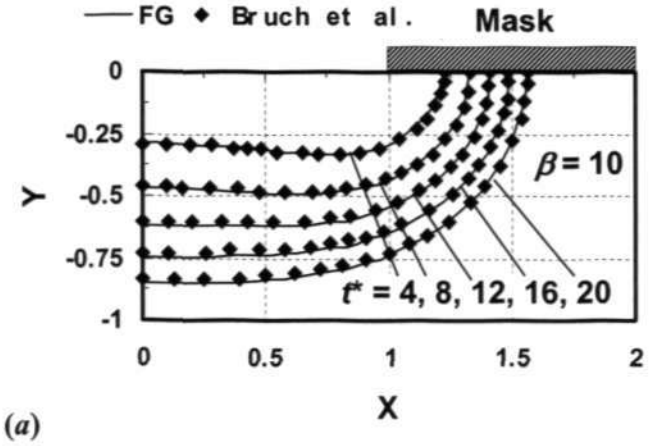

(*a*)

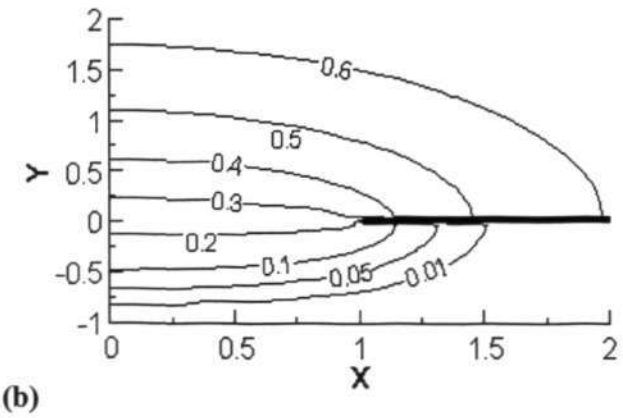

(b)

Figure 4.7 Etched profiles and concentration distribution for $\beta = 10$ and infinitely thin mask: (*a*) comparison of etched profiles with the variational inequality approach; (b) concentration contour at $t^* = 20$.

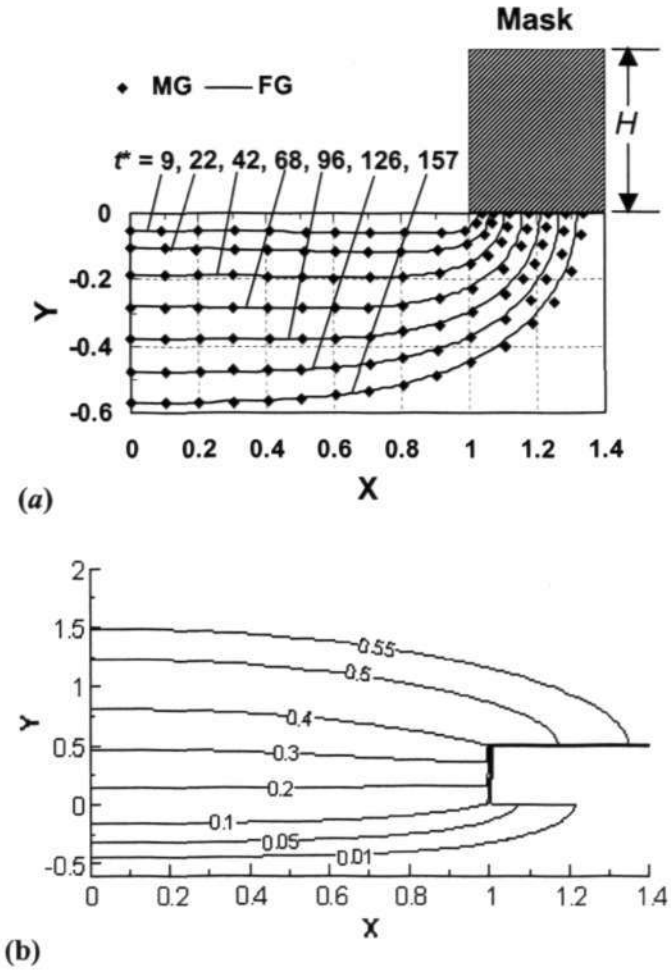

Figure 4.8 Etched profiles and concentration distribution for β = 100 and finite mask thickness (H = 0.5): (a) comparison of etched profiles with MG method; (b) concentration contour at t^* = 126.

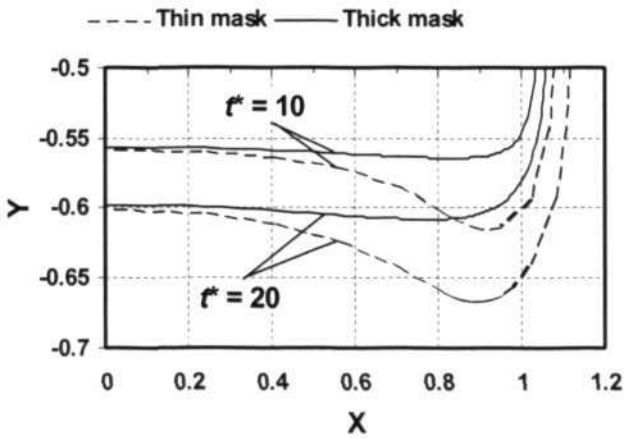

Figure 4.9 Effect of mask thickness on bulging of etched profile for β = 100.

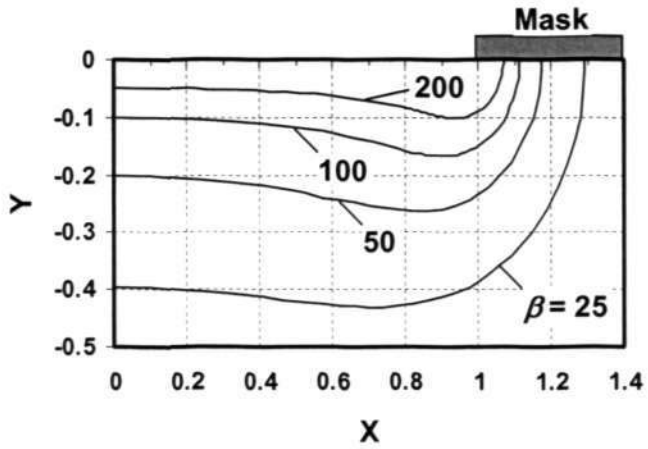

Figure 4.10 Effect of initial etchant concentration (in terms of β) on etched profile evolution at $t^* = 20$ for infinitely thin mask.

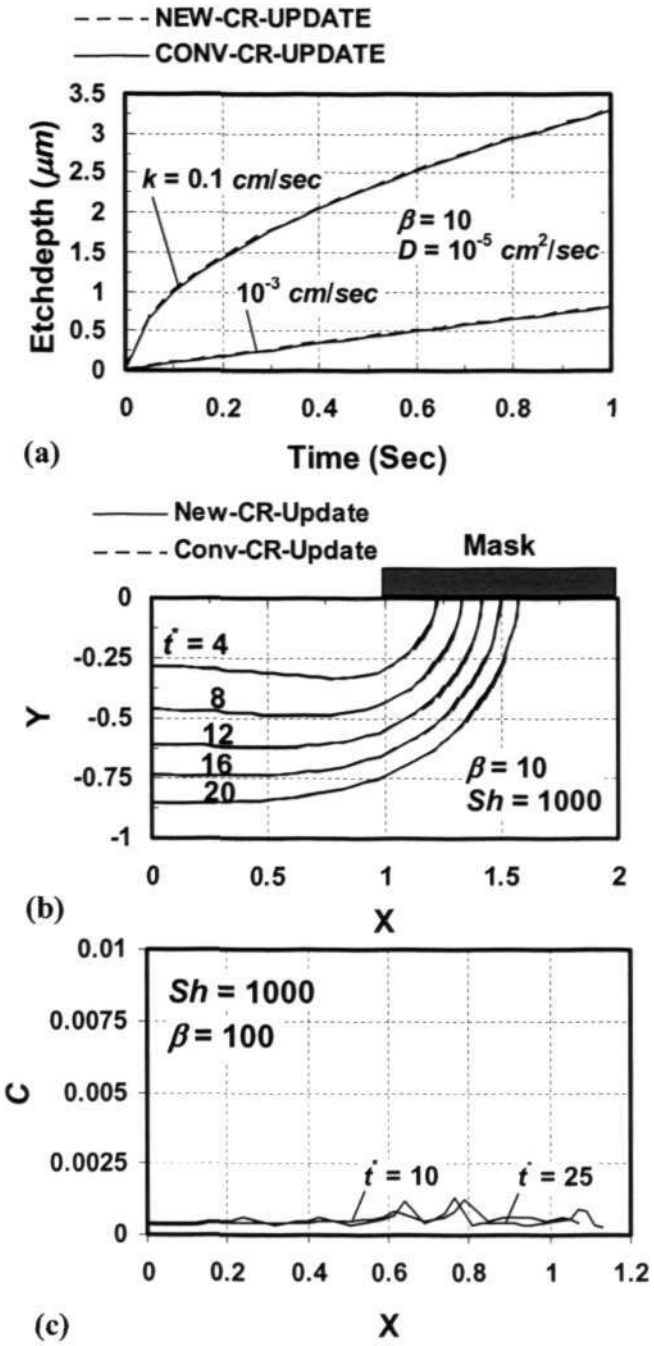

Figure 4.11 Comparison of two update procedures of reacted concentration (c_R): (a) One-dimensional etching; (b) Two-dimensional diffusion-controlled etching (Sh = 1000); (c) Etchant concentration distribution along the interface for Sh = 1000.

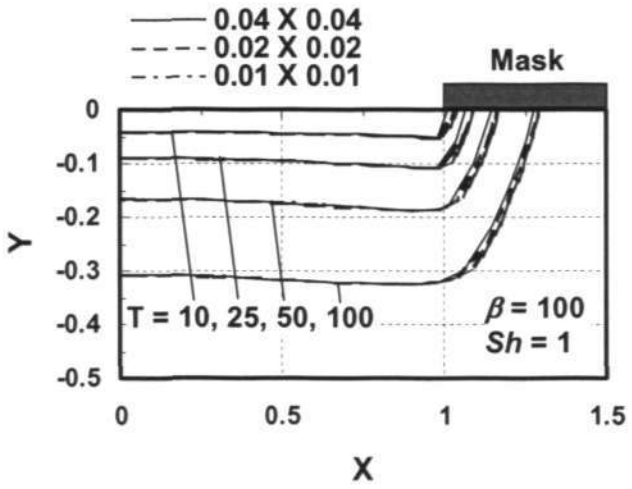

Figure 4.12 Grid-independence test for non-dimensional etching parameter $\beta = 100$ and $Sh = 1$.

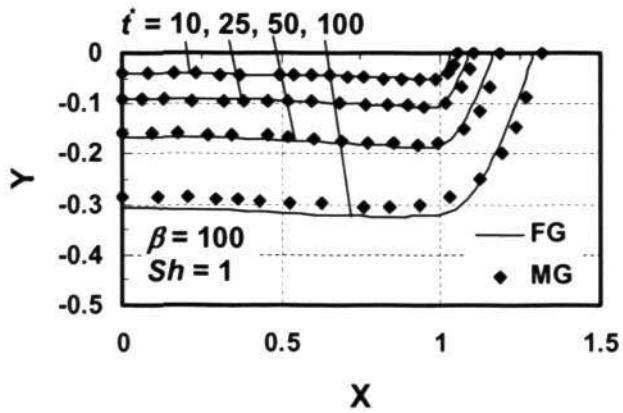

Figure 4.13 Comparison of etch profiles with MG method (Sudirham et al., 2004) for reaction-controlled etching with $Sh = 1.0$ and $\beta = 100$.

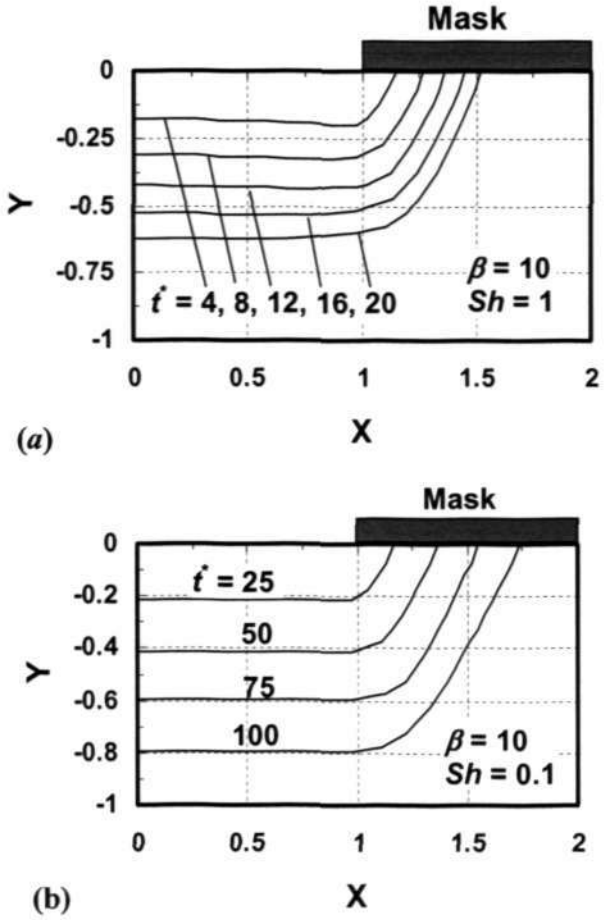

Figure 4.14 Evolution of etch profiles at different time levels for finite reaction at the interface with $\beta = 10$: (a) Evolution of etch profiles for $Sh = 1.0$; (b) Evolution of etch profiles for $Sh = 0.1$.

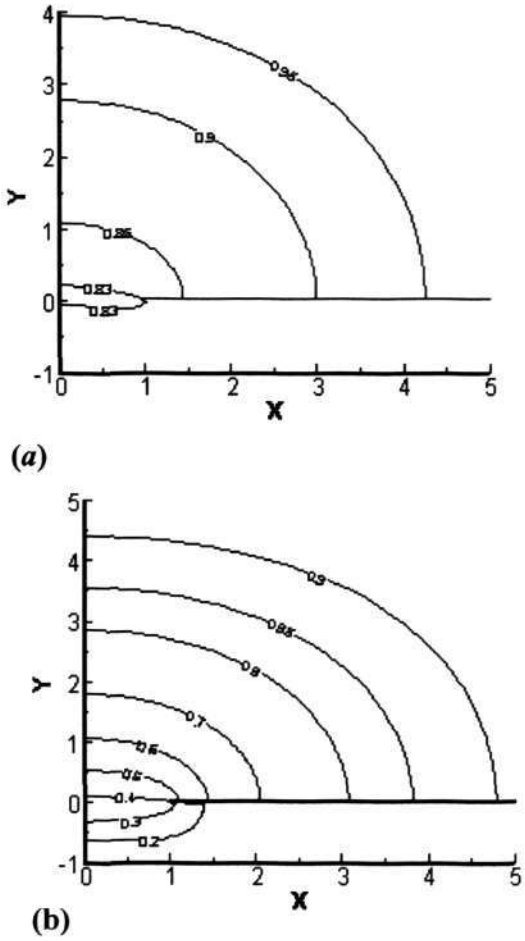

Figure 4.15 Concentration contours at $t^* = 20$ for $\beta = 10$: (a) contours for $Sh = 0.1$ and (b) contours for $Sh = 1.0$.

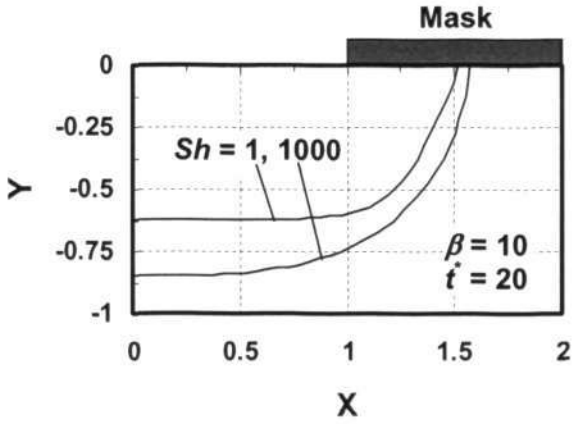

Figure 4.16 Effect of reaction rate on etch profile shape.

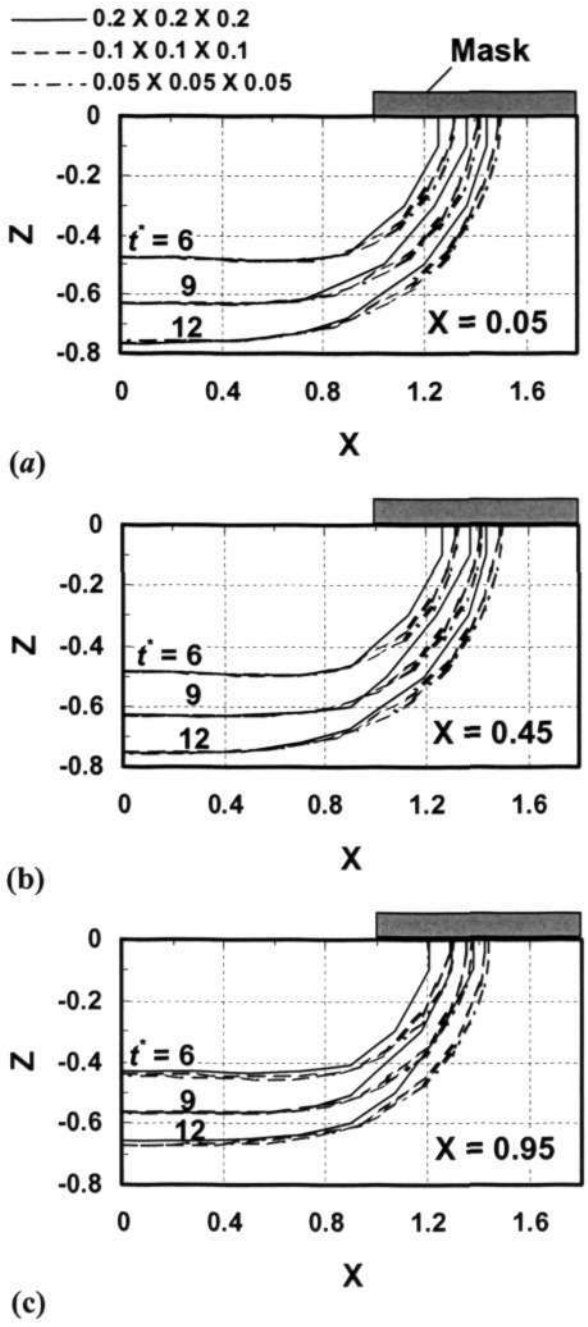

Figure 4.17 Grid independence study at three different locations in XZ-plane for $\beta = 10$.

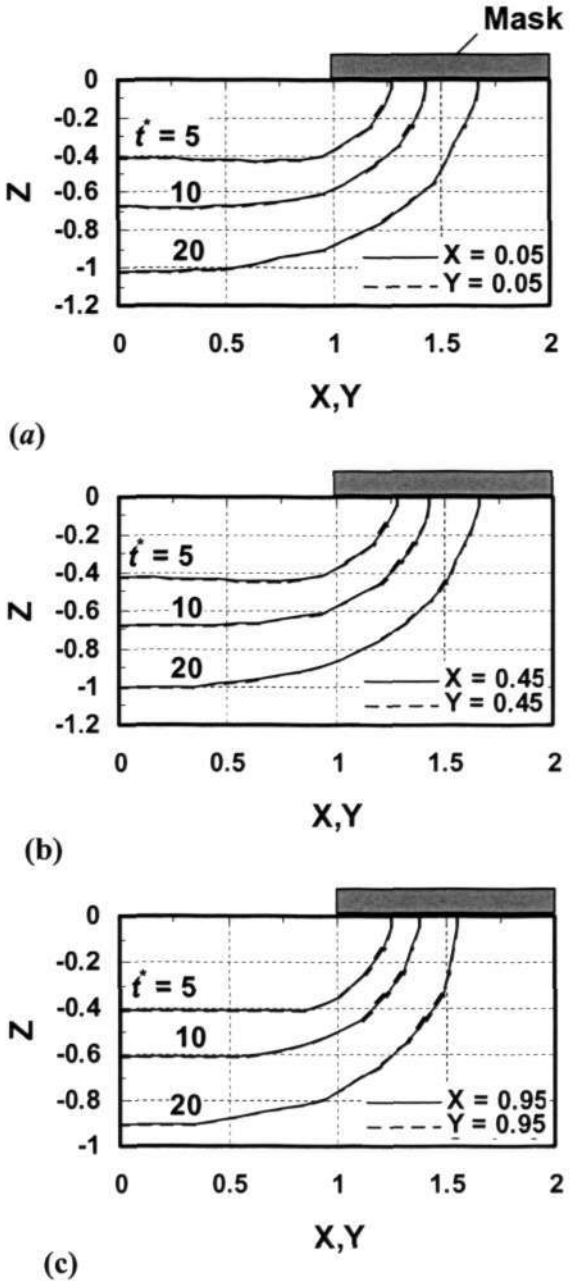

Figure 4.18 Etchfronts at three different sections in XZ- and YZ-plane cuts for $\beta = 10$.

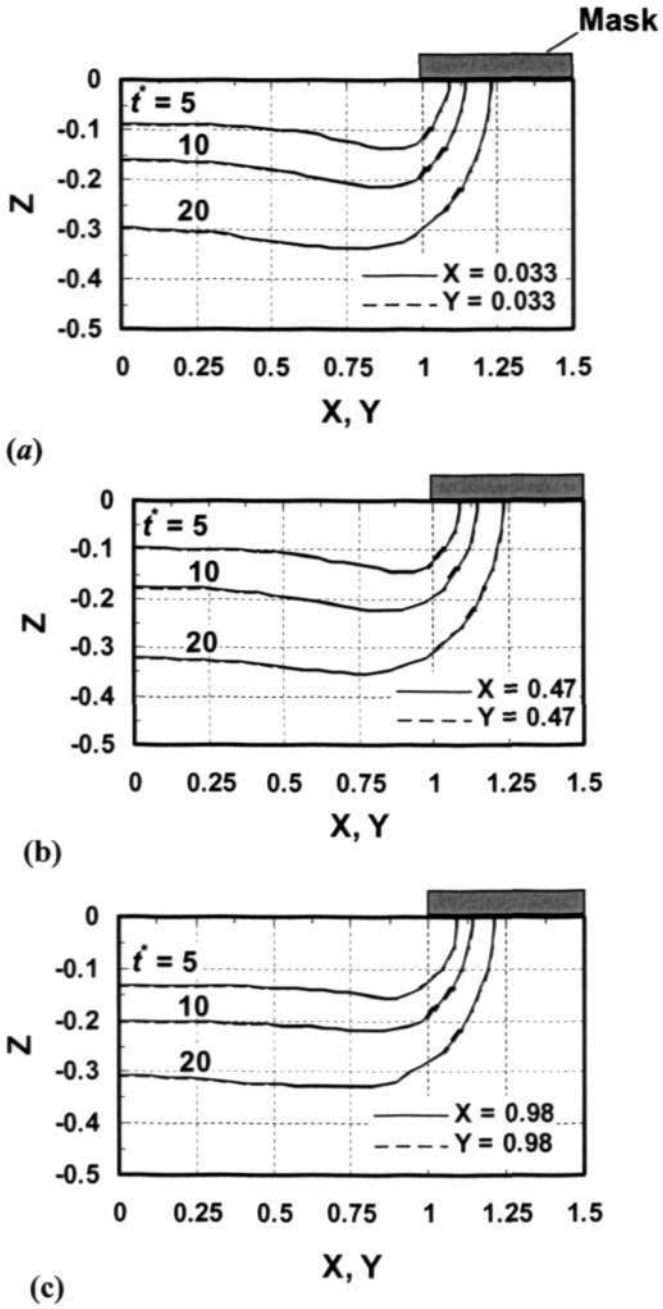

Figure 4.19 Etchfronts at three different sections in XZ- and YZ-plane cuts for $\beta = 50$.

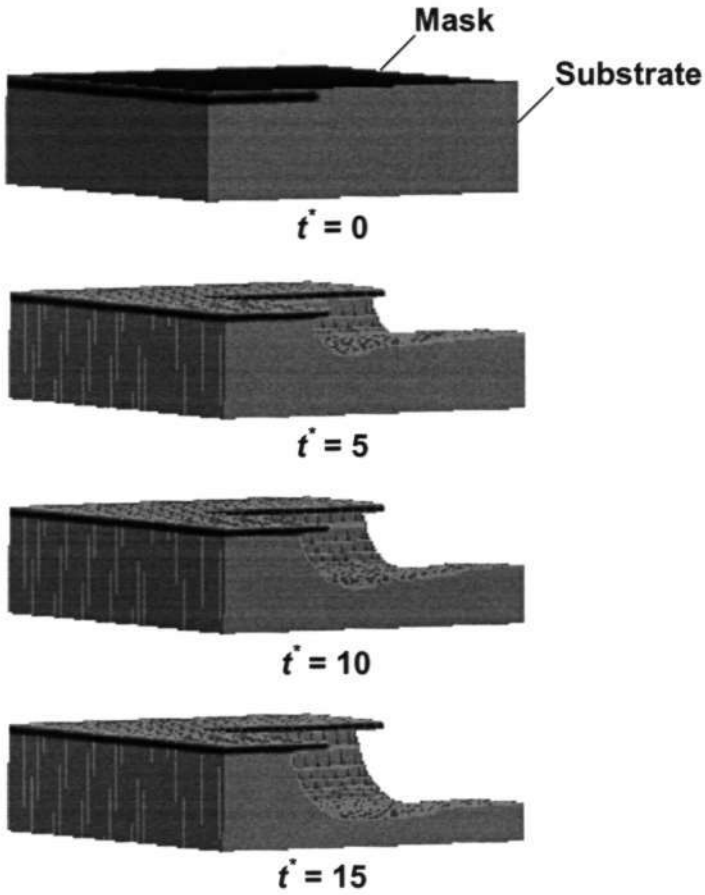

Figure 4.20 Evolution of etch surfaces at different times during etching with infinitely thin mask ($H = 0.005$) and $\beta = 50$.

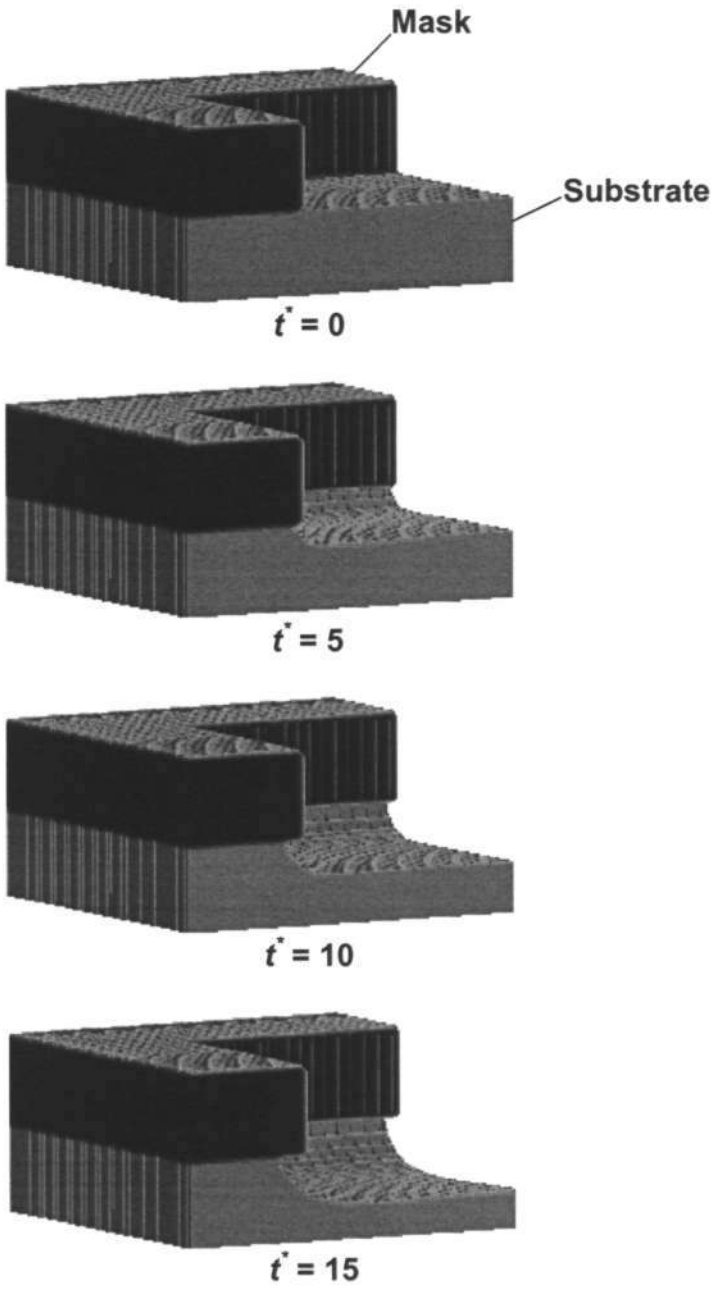

Figure 4.21 Evolution of etch surfaces at different times during etching with finite mask thickness ($H = 0.4$) and $\beta = 50$.

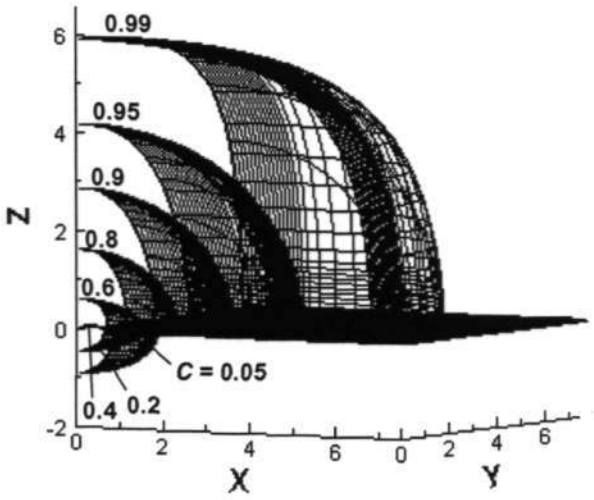

Figure 4.22 Concentration contours at $t^* = 20$ for $\beta = 10$ and infinitely thin mask.

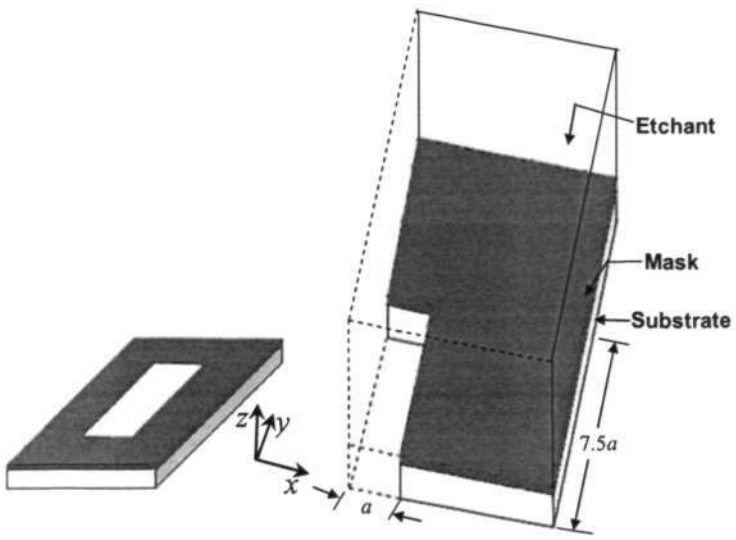

(*a*) (b)

Figure 4.23 Schematic for transformation of a three-dimensional etching problem to a two-dimensional etching problem.

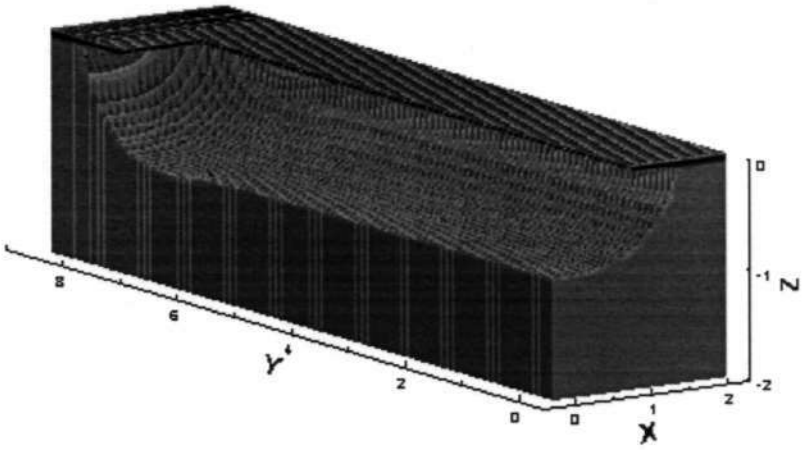

Figure 4.24 Evolution of an etched surface in a rectangular opening at $t^* = 20$ for $\beta = 10$.

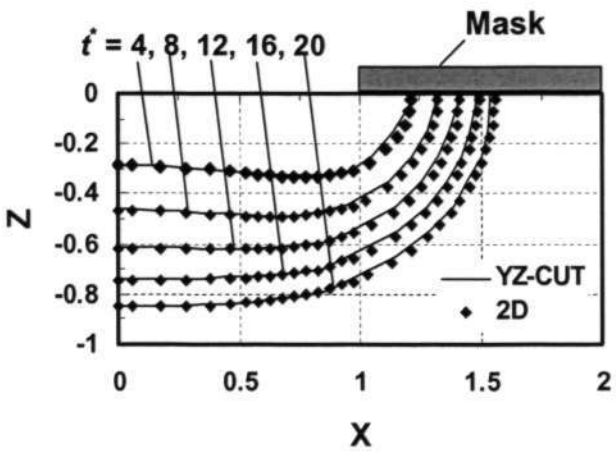

Figure 4.25 Comparison of the sections of three-dimensional etchfronts (taken from YZ-plane near the origin) with the two-dimensional etchfronts for $\beta = 10$.

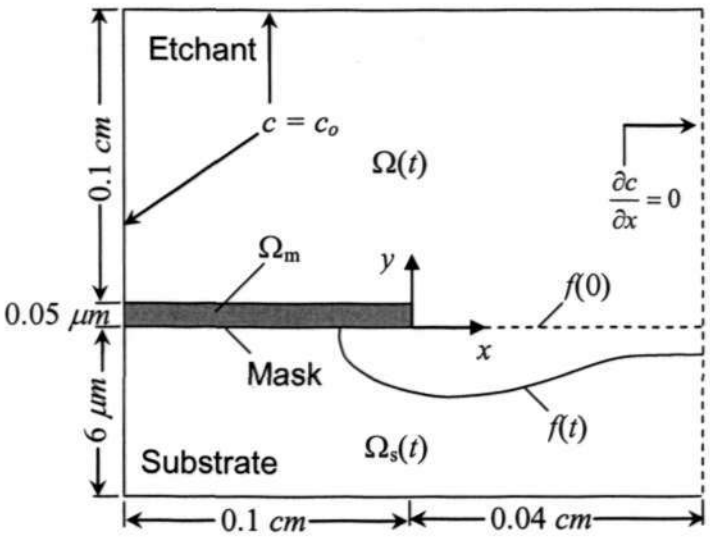

Figure 4.26 The computational domain for experimental validation.

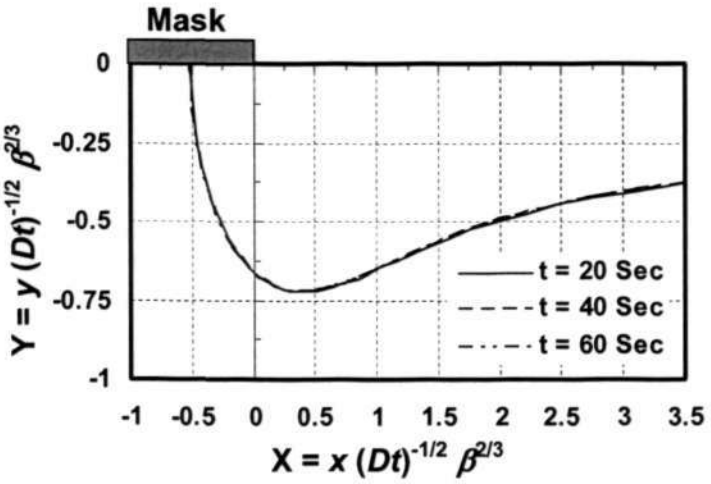

Figure 4.27 Evolution of etchfronts at different time near the mask corner region.

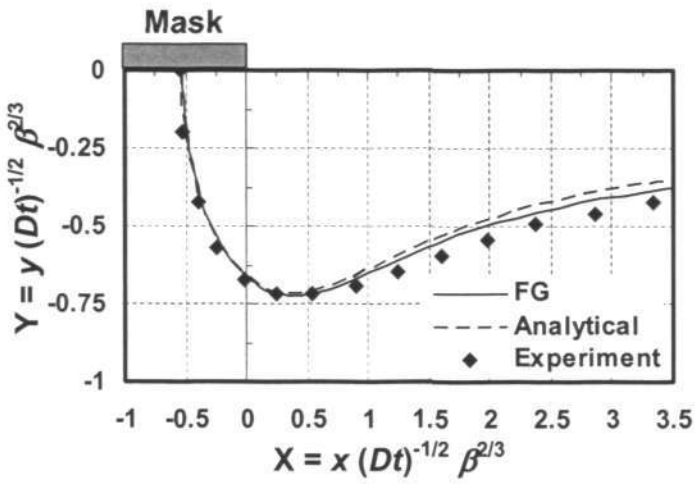

Figure 4.28 Comparison of etch profile obtained using the present FG method with the analytical asymptotic solution and the experiment.

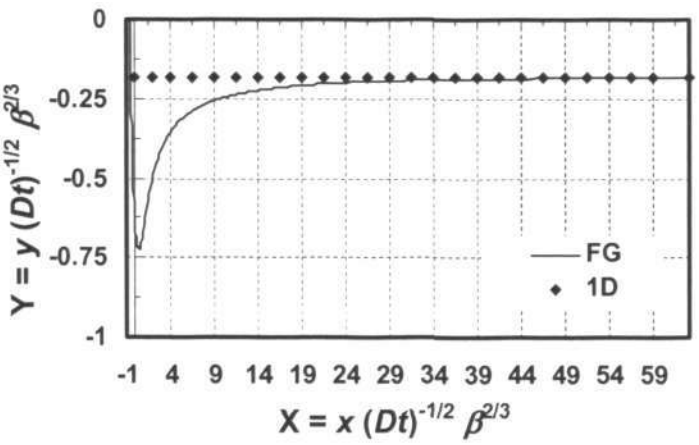

Figure 4.29 Comparison of the etchfront obtained using the FG method with the one-dimensional (1-D) etchfront.

CHAPTER 5

CONCLUSIONS AND RECOMMENDATIONS

5.1 Conclusions

As discussed earlier, the physical and chemical mechanism of the wet chemical etching process is investigated numerically. A new numerical model is developed to model this wet etching (WCE) process under different etching conditions. The new model is based on the total concentration fixed-grid (FG) approach. It is analogous to the enthalpy method used for modeling melting/solidification problems. A new parameter called as the total concentration is defined which is the sum of the unreacted etchant concentration and the reacted etchant concentration. The reacted concentration of etchant is used to predict the etchfront propagation during etching. The conventional governing equation for the wet etching process is reformulated based on the newly defined total concentration. The modified governing equation includes the interface condition. Using this proposed approach, the etchfront can be found implicitly.

The new FG method is applied to model the one-dimensional WCE process. Two limiting cases are studied: (1) the diffusion-controlled etching and (2) the reaction-controlled etching. These two cases differ from each other by the rate of reaction of etchant with the substrate at the interface. As discussed before, the diffusion-controlled etching is associated with infinitely fast reaction at the interface which makes the etchant concentration at the interface to zero. The etching process is governed by the diffusion of etchant to the interface. In reaction-controlled etching, the reaction rate is finite and hence, finite etchant concentration at the interface. The

etching process in this case is governed by the rate of reaction at the interface. The etch depth and the etchant concentration distribution are compared with the available exact solution and the numerical moving grid (MG) solution. A good agreement is found between present FG method and existing exact solution and MG method. The effect of the rate of reaction on the etching process is investigated by varying the rate constant of reaction for a given etchant-substrate combination. It is found that by increasing the rate constant of reaction, the etching approaches to the diffusion-controlled limit and highest etch depth at a given time is found for diffusion limited condition. The effect of initial etchant concentration on the etching process is also investigated. As expected, with increase in the initial etchant concentration, the etch depth is higher at a given etching time and hence the etch rate.

The proposed FG method is extended to model the two-dimensional WCE process. The presence of inert mask makes the etching process multidimensional by protecting certain portions of the substrate from being etched by direct contact with the etchant. Two limiting etching conditions as discussed in previous paragraph on the etchfront evolution are investigated. A new update procedure of the reacted concentration (c_R) is developed for reaction limited etching. The conventional iterative c_R update procedure is applicable for iso-concentration interface as the case with diffusion limited etching. However, in reaction limited etching, the interface is not a iso-concentration interface as the etchant concentration varies along the interface due to the two-dimensional nature of the problem. The etchant concentration distribution is highly non-linear especially near the mask corner, where there is abrupt rise and fall of etchant concentration along the interface. As a result, the conventional iterative update procedure of c_R fails to accurately predict the front. Hence, a new c_R update

procedure is developed considering the spatial variation of etchant concentration along the interface. It is found that the two c_R update procedures produced the same etchfront in diffusion limited etching. However, the conventional c_R update procedure is easy to implement compared to the new update procedure as in the new procedure, one has to evaluate the normal concentration gradient which is not so straightforward in multidimensional etching. Hence, the new c_R update procedure can be applied where the etchant concentration varies along the interface like the case with reaction limited etching. The etchfront evolution is compared with the available analytical and numerical solutions. The present FG method is found to predict the two-dimensional etchfront accurately. The effect of mask thickness on the etchfront evolution is studied. It is found that by increasing the mask thickness, the bulging effect and the underetching can be minimized. The effect of the rate of reaction on the etchfront shape evolution is studied. It is found that the slope of the etching profile in the underetching region increases as the reaction rate at the interface increases. Hence, the bulging of the etch profile near the mask corner is more pronounced when etching is diffusion limited.

The proposed FG method is further extended to model the three-dimensional wet etching. A diffusion-controlled etching condition is examined. The effect of the initial etchant concentration on the etch surface evolution is studied based on the dimensionless etching parameter β. It is found that the etch surface moves faster with low value of β. This is because of the high initial etchant concentration with low β value. The effect of the mask thickness on the etch surface evolution with time is studied and a similar nature of the etchfront surface is found as discussed in two-dimensional etching. An etching condition is studied where one of

cavity opening dimension is taken large enough and it is found that far away from the mask corner, the etchfront is two-dimensional in nature.

The proposed FG method is validated with the available experimental results while etching GaAs in $HCl/H_2O_2/H_2O$ etchant solution. The etchfront obtained using the FG method is compared with the etchfront obtained by experiment and a good agreement is found which confirms the validity of the proposed FG method.

5.2 Recommendations

The new numerical model based on the fixed-grid method is capable of describing the physical and chemical mechanism involved in the wet chemical etching process. The proposed method is capable to model two limiting etching conditions: the diffusion-controlled and the reaction-controlled etching. However, in reaction-controlled etching, a first order reaction rate is assumed. The capability of the proposed method can be tested for higher order reaction rates. The proposed fixed-grid method can be extended to study the etched surface evolution in three-dimensional etching under reaction-controlled etching condition using the new c_R update procedure.

An isothermal etching condition is assumed while modeling the etching process. Hence, the rate constant of reaction is assumed constant. However, the rate constant usually varies with temperature according to the Arrhenius law (Laidler). So, while modeling the non-isothermal wet etching process (also known as thermally driven chemical etching process) the temperature dependence of the rate constant has to be taken into account which leads to non-linear

boundary condition at the interface. Along with the species transport equation the heat diffusion equation needs to be solved to get the temperature distribution at the etchant-substrate interface. A common example of such kinds of etching process is the laser assisted wet chemical etching. In this process the laser beam heat the surface of the substrate and hence enhance the reaction rate thereby increasing the etch rate.

In the present model the etchant is assumed stationary. Hence, the convection effect is neglected. For getting higher etch rate, the etchant solution is forced to flow over the substrate. Then the resulting problem will be convection driven etching, where one needs to solve the continuity equation, the momentum equation and the convection-diffusion species transport equation. The present model can be extended to model this above etching process by including the convection term in the modified governing equation.

The performance of the proposed method to simulate the etching process using unstructured mesh can be tested. The unstructured mesh system is generally needed, when the initial boundaries before etching are highly irregular in shape. The unstructured mesh system can accurately capture the initial highly irregular domain boundaries.

A wet etching experiment can be conducted to validate the present method under different etching conditions. The etching conditions include the diffusion limited and the reaction limited etching. The effect of the etchant concentration and temperature on the wet etching process can be investigated experimentally and the model prediction can be validated.

REFERENCES

Adalsteinsson, D. and Sethian, J., 1995a, "A Level Set Approach to a Unified Model for Etching, Deposition, and Lithography I: Algorithms and Two-Dimensional Simulations", *Journal of Computational Physics*, *Vol. 120*, *pp. 128-144*.

Adalsteinsson, D. and Sethian, J., 1995b, "A Level Set Approach to a Unified Model for Etching, Deposition, and Lithography II: Three-Dimensional Simulations", *Journal of Computational Physics*, *Vol. 122*, *pp. 348-366*.

Asaumi, K., Iriye, Y., and Sato, K., 1997, "Anisotropic-Etching Process Simulation System MICROCAD Analyzing Complete 3D Etching Profiles of Single Crystal Silicon", *Proceedings of IEEE MEMS 1997*, *Nagoya*, *pp. 412-417*.

Brent, A. D., Voller, V. R. and Reid, K. J., 1988, "Enthalpy-Porosity Technique for Modeling Convection-Diffusion Phase Change: Application to the Melting of a Pure Metal", *Numerical Heat Transfer*, *Vol. 13*, *pp. 297-318*.

Bruch, Jr., J. C., Papadopoulos, C. A., Sloss, J. M., 1993, "Parallel Computing Used in Solving Wet Chemical Etching Semiconductor Fabrication Problems", *GAKUTO International Series*, *Mathematical Sciences and Applications*, *Vol. 1*, *Nonlinear Mathematical Problems in Industry*, pp. 281-292.

Cho, S. R., Kim, J., Oh, K. S., Yang, S. K., Baek, J. M., Jang, D. H., Kim, T. I. and Jeon, H., 2002, "Enhanced Optical Coupling Performance in an InGaAs Photodiode Integrated with Wet-Etched Microlens", *IEEE Photonics Technology Letters*, *Vol. 14*, *No. 3*, *pp. 378-380*.

Chun, C. K. and Park, S. O., 2000, "A Fixed-Grid Finite-Difference Method for Phase Change Problems", *Numerical Heat Transfer - Part B, Vol. 38, pp. 59-73.*

Crank, J., 1984, "Free and Moving Boundary Problems", *Clarendon Press, Oxford.*

Declercq, M. J., Gerzberg, L. and Meindl, J. D., 1975, "Optimization of the Hydrazine-Water Solution for Anisotropic Etching of Silicon in Integrated Circuit Technology", *Journal of Electrochemical Society, Vol. 122, pp. 545-52.*

Driesen, C. H., 1999, "Simulation of Convection-Driven Wet Chemical Etching", *PhD. Thesis, University of Twente, The Netherlands.*

Eaton, W. P., Smith, J. H. and Jarecki, R. L., 1996, "Release-Etch Modeling for Complex Surface Micromachined Structures", *Micromachined Devices and Components, Proceedings of the SPIE, Vol. 2882, Austin, TX, Oct 14-15.*

Elwenspoek M., 1993, "On the Mechanism of Anisotropic Etching of Silicon", *Journal of the Electrochemical Society, Vol. 140, pp. 2075-2080.*

Elwenspoek, M., Gardeniers, H., de Boer, M. and Prak, A., 1994, "Micromechanics", *Report No. 122830, University of Twente, Twente, The Netherlands.*

Elwenspoek, M. and Jansen, H. V., 1998, "Silicon Micromachining", *Cambridge Studies in Semiconductor Physics and Microelectronic Engineering: 7, Cambridge University Press.*

Finne, R. M. and Klein, D. L., 1967, "A Water-Amine-Complexing Agent System for Etching Silicon", *Journal of the Electrochemical Society, Vol. 114, pp. 965-70.*

Georgiadou, M. and Alkire, R., 1993, "Anisotropic Chemical Etching of Copper Foil-Experimental Studies on Shape Evolution", *Journal of the Electrochemical Society, Vol. 140, No. 5, pp. 1348-1355.*

Georgiadou, M. and Alkire, R., 1994, "Anisotropic Chemical Pattern Etching of Copper Foil", *Journal of the Electrochemical Society, Vol. 141, No. 3, pp. 679-689.*

Gravesen, P., Branebjerg, J. and Jensen, O. S., 1993, "Microfluidics- a Review", *Journal of Micromechanics and Microengineering, Vol. 3, pp. 168-182.*

Hoffman, K. H. and Sprekels, J., 1990, "Free Boundary Problems: Theory and Applications", *Longman Scientific Technical, Vol. 1, pp. 89.*

Hu, H. and Argyropoulos, S. A., 1996, "Mathematical Modelling of Solidification and Melting: A Review", *Modelling and Simulation in Material Science and Engineering, Vol. 4, pp. 371-396.*

Jianqiang, L. and Yu-Chong, T., 1993, "In Situ Monitoring and Universal Modelling of Sacrificial PSG Etching using Hydrofluoric Acid", *IEEE 0-7803-0957-2/93.*

Javierre, E., 2003, "Numerical Methods for Dissolution Problems", *Report, TUDelft, pp. 1-24.*

Javierre, E, Vuik, C., Vermolen, F. J. and Van Der Zwaag, S., 2005, "A Comparison of Numerical Models for One-Dimensional Stefan Problems", *STW Report, TUDelft, pp. 1-18.*

Kao, Alan S., Stenger, Harvey G., Christos G., Covert, Kathleen L. and Kurowski, John A., 1992, "Etch Profiles Development in Spray Etching Processes", *Journal of the Electrochemical Society, Vol. 139, No. 8, pp. 2202-2211.*

Kaneko, K., Noda, T., Sakata, M. and Uchiyama, T., 2003, "Observation and Numerical Simulation for Wet Chemical Etching Process of Semiconductors", *4th ASME_JSME Joint Fluids Engineering Conference, Honolulu, Hawaii, USA, July 6-10.*

Kendall, D. L., 1990, "A New Theory for the Anisotropic Etching of Silicon and Some Underdeveloped Chemical Micromachining Concepts", *Journal of Vacuum Science and Technology A, Vol. 8, No. 4, pp. 3598-3605.*

Kern, W., 1978, "Chemical Etching of Silicon, Germanium, Gallium Arsenide, and Gallium Phosphide", *Radio Corporation of America Review article, Vol. 39, pp. 278-308.*

Kern, W. and Deckert, C. A., 1978, "Chemical Etching", *Thin Film Processes, J. L. Vossen and W. Kern, Eds. Orlando: Academic Press.*

Kikyuama, H., Miki, N., Saka, K., Takano, J., Kawanabe, I., Miyashita, M. and Ohmi T., 1991, "Principles of Wet Chemical Processing in ULSI Microfabrication", *IEEE Transactions on Semiconductor Manufacturing, Vol. 4, No. 1, pp. 26-35.*

Klein, D. L. and D'Stefan, D. J., 1962, "Controlled Etching of Silicon in the HF-HNO_3 System", *Journal of the Electrochemical Society, Vol. 109, pp. 37-42.*

Koide, A., Sato, K. and Tanaka, S., 1991, "Simulation of Two-Dimensional Etch Profile of Silicon during Orientation-Dependent Anisotropic Etching", *Proceedings of IEEE MEMS 1991, pp. 216-220.*

Kovacs, G. T. A., Maluf, N. I. and Petersen, K. E., 1998, "Bulk Micromachining of Silicon", *Proceedings of the IEEE, Vol. 86, No. 8, pp. 1536-51.*

Kuiken, H. K. and Tijburg, R. P., 1983, "Centrifugal Etching: A Promising Tool to Achieve Deep Etching Results", *Journal of the Electrochemical Society*, *Vol. 130*, *No. 8*, *pp. 1722-1735*.

Kuiken, H. K., 1984a, "Etching: A Two-Dimensional Mathematical Approach", *Proceedings of the Royal Society of London. Series A*, *Mathematical and Physical Sciences*, *Vol. 392*, *Issue 1802*, *pp. 199-225*.

Kuiken, H. K., 1984b, "Etching Through a Slit", *Proceedings of the Royal Society of London. Series A*, *Mathematical and Physical Sciences*, *Vol. 396*, *Issue 1810*, *pp. 95-117*.

Kuiken, H. K., Kelly, J. J. and Notten, P. H. L., 1986, "Etching Profiles at Resist Edges – I Mathematical Models for Diffusion-Controlled Cases", *Journal of the Electrochemical Society*, *Vol. 133*, *No. 6*, *pp. 1217-1226*.

Kuiken, H. K., 1990, "Free Boundary Problems: Theory and Applications", *K.H. Hoffmann and J. Sprekels editors*, *Vol. 1*.

Kuiken, H. K., 1998, "A Free-Convection Boundary-Layer Model for the Centrifugal Etching of an Axisymmetric Cavity", *Journal of Engineering Mathematics*, *Vol. 34*, *pp. 181-200*.

Kuiken, H. K., 2003, "A Mathematical Model for Wet-Chemical Diffusion-Controlled Mask Etching through a circular Hole", *Journal of Engineering Mathematics*, *Vol. 45*, *pp. 75-90*.

La Magna, A., D'Arrigo, G., Garozzo, G. and Spinella, C., 2003, "Computational Analysis of Etched Profile Evolution for the Derivation of 2D Dopant Density Maps in Silicon", *Materials Science and Engineering B, Vol. 102, No. 1-3, pp. 43-48.*

Laidler K. J., "Chemical Kinetics", *Third Edition, Harper and Row Publisher, New York.*

Lee, D. B., 1969, "Anisotropic Etching of Silicon", *Journal of Applied Physics, Vol. 40, pp. 4569-74.*

Li, W. J., Shih, J. C., Mai, J. D., Ho, C-M., Jianqiang, L. and Tai, Y-C., 1998, "Numerical Simulation for the Sacrificial Release of MEMS Square Diaphragms", *First International Conference on MSMSSA, San Jose, USA.*

Liu, J. and Yu-Chong, T., 1993, "In Situ Monitoring and Universal Modelling of Sacrificial PSG Etching using Hydrofluoric Acid", *IEEE 0-7803-0957-2/93.*

Madou, M. J., "Fundamentals of Microfabrication", *2nd edition, CRC Press.*

Mastrangelo, C. H., Zhang, X. and Tang, W. C., 1995, "Surface Micromachined Capacitive Differential Pressure Sensor with Lithographically-Defined Silicon Diaphragm", *The 8th International Conference on Solid-State Sensors and Actuators, Eurosensor XI, Stockholm, June 25-29, pp. 612-615.*

Meerakker, J. E. A. M. van den and Vegchel, J. H. C. van, 1989, "Silicon Etching in CrO_3-HF Solutions", *Journal of the Electrochemical Society, Vol. 136, No. 7, pp. 1949-1957.*

Meerakker, J. E. A. M. van den, Elfrink, R. J. G., Roozeboom, F. and Verhoeven, J. F. C. M., 2000, "Etching of Deep Micropores in 6 in. Si Wafers", *Journal of the Electrochemical Society, Vol. 147, No. 7, pp. 2757-2761.*

Monguchi, T., Fujioka, H., Ono, K., Baba, Y. and Oshima, M., 2000, "Effects of Wet Etching on Photoluminescence of Porous Silicon", *Journal of the Electrochemical Society, Vol. 147, No. 2, pp. 602-605.*

Monk, D. J., Soane, D. S. and Howe, R. T., 1991, "Sacrificial Layer SiO_2 Wet Etching for Micromachining Applications", *International Conference on Solid-State Sensors and Actuators: Transducers '91, IEEE, San Franciscisco, CA, pp. 647-650.*

Monk, D. J., Soane, D. S. and Howe, R. T., 1994, "Hydrofluoric Acid Etching of Silicon Dioxide Sacrificial Layers – II Modeling", *Journal of the Electrochemical Society, Vol. 141, No. 1,* pp. 270-274.

Nedjar, B., 2002, "An Enthalpy-Based Finite Element Method for Non-Linear Heat Problems Involving Phase Change", *Computers and Structures, Vol. 80, pp. 9-21.*

Nielsen, H. and Hackleman, D., 1983, "Some Illumination on the Mechanism of SiO_2 Etching in HF Solutions", *Journal of the Electrochemical Society, Vol. 130, No. 3, pp. 708-712.*

Notten, P. H. L., Kelly, J. J. and Kuiken, H. K., 1986, "Etching Profiles at Resist Edges – II Experimental Confirmation of Models Using GaAs", *Journal of the Electrochemical Society, Vol. 133, No. 6, pp. 1226-1232.*

Ozisik, M. N., "Heat Conduction", *2^{nd} Edition, Wiley-Interscience publication.*

Patankar, S. V., 1980, "Numerical Heat Transfer and Fluid Flow", *W. J. Minkowycz and E. M. Sparrow, Editors, Hemisphere Publishing Corporation.*

Petersen, K. E., 1982, "Silicon as a Mechanical Material", *Proceedings of the IEEE, Vol. 70, pp. 420-457.*

Pister, K. S. J., Judy, M. W., Burgett, S. R. and Fearing, R. S., 1992, "Microfabricated Hinges", *Sensors and Actuators A, Vol. 33, pp. 249-256.*

Prakash, C., Samonds, M. and Singhal, A. K., 1987, "A Fixed-Grid Numerical Methodology for Phase Change Problems Involving a Moving Heat Source", *International Journal of Heat and Mass Transfer, Vol. 30, No. 12, pp. 2690-2694.*

Rath, P., Chai, J. C., Zheng, H. Y., Lam, Y. C., Murukeshan, V. M. and Zhu, H., "A fixed-grid approach for diffusion- and reaction-controlled wet chemical etching", *International Journal of Heat and Mass Transfer, Vol. 48, No. 11, pp. 2140-2149.*

Resnik, D., Vrtacnik, D., Aljancic, U., Mozek, M., Amon, S., 2003, "Different Aspect Ratio Pyramidal Tips Obtained by Wet Etching of (100) and (111) Silicon", *Microelectronics Journal, Vol. 34, pp. 591-593.*

Robbins, H. and Schwartz, B., 1959, "Chemical Etching of Silicon-I: The System, HF, HNO_3, and H_2O", *Journal of the Electrochemical Society, Vol. 106, pp. 505-8.*

Sakaino K., Kawabata Y., and Adachi S., 2000, "Etching Characteristics of Si (100) Surfaces in an Aqueous NaOH Solution", *Journal of the Electrochemical Society, Vol. 147, No. 4, pp. 1530-1534.*

Salo, T., Vancura, T. and Baltes, H., 2004, "Modelling of Sacrificial Aluminium Etching in Complex Geometries", *Journal of Micromechanics and Microengineering, Vol. 14, pp. S123-S127.*

Schwartz, B. and Robbins, H., 1976, "Chemical Etching of Silicon-IV: Etching Technology", *Journal of the Electrochemical Society, Vol. 123, pp. 1903-1909.*

Schwartz, B. and Robbins, H., 1976, "Chemical Etching of Silicon-IV: Etching Technology", *Journal of the Electrochemical Society, Vol. 123, pp. 1903-1909.*

Seidel, H., Csepregi, L., Heuberger, A. and Baumgärtel , H., 1990, "Anisotropic Etching of Crystalline Silicon in Alakaline Solutions", *Journal of the Electrochemical Society, Vol. 137, No. 11, pp. 3612-3625.*

Seidel, H., Csepregi, L., Heuberger, A. and Baumgärtel , H., 1990, "Anisotropic Etching of Crystalline Silicon in Alakaline Solutions-I. Orientation dependence and Behavior of Passivation layers", *Journal of the Electrochemical Society, Vol. 137, No. 11, pp. 3612-3625.*

Seidel, H., Csepregi, L., Heuberger, A. and Baumgärtel , H., 1990, "Anisotropic Etching of Crystalline Silicon in Alakaline Solutions-II. Influence of Dopants", *Journal of the Electrochemical Society, Vol. 137, No. 11, pp. 3626-3632.*

Shamsundar, N. and Sparrow, E. M., 1975, "Analysis of Multidimensional Conduction Phase Change via the Enthalpy Method", *Journal of Heat Transfer, Vol. 97, pp. 333-340.*

Shin, C. B. and Economou, D. J., 1989, "Effect of Transport and Reaction on the Shape Evolution of Cavities during Wet Chemical Etching", *Journal of the Electrochemical Society, Vol. 136, No. 7, pp. 1997-2004.*

Shin, C. B. and Economou, D. J., 1991, "Forced and Natural Convection Effects on the Shape Evolution of Cavities During Wet Chemical Etching", *Journal of the Electrochemical Society, Vol. 138, No. 2, pp. 527-538.*

Shin, C. B. and Economou, D. J., 1990, "Mass Transfer by Natural and Forced Convection in Open Cavities", *International Journal of Heat and Mass Transfer, Vol. 33, No. 10, pp. 2191-2205.*

Spiering, V. L., Lammerink, T. S. J., Jansen, H. V., Fluitman, J. H. J. and Van der Berg, A., 1996, "Technologies and Microstructures for Separation Techniques in Chemical Analysis", *Proceedings of SPIE, Vol. 2882, Austin, Texas, pp. 91-100.*

Stefan, J., 1889, *S B Wein Akad. Mat. Natur., Vol. 98, pp. 473-484, 965-983.*

Stefan, J., 1891, "Uber Die Theorie Der Eisbildung, Inbesondere Uber Die Eisbildung Im Polarmir", *Ann. Chem. Phys., Vol. 42, pp. 269-286.*

Stocker, D. A., Geopfert, I. D., Schubert, E. F., Boutros, K. S. and Redwing, J. M., 2000, "Crystallographic Wet Chemical Etching of p-Type GaN", *Journal of the Electrochemical Society, Vol. 147, No. 2, pp. 763-764.*

Striemer, C. C. and Fauchet, P. M., 2002, "Dynamic Etching of Silicon for Broadband Antireflection Applications", *Applied Physics Letters, Vol. 81, No. 16, pp. 2980-2982.*

Sudirham, J. J., Van Damme, R. M. J. and Van Der Vegt, J. J. W., 2004, "Space-Time Discontinuous Galerkin Method for Wet Chemical Etching of Microstructures", *Memorandum No. 1720, Faculty of EEMCS, University of Twente, The Netherlands.*

Swaminathan, C. R. and Voller, V. R., 1992, "A General Enthalpy Method for Modeling Solidification Processes", *Metallurgical Transactions B, Vol. 23, pp. 651-664.*

Tabata, O., Asahi, R. and Sugiyama, S., 1990, "Anisotropic Etching with Quarternary Ammonium Hydroxide Solutions", *in Technical Digest: 9th Sensor Symposium, Tokyo, Japan, pp. 15-18.*

Tarzia, D. A., 2000, "A Bibliography on Moving-Free Boundary Problems for the Heat-Diffusion Equation: The Stefan and Related Problems", *MAT-Series A, No. 2.*

Tjerkstra, R. W., 1999, "Isotropic Etching of Silicon in Fluoride Containing Solutions as a Tool for Micromachining", *PhD. Thesis, University of Twente, The Netherlands.*

Turner, D. R., 1958, "Electropolishing Silicon in Hydrofluoric Acid Solutions", *Journal of the Electrochemical Society, Vol. 105, pp. 402-408.*

Ulhir, A., 1956, "Electrolytic Shaping of Germanium and Silicon", *Bell System Technology Journal, Vol. 35, pp. 333-47.*

Vakanas, George P., Tseng, Ampere A. and Winer, Paul, 2002, "Laser-assisted chemical etching for embedded microchannels and overhanging microstructures on Si/SiO_2 substrates", *Journal of Laser Applications, Vol. 14, No., pp. 185-190.*

Van der Berg, A. and Lammerink, T. S. J., 1998, "Micro Total Analysis Systems: Microfluidic Aspects, Integration Concept and Applications", *Topics in Current Chemistry*, *Vol. 194*, *pp. 22-49*.

Veenendaal, E. van, Nijdam, A. J., Suchtelen, J. van, Sato, K., Gardeniers, J. G. E., Enckevort, W. J. P. van, Elwenspoek, M., 2000, "Simulation of Anisotropic Wet Chemical Etching Using a Physical Model", *Sensors and Actuators*, *Vol. 84*, *pp. 324-329*.

Voller, V. R. and Cross, M., 1981, "Accurate solutions of moving boundary problems using the enthalpy method", *International Journal of Heat and Mass Transfer*, Vol. 24, pp. 545-556.

Voller, V. R., Prakash, C., 1987, "A Fixed Grid Numerical Modelling Methodology for Convection-Diffusion Mushy Region Phase-Change Problems", *International Journal of Heat and Mass Transfer*, *Vol. 30*, *No. 8*, *pp. 1709-1719*.

Voller, V. R., Swaminathan, C. R. and Thomas, B. G., 1990, "Fixed Grid Techniques for Phase Change Problems: A Review", *International Journal of Numerical Methods in Engineering*, *Vol. 30*, *pp. 875-898*.

Voller, V. R. and Swaminathan, C. R., 1991, "General Source-Based Method for Solidification Phase Change", *Numerical Heat Transfer*, *Vol. 19*, *pp. 175-189*.

Vuik, C. and Cuvelier, C., 1985, "Numerical Solution of an Etching Problem", *Journal of Computational Physics*, *Vol. 59*, *pp. 247-263*.

Vuik C., Segal A. and Vermolen F. J., 2000, "A Conservative Discretization for a Stefan Problem with an Interface Reaction at the Free Boundary", *Computing and Visualization in Science, Vol. 3, pp. 109-114.*

White R. E., 1982, "An Enthalpy Formulation of the Stefan Problem", *SIAM Journal on Numerical Analysis, Vol. 19, pp. 1129-1157.*

Williams, K. R. and Muller, R. S., 1996, "Etch Rates for Micromachining Processing", *Journal of Micromechanical Systems, Vol. 5, No. 4, pp. 256-269.*

Wolf, S. and Tauber, R. N., "Silicon Processing for the VLSI era", *2000 edition.*

Zeng, X. and Xin, M. D., 1991, "An Implicit Finite Difference Solution of Phase Change Problems via Coupling The Enthalpy and Moving Boundary", *HTD-Vol. 159, Phase Change Heat Transfer.*